NEUTRON MODERATOR DESIGNS FOR A LOW VOLTAGE ACCELERATOR

A Thesis

Submitted to the Graduate Faculty of the
Louisiana State University and
Agricultural and Mechanical College
in partial fulfillment of the
requirements for the degree of
Master of Science

in

The Department of Nuclear Engineering

by
David William Kiesel
B.S., Louisiana State University, 1966
J.D., Louisiana State University, 1970
June, 1970

151

ACKNOWLEDGMENT

The author is indebted to Dr. Frank A. Iddings for his guidance and aid in making this thesis possible. Thanks must also go to Dr. Edgar L. Steele for his suggestions in selection of foils. A special appreciation is due Dr. Norman A. Bostrom of Accelerators, Inc. for making available the neutron generator and other equipment.

TABLE OF CONTENTS

PAGE

TABLES

FIGURES

PAGE

PAGE

PAGE

GRAPHS

PAGE

ABSTRACT

Neutrons with energy below 0.41 eV were detected by counting indium foils irradiated at pre-determined positions from the target of an Accelerators, Inc. neutron generator operated at 150 KV. The fast neutrons produced by the neutron generator were determined by counting ^{18}F from $^{19}F(n,2n)^{18}F$ in Teflon or ^{62}Cu from $^{63}Cu(n,2n)^{62}Cu$.

The effect of different moderator designs on the yield of neutrons with energy below 0.41 eV was determined. The results indicate that the thermal flux at a predetermined position can be increased by use of scattering materials around the target. Experimental results also indicate that certain arrangements of scattering materials produce more thermal flux at the predetermined position than other arrangements. Of the scattering material arrangements tested optimal results were obtained when using a hydrocarbon scatterer shaped into a paraboloid cavity, the vertex of which was 6.35 cm from the neutron generator target.

CHAPTER I. INTRODUCTION

The industrial demand for fast, accurate nondestructive quality control methods has lead to increased interest in the relatively new fields of activation analysis and neutron radiography. Activation analysis has become an extremely useful tool to industry to detect trace impurities in a product. By irradiating an element with some particle, such as neutrons, one can produce an unstable isotope. Since each isotope produces a characteristic energy spectrum as it decays, the isotope can be identified.[1] By knowing the isotope produced and the reaction used to produce it one can determine what elements are to be found in the sample irradiated. In activation analysis it is sometimes desireable to irradiate the samples with thermal rather than fast neutrons. This is particularly true when trying to detect trace quantities of certain elements. The primary reason being that the capture cross-section of an element for certain reactions are larger for thermal, than for fast neutrons. See Table I[2] for an illustration of the energy dependance of captive cross sections.

---

[1]Heath, R.L., Scintillation Spectrometry Gamma-Ray Spectrum Catalogue (2nd Ed.), TID-4500, IDO-16880-2, August, 1964.

[2]Templin, L.J., ed., Reactor Physics Constants, U.S. Atomic Energy Commission Division of Technical Information, ANL-5800 (2nd Ed.), 1963 pp. 37-40.

Element	(0.01 MeV)	(1 MeV)
Na^{23}	4 mb	0.1 mb
Nb^{93}	0.7 b	0.03 b
Zr^{90}	0.05 b	0.006 b
Mo	0.7 b	0.02 b
Ta^{181}	2.0 b	0.05 b
Th^{232}	1.0 b	0.1 b
U^{238}	0.6 b	0.1 b
Bi^{209}	3.0 b	2.0 b
Pu^{239}	1.2 b	0.1 b

Table I.

Illustration of Dependance of Capture
Cross Sections on Energies
(n,γ) Reaction

Another reason for desiring thermal neutrons rather than fast neutrons would be to prevent a certain reaction from taking place. This may be done since certain reactions will not occur if the bombarding neutron is below a certain energy called the threshold energy. Table II gives an illustrative listing of the threshold energy for neutron reactions with different elements and some of their isotopes. For a complete listing one may refer to Thresholds of Neutron Induced Reactions by R.J. Howerton, et al.[3]

---

[3]Howerton, R.J.,et al., Thresholds of Neutron-Induced Reactions (May, 1964), TID-21627.

Element	(n,p) Thresholds
$_{3}Li^{6}$	3.19
$_{6}C^{12}$	13.63
$_{11}Na^{23}$	3.76
$_{29}Cu^{63}$	0.0
$_{9}F^{19}$	4.24
$_{13}Al^{27}$	1.90
$_{30}Zn^{64}$	0.0
$_{55}Cs^{123}$	0.0
$_{49}In^{115}$	0.68
$_{48}Cd^{114}$	3.85

Table II.

Illustrative Listing of (n,p)
Thresholds for Different Elements

Neutron radiography has become a useful complement to x-ray and gamma-ray techniques in quality control testing. The x-ray and gamma-ray have the characteristic of being able to penetrate large thicknesses of light elements such as hydrogen and carbon, but not large thicknesses of heavy elements such as iron and lead. On the other hand, the neutron will penetrate deep into the heavy elements, but will be stopped by relatively light elements such as hydrogen and carbon. Utilizing this characteristic of neutrons it is possible to obtain radiographs of light element material encased in heavy element materials without destroying the casing.

These radiographs are obtained by either a direct or a transfer method.[4] In the direct method, a beam of thermal neutrons which has been collimated strikes the specimen and then falls on a screen (See Figure 1). The screen is made radioactive by the striking thermal neutrons. If the screen is made of material such as lithium or boron, alpha particles will be emitted. The nuclear reactions are

$$(1)\quad {}^{6}Li + n \rightarrow {}^{4}\alpha + {}^{3}H$$

$$(2)\quad {}^{10}B + n \rightarrow {}^{4}\alpha + {}^{7}Li$$

These emitted alpha particles are used to excite a fluorescent screen, such as ZnS(Ag), and the light produced exposes the film located between the screens.

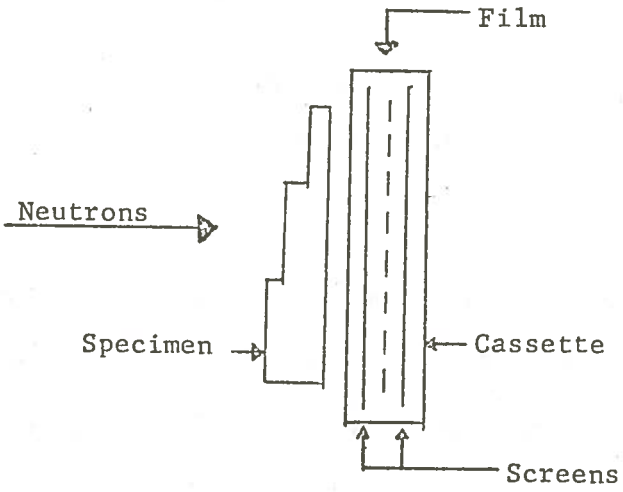

Figure 1.
Direct Neutron Radiography

---

[4]Iddings, F.A., "Utilization of a Low Voltage Accelerator for Neutron Radiography," 7th Symposium on Nondestructive Evaluation of Components and Materials in Aerospace, Weapons Systems and Nuclear Applications (April, 1969), pp. 364-5.

In the transfer method the collimated beam of thermal neutrons also strikes the specimen as before. This time only a screen is behind the specimen (See Figure 2). This irradiated screen is then removed, placed in a cassette, and contacted with the film.

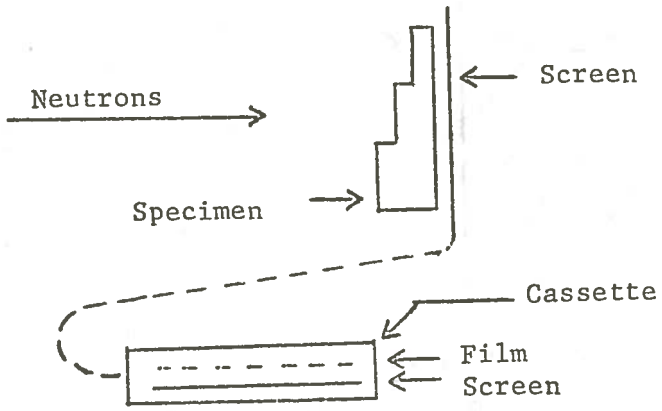

Figure 2
Diagram of Transfer Neutron Radiography

Regardless of the method employed to expose the film, sharp imaging of the specimen is obtained only when the beam of thermal neutrons is well collimated. The collimation of the beam results in a large loss of the total thermal neutrons produced because those thermal neutrons which are not parallel with the line between the specimen and the target must be screened out (See Figure 3).

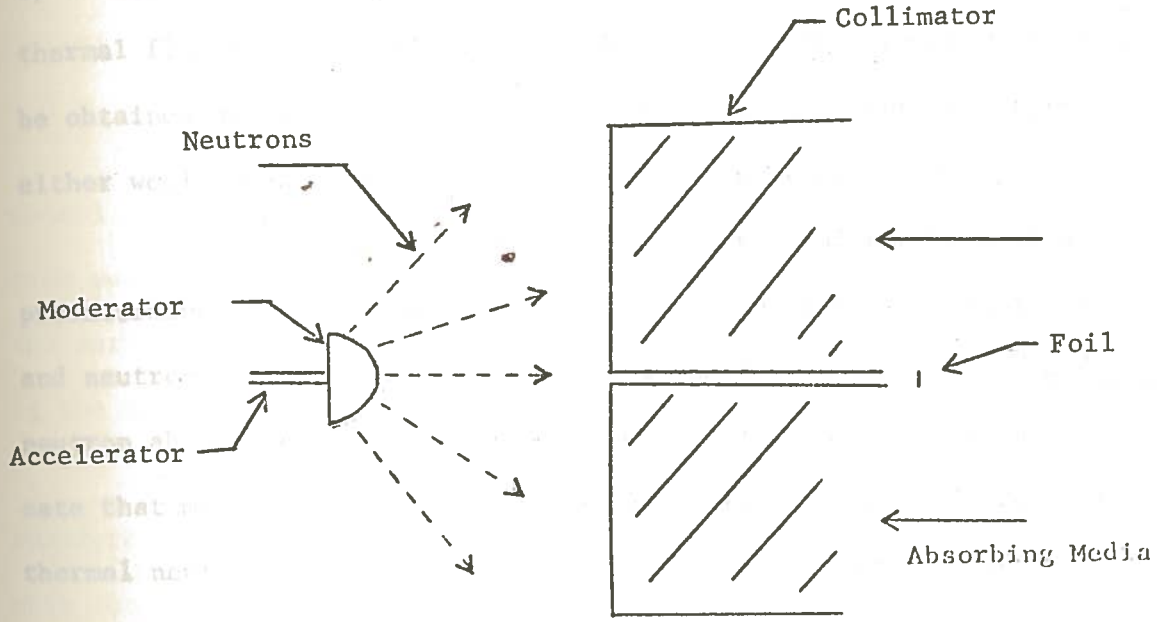

Figure 3

Loss of Thermal Neutrons after Uniform Moderation Due to Collimation

A 150 KV neutron generator running at four milliamperes will produce approximately 3.1×10^{11} fast neutrons/(sec-cm^2) when using a five curie tritium target and deuterium gas.[5] Using prior moderating designs thermal fluxes after moderation have been of the order of 1×10^{9} neutrons/(sec-cm^2) and 1×10^{6} neutrons/(sec-cm^2) after satisfactory collimation at the object position.[6] With a thermal flux of

---

[5]Iddings, Ibid., p. 364.

[6]Private communication with Dr. F. A. Iddings.

this magnitude satisfactory images may be obtained using exposures of up to ten minutes with fast screens.[7] If one could obtain larger thermal fluxes after collimation either better image resolution could be obtained or shorter irradiation time used.[8] An improvement in either would open up new industrial uses of neutron radiography.

As noted above an increase in the thermal neutrons at a predetermined position would be a benefit to both activation analysis and neutron radiography. The preferred scattering directions[9] and neutron absorption characteristics[10] which all isotopes possess indicate that moderator design might be successfully used to increase the thermal neutron flux at a predetermined position. Dr. D.C. Cutforth has published an article dealing with moderator designs when using an isotopic source.[11] However, no published work has been done with moderator designs when using a neutron generator. Dr. Cutforth has indicated he has done some work in this area, but nothing has been published.[12] The current lack of information in moderator designs for neutron generators and the potential importance of successful designs produces a fertile field of research.

---

[7] Ibid.

[8] Chernick, B.E., "Neutron Radiography-Utilization of Neutrons From A Cockcroft-Walton Accelerator," Thesis, Louisiana State University (1966).

[9] Goldberg, M.D., V.M. May, and J.R. Stein, "Angular Distribution in Neutron-Induced Reactions," BNL-400 (2nd Ed.), October, 1962.

[10] Ibid.

[11] Cutforth, D.C., "On Optimizing an Sb-Be Source for Neutron Radiographic Application," Materials Evaluation, Vol. XXVI, No. 4 (Dec., 1968), p. 49.

[12] Private Communication with Dr. D.C. Cutforth, Argonne National Laboratories, Idaho Falls, Idaho.

CHAPTER II

THEORY OF NEUTRON MODERATION AS APPLIED TO A LOW VOLTAGE NEUTRON ACCELERATOR

This chapter shall examine both a mathematical and an experimental approach. In the first, consideration is given to what information must be known, what assumptions must be made, the reliability of the mathematical model to similar physical problems, and the applicability of the mathematical model to the present physical problem.

In the experimental approach flux distribution from an unmoderated target, angle of scatter, and energy loss are discussed with the purpose of constructing physical models.

A. Mathematical Techniques for Describing The Neutron Flux Distributions

Any discussion of neutron moderation requires inquiries into neutron velocity (or energy), neutron direction, mass of moderating media, as well as the time relation with the above.

Many texts may be found describing this flight.[13] The final equation derived is referred to as the Boltzmann Transport Equation.

Consider the following diagram:

---

[13]Isbin, H.S., Introductory Nuclear Reactor Theory, Reinhold Publishing Corp., New York (1963), pp. 326-329.

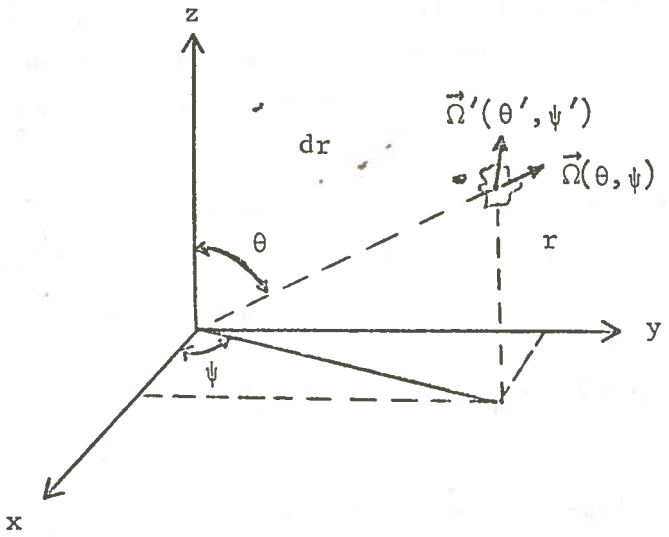

Figure 4

Vector Parameters Used to Specify
Neutron Distribution

It is seen that the following neutron balance may be written:

I [Number of neutrons moving in direction $\vec{\Omega}(\theta,\Psi)$ with speed $d\nu$ about ν which appear per unit time from sources in dr.]

+

II [Number of neutrons moving in direction $\vec{\Omega}(\theta,\Psi)$ with speed $d\nu$ about ν in dr gained per unit time from scattering collisions which scatter the neutron from all directions $\vec{\Omega}'(\theta',\Psi')$ to $\vec{\Omega}(\theta,\Psi)$.]

-

III [Net number of neutrons moving in direction $\vec{\Omega}(\theta,\Psi)$ with speed $d\nu$ about ν that are lost per unit time by leakage through the boundaries of dr.]

-

IV [Number of neutrons moving in direction $\vec{\Omega}(\theta,\gamma)$ with speed $d\nu$ about ν which are removed per unit time from $d\nu$ by absorption collisions]

V [Number of neutrons moving in direction $\vec{\Omega}(\theta,\gamma)$ with speed $d\nu$ about ν which are removed per unit time from $d\nu$ by being scattered into a new direction]

=

VI [Change per unit time in net number of neutrons moving in direction $\vec{\Omega}(\theta,\gamma)$ with speed $d\nu$ about ν in $d\nu$.]

Expressed mathematically, this becomes

$$S(r,\nu,\vec{\Omega},t) + \int_{\nu',\Omega'} \phi(r,\nu',\vec{\Omega}',t)\Sigma_s(\nu')f(\nu,\vec{\Omega};\nu',\vec{\Omega}')d\nu'd\Omega'$$

$$- \vec{\Omega}\cdot\nabla\phi(r,\nu,\vec{\Omega},t) - \Sigma_a(\nu)\phi(r,\nu,\vec{\Omega},t) - \Sigma_s(\nu)\phi(r,\nu,\vec{\Omega},t)$$

$$= \frac{1}{\nu}\frac{\partial}{\partial t}\phi(r,\nu,\vec{\Omega},t)$$

where

$r \equiv$ position of the neutron

$\nu \equiv$ velocity of neutron

$\vec{\Omega} \equiv$ initial direction of the neutron

$t \equiv$ time

$\phi \equiv$ neutron flux

$\Sigma_s \equiv$ scattering cross-section

$f \equiv$ distribution function

$\Sigma_a \equiv$ absorption cross-section

$S \equiv$ source term

By rearranging the above equation the standard form of the Boltzmann Transport Equation is obtained by assuming $\phi(r,\nu,\vec{\Omega},t)$ is time independent

$$\Sigma_t(\nu)\phi(r,\nu,\vec{\Omega},t) + \vec{\Omega}\cdot\nabla\phi(r,\nu,\vec{\Omega},t) =$$

$$S(r,\nu,\vec{\Omega},t) + \int_{\nu',\vec{\Omega}'} \phi(r,\nu',\vec{\Omega}',t)\Sigma_s(\nu')f(\nu',\vec{\Omega}';\nu,\vec{\Omega}')dr'd\vec{\Omega}'$$

where

$$\Sigma_t \equiv \Sigma_a + \Sigma_s$$

The solution of this equation in terms of $\phi(r,\nu,\vec{\Omega},t)$ would yield the number of neutrons with a given velocity (i.e., energy) at a certain position, r, at time t; provided, the correct constants could be substituted into the solution.

The three most common mathematical techniques to solve the Boltzmann Transport Equation are the "straight-ahead" approach, method of moments, and the Monte Carlo method.

The least desirable of the three techniques is the "straight-ahead" approach. The calculation time, even with computers, is prohibitive.[14] Even if the available codes[15] are used the theoretical prediction will not be the same as the experimental results. The best would be a deviation of about 20 per cent.[16]

---

[14]Fitzgerald, J.J., G.L. Brownell, and F.J. Mahoney, Mathematical Theory of Radiation Dosimetry, Gorden and Breach Science Publishers, New York (1967), pp. 476-477.

[15]Heller, J. and H. Heller, Physics Review, 93:93A (1954).

[16]Goldstein, H., Fundamental Aspects of Reactor Shielding, Addison-Wesley, Reading, Mass. (1959).

The prohibitive solution time of the "straight-ahead" approach led to the development of the moments method. This semi-numerical technique utilized Le Gendre approximations and transform functions. The advantage over the former being that the integro-differential three variable equation is replaced by a denumerably infinite system of Volterra integral equations.[17] These equations may be expressed by

$$\Sigma_t(E)M_{nl}(E) = \sum_i \sum_\alpha n^{(i)} \int_E^\infty dE' \sigma_e^{(i,\alpha)}(E' \to E) M_{nl}(E') +$$

$$\frac{1}{2l+1}\left[(l+1)M_{n-1,l+1}(E) + lM_{n-1,l-1}(E)\right] +$$

$$S(E)\delta_{no}\delta_{lo}$$

where

$$M_{nl}(E) = \frac{1}{2(n!)}\left[\int_{-\infty}^{+\infty} Z^n \, 2\pi \int_{-1}^{+1} P_l(\omega)N(Z,\omega,E)d\omega\right] dz$$

$$\sigma_l^{(i,\alpha)}(E' \to E) = 2\pi \int_{-1}^{+1} d\mu_o P_l \mu_{op}^{(i,\alpha)}(E' \to E)$$

$$\mu_o \equiv \vec{\Omega}' \cdot \vec{\Omega}.$$

Here $M_{nl}(E)$ is the integral transform. Now to find the neutron distribution, it is necessary to "invert" the transformation by using

---

[17] Krumbein, A.D., and B.D. O'Reilly, "Transport Method," Engineering Compendium on Radiation Shielding, Vol. I, Springer-Verlag, New York (1968), p. 131.

$$\frac{1}{2(n!)} \int_{-\infty}^{+\infty} Z^n dz\, N(E,Z,\omega) = \sum_{l=0}^{\infty} \frac{2l+1}{4\pi} M_{nl}(E) P_l(\omega).^{18}$$

Since it is the number density which is sought, $l = 0$. This leads to

$$M_{no}(E) = \frac{4\pi}{1} \cdot \frac{1}{2(n!)} \int_{-\infty}^{+\infty} Z^n dz\, N(E,Z,\omega)$$

$$= \frac{2\pi}{n!} \int_{-\infty}^{+\infty} Z^n\, dz \left[\frac{1}{4\pi} N_o(Z,E)\right]$$

$$= \frac{1}{2(n!)} \int_{-\infty}^{+\infty} Z^n dz\, N_o(Z,E)$$

Approximations for $N_o(Z,E)$ lead to a solution for $M_{no}(E)$. One approximation used is the Spencer Function Fitting Method.[19] This method assumes $N_o(Z,E)$ can be approximated by the function

$$N_o(Z,E) \approx \sum_{i=1}^{I+1} \frac{A_i}{\sqrt{B_i}} f\left(\frac{Z}{\sqrt{B_i}}\right).$$

The difficulty lies in selecting the suitable function for $f\left(\frac{Z}{\sqrt{B_i}}\right)$. The selections made to this time have not yielded results corresponding to the experimental data when measuring close to the source.[20] In more recent studies by O'Reilly and Lewis[21] functions of the form

---

[18] Ibid., p. 132.

[19] Spenser, L.V., "Penetration and Diffusion of X-Rays", Mathematical Techniques, NBS Report 1442 (March 1952).

[20] Ibid., p. 134.

[21] Ibid.

$f(Z) = Z^2 e^{-a|Z|} + e^{-bZ^2}$; a and b are positive constants

have produced more accurate results in the neighborhood of a source plane surrounded by one media. Even with this improvement the theoretically determined flux oscillates about the experimental flux in the neighborhood $\sim 1\text{cm} \leq Z \leq \sim 5\text{cm}$ from the source.

Because of the failure of the moments method to accurately predict the flux within the region described above its application to the present study would not be desireable. There are other complications that also rule out the use of this method. The neutron generator is not a uniform source of neutrons. The neutron output is a function of the target life. As the target life increases the neutron output decreases. There is also no precise geometrical shape to the target area struck which emits neutrons. Furthermore, there are several different media surrounding the target. Each possesses its own neutron moderating characteristics. The combined effect of these deviations would lead to unpredictable error with the use of the moments method.

The most used mathematical technique to describe the flight of neutrons through different media is the Monte Carlo method.[22] The flight through the media is mathematically simulated. Random numbers are chosen from a distribution describing the molecular interactions. From this the neutron path is determined. Then using cross sectional data, the neutron path history can be recorded.

---

[22]Kahn, H., "Randon Sampling (Monte Carlo) Techniques in Neutron Attenuation Problems," Nucleonics 6, 27 (1950).

The major difficulties with the Monte Carlo method are the need for a great many neutron histories and the need for much nuclear data and cross sections. Of the two, the accuracy of the cross sections results in the greatest error. Biro[23] lists the different neutron cross sections needed to establish a Monte Carlo code:

1. Total cross section, σ_T (E)
2. Cross sections for elastic scattering
   (a) Total cross section, σ_n (E)
   (b) Angular distribution of elastically scattered neutrons σ_n ($E_1\theta$)
3. Cross sections for inelastic scattering
   (a) Total cross section $\sigma_{n'}$ (E)
   (b) Energy distribution of the scattered neutrons $\sigma_{n'}$ (E;E′)
   (c) Energy and angle distribution of the scattered neutrons $\sigma_{n'}$ (E;E′, θ)
4. Cross sections for neutron multiplicative processes
   (a) Fission cross section, σ_f(E), and multiplicity N(E)
   (b) Cross sections for the (n,2n) reaction: σ_{2n}(E), σ_{2n} (E;E′)
5. Cross sections for other neutron-producing reactions, for example, $\sigma_{n',\alpha}$(E) for the $^{12}C(n,n'\alpha)^{8}Be$ reaction.
6. Cross sections for processes in which the neutron disappears
   (a) Radiative capture, σ_γ
   (b) Charged particle reactions, (n,p), (n,d), (n,α), etc.

---

[23]Krumbein and O'Reilly, Ibid., p. 118.

The greatest error is found near the neutron source.[24] Again there is little comparative data between experimental and theoretical results. An examination of the available codes[25,26,27] reveals that all the codes assume an isotropic point source or volume distributed fission or monoenergetic sources. Although in reactor shielding problems these assumptions are valid because the interest is at great distances from the source; on the other hand, neutron fluxes near the source are of interest in this study. For the above reasons this theoretical approach would not be expected to yield accurate results in the physical situation of this study.

B. Unmoderated Neutron Flux Distribution From a Low Voltage Neutron Accelerator Target

In attempting to maximize the thermal (neutrons with energy of 0.41 eV or less) neutron flux at a predetermined position, a first point of interest would be to establish the flux pattern before any moderating material has been placed around the accelerator target.

As used in this study neutrons were produced by the low voltage accelerator when deuterium that has been fed into a vacuum is

---

[24] Ibid., p. 112.

[25] Guber, W., and M. Shapiro, "A Description of the SANE and SAGE Programs," UNUCOR-633, United Nuclear Corp., 1963.

[26] Eisenman, B., and E. Hennessy, "ADONIS-An IBM 7090 Monte Carlo Shielding Code," UNUCOR-635, United Nuclear Corp., 1963.

[27] Eisenman, B., and F.R. Nakache, "UNC-SAM, A Fortran Monte Carlo System for the Evaluation of Neutron or Gamma-Ray Transport in 3-Dimensional Geometry," UNC-5093, United Nuclear Corp., 1964.

accelerated by a potential difference (150 KV) into a target. The target may be made of any material that will emit neutrons when struck by the deuterium. In this study tritium embedded in a titanium on a copper sheet was used as the target. The resulting reaction

$$_1H^2 + {}_1H^3 \rightarrow {}_0n^1 + {}_2He^4$$

produces 14.3 MeV neutrons.

In the literature many articles are found dealing with the neutron flux distribution from the target of a low voltage neutron accelerator. B.T. Kenna and F.J. Conrad[28] revealed that within six centimeters of the target the neutron flux is uniform except in directions of the target plane. The neutron distribution in their study was determined by counting activated copper foils placed at predetermined positions around the target.

The findings of Kenna and Conrad have been confirmed by E.B. Andresen.[29] His results are illustrated in Figure 5.

---

[28]Kenna, B.J., and F.J. Conrad, "Fast Neutron Flux Patterns For A 14-MeV Neutron Generator," Health Physics, 12:564-6 (April 1966).

[29]Andresen, E.G., "Angular Distribution of Neutrons From a Phillips Neutron Generator PW-5300," Messtecknik 76:81-3 (April 1968).

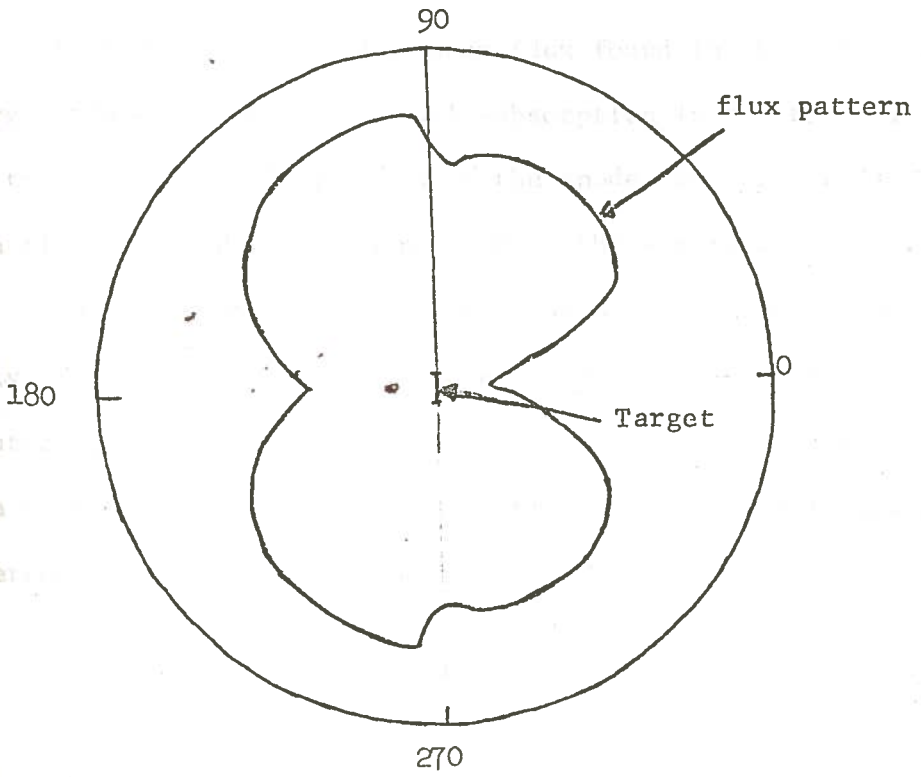

Figure 5

Unmoderated Neutron Flux Distribution
From the Target of a Low Voltage
Neutron Accelerator

Related articles whose conclusions verify those reached above have been written by Chiro Shinomiya and Toshiaki Kishikawa,[30] J. Op. de Beeck,[31] and G. Oldham and D.M. Bibby.[32]

---

[30]Shinomiya, C., and T. Kishikawa, "Geometry Calculations and Flux Measurements for Fast Neutron Irradiations with an Accelerator," Kumamoto Daigaku Kogukubu Kenkya Hokoku, Kumamoto Univ., Japan, Vol. 16: No. 3, pp. 68-74.

[31]Op de Beeck, J., "Neutron Flux Distribution Around Disk-Shaped Source of Accelerator-type Neutron Generators," Journal of Radioanalytical Chemistry 1:313-23 (July 1968).

[32]Oldham, G., and D.M. Bibby, "Neutron Flux Distributions Around the Target of a 14-MeV Neutron Generator," Nuclear Energy, 167-9 (Nov. - Dec. 1968).

Andresen explains the lower flux found in the directions in the target plane as a result of self-absorption in the target. He also states that the high voltage lead at the anode side also reduces the neutron flux recorded in the direction of the accelerator tube.[33]

The above articles indicate that although the target may randomly emit neutrons and that there is no preferred direction for the neutrons, the physical structure of the low voltage accelerator is such that preferred directions are created. This fact must be considered when designing moderator systems.

---

[33]Andresen, Ibid., p. 81-3.

CHAPTER III

EXPERIMENTAL TECHNIQUES FOR DETERMINATION OF NEUTRON FLUX DISTRIBUTION

Three series of experiments were conducted in this study. Series I was designed to gather information on the neutron flux pattern obtained when no moderator was placed around the accelerator target assembly. Several experiments were also included within this series to examine the change in the neutron flux pattern when a polyethylene hemispherical moderator is placed around the accelerator target assembly. Both of the objectives described above were limited to neutrons with energy above 10.0 MeV (when copper foils were used) or 0.41 eV (when indium foils were used). In Series II similar experiments were run, except only neutrons with energies below 0.41 eV were considered. Finally in Series III experiments were designed to study the effect of various moderator designs on the neutron flux pattern. Comparisons are then made between the five basic designs tested.

Several technique problems common to experiments in each of the series were present. High background activity at the scintillation crystal, neutron scatter from the surroundings, and uniformity of foils are examples of problems common to each of the series. Several experiments presented problems unique to that experiment. The problem of self-absorption within the indium foils, large statistical errors possibly due to low activation of the foils, and

normalization of the data because of long time delays before the copper foils were counted were some of the special problems encountered.

This chapter shall then concern itself with a general discussion of the experimental procedure and, secondly, to the common and special problems encountered.

A. General Procedure for Determination of Neutron Flux Patterns From the Target of a Low Voltage Accelerator

A selection is made as to the foil composition, size, and positioning about the target. The interdependence of the conditions on one another and the effects of the selection is discussed in greater detail in later sections of this paper. At this point it is sufficient to say experiments were run using copper, indium, and teflon foils. These foils were then placed at pre-determined distances from the accelerator target. Distances of one, two, and three feet were selected depending on the experiment.

The foils were attached by tape to a wooden rod supported by a wooden arc suspended from the ceiling of the experiment room by nylon cord (See photograph 1). The wooden rods were connected to the arc by adjustable clamps. This allowed the rods to be positioned so that the foil taped on the end could be placed where desired. Finally, the arc and rod were marked in order that the position of foil could be determined.

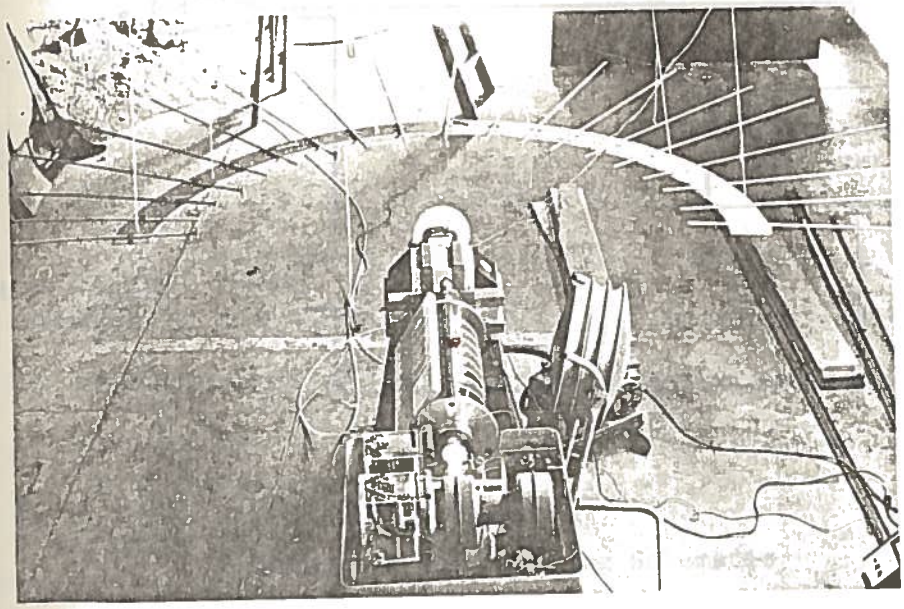

Photograph 1.
Foil Placement and Support System

Once the foils have been positioned stable accelerator operating conditions are obtained. When these have been obtained the high voltage is adjusted to approximately 150 KV during operation. After the accelerator voltage has been turned off the activated foils were retrieved and hand carried to a 3" x 3" NaI(Tl) scintillation crystal located about 100 feet from the accelerator. This process took about two minutes on the average.

The crystal was shielded by 10" of water, 8" of concrete, and 2" of lead in order to prevent activation of the crystal and elimination of background counts. Connected to the crystal was a photomultiplier tube and a multichannel analyzer (See Figure 6).

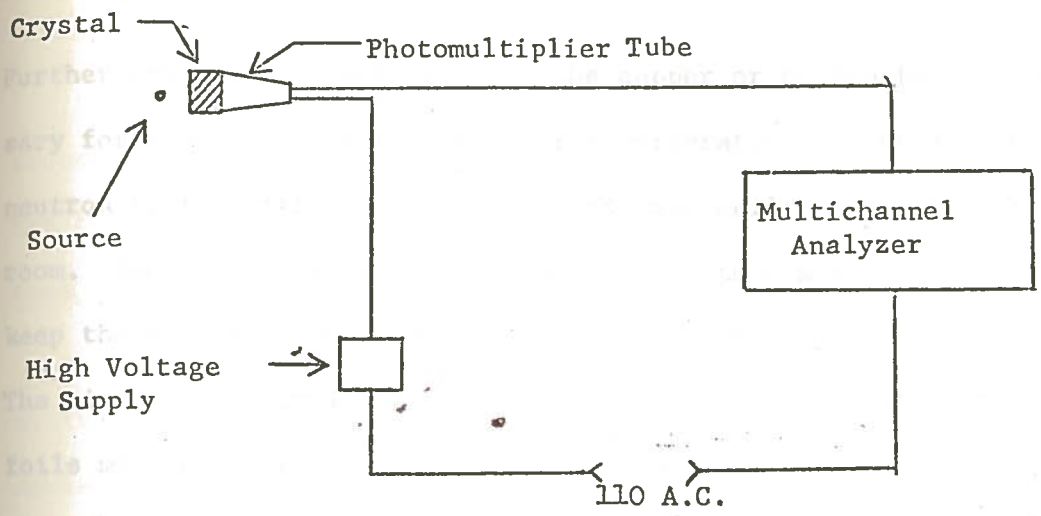

Figure 6
Detection and Counting Schematic

The counts thus obtained were then recorded. When a copper foil was activated the 0.511 MeV photons produced by annihilation were counted. This was also true when the teflon foils were used. However, when indium was the foil the 1.09 and 1.27 MeV gammas produced were counted.

Many important considerations are necessary if the above experimental technique is to yield accurate results. It is important that the deuterium strike the center of the tritium-copper target and that the diameter of the deuterium beam be as small as possible. If the beam is not centered, the neutron distribution from the target will be effected. From geometry considerations the closer the measurements to the target the more critical beam centering becomes. It is also important that the deuterium beam remain constant in intensity.

Furthermore, exact positioning of the copper or teflon foils is necessary for accurate results. Another consideration is the amount of neutron scatter from the walls, floors, and ceilings of the experiment room. One should try to reduce the scatter to a minimum and try to keep the amount constant at all positions where foils will be placed. The time delay from irradiating the foils to counting the activating foils may become critical depending on the foil used. In this connection the background at the NaI(Tl) scintillation crystal is important if it is of the same order of magnitude as the counts received from the activated foil. Each of these are discussed in more detail below.

Subsection A.1. Positioning and Size of the Deuterium Beam on the Accelerator Target

The importance of centering the deuterium beam on the accelerator target is apparent upon a close examination of the target assembly (See Figure 7).

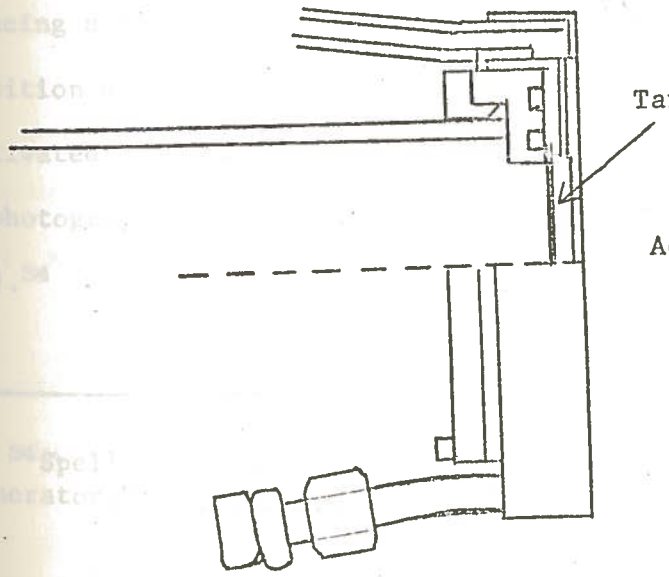

Figure 7
Accelerator Target Assembly

Figure 7

Because of the location of the target within the target assembly there are moderating media behind the target. In particular are the aluminum housing supports, and more important, in regard to fast neutron moderation, is the circulating water behind the target.

If the beam struck the lower part of the target those neutrons produced traveling in an upward direction (small angular deviation from the target plane) would have to pass through a greater distance of moderating media. This would increase the probability of collision, and hence the possibility that the 14.3 MeV neutron will be moderated so that its resultant energy will be below the threshold energy for the foil (10.0 MeV for copper and 11.0 MeV for F^{19}). If this happens the foil will not be activated by this neutron. Therefore, a depression of the flux in certain areas will occur if the beam is not centered. This fact is born out by the experiments run. More detail on this subject will be found in Chapter IV.

The position of the beam on the target was determined by placing a copper foil over the target. The foil was marked so its position on the target could be determined later. The foil was then activated. By placing the activated foil in contact with Polaroid film a photograph can be obtained in a short period of time (See Photograph 2).[34]

---

[34]Spell, W.H., and F.A. Iddings, "Beam Centering in a Neutron Generator," Analytical Chimista Acta, 40 (1968), pp. 515-516.

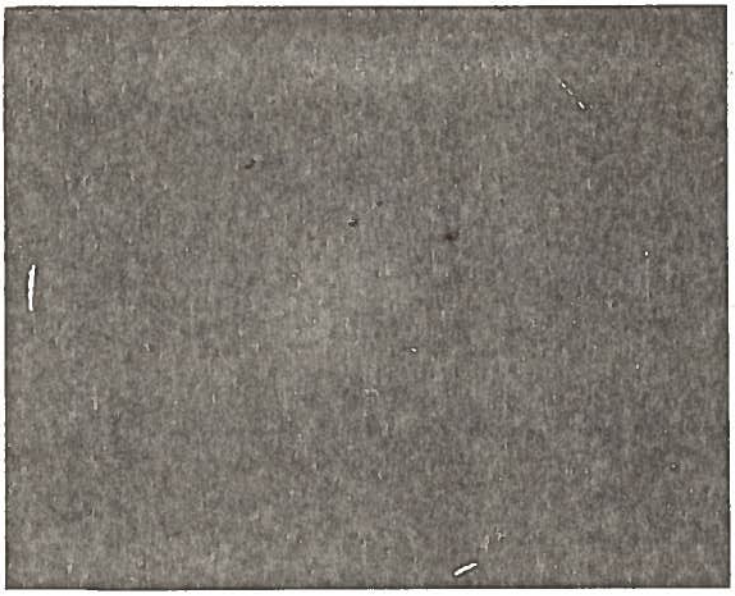

Top of
Target

Photograph 2

Neutron Radiograph of Deuterium Beam Position
(2 minute irradiation, 30 second exposure)

Subsection A.2. Deuterium Beam Size Considerations

In considering the deuterium beam size one must take into account target lifetime and the geometric relationship between the foil and the area struck by the beam.

Generally speaking, the smaller the deuterium beam the shorter the lifetime of the target. Lifetime of the target refers to the length of time the beam may strike the target before the

tritium is depleted. For a given beam size a standard target lifetime graph is given below:[35]

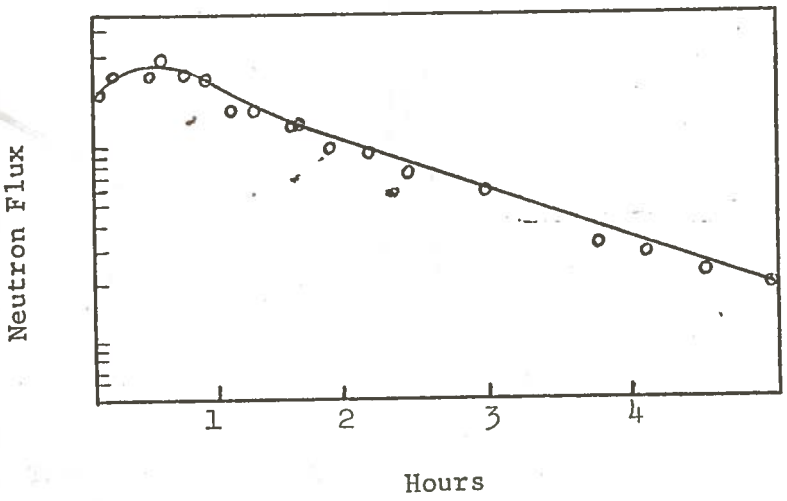

Figure 8
Average Target Lifetime

As the tritium is depleted the total number of neutrons produced decreases. After sufficient beam time the number of neutrons produced will not be great enough to activate the foils if they are positioned two feet away from the target. Therefore one must not decrease the beam to a size that will deplete the target too rapidly.

As to geometry considerations see figure 9.

---

[35]Iddings, F.A., "Utilization of a Low Voltage Accelerator for Neutron Radiography," 7th Symposium on Nondestructive Evaluation of Components and Materials in Aerospace, Weapons Systems and Nuclear Applications (April, 1969), p. 370.

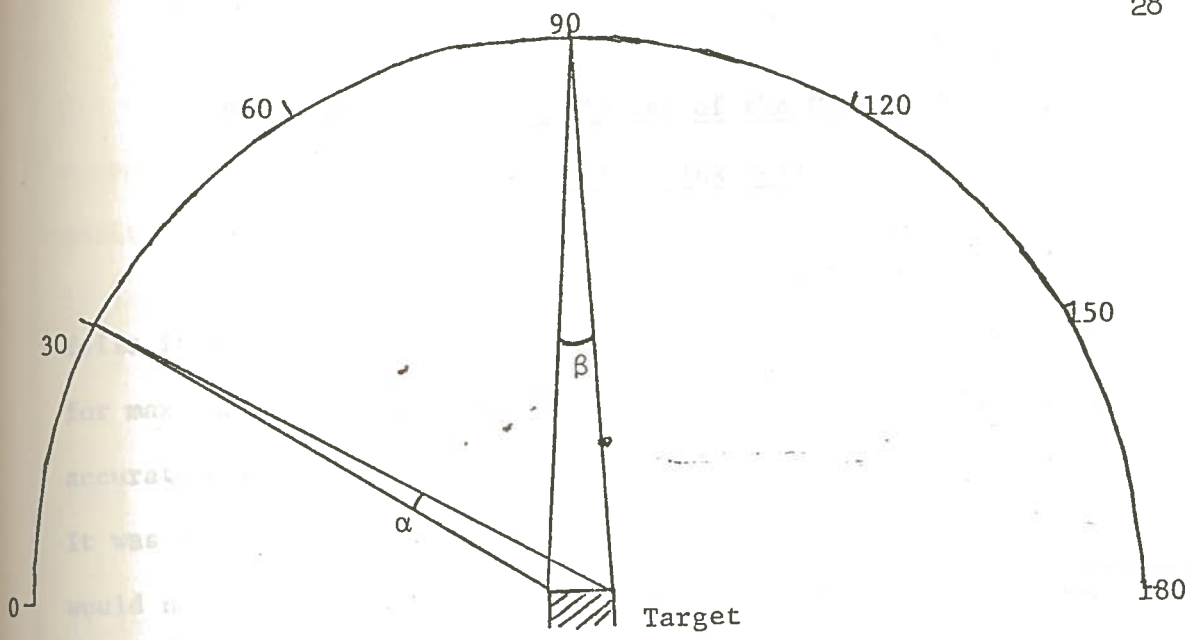

Figure 9
Top View of Geometric Relationship Between the Struck Area of the Target and the Foils

One can see that the larger the beam size (i.e., area of target struck by the deuterium beam) the greater the probability of a neutron striking the foil located at the 90^{o} position. This is made explicitly clear in comparing the angles α and β. Since $\alpha < \beta$ then more neutrons will strike the foil at position 90^{o}.

When one considers that the fast neutron flux at the target cooling jacket is approximately 1×10^{9} neutrons/sec-cm^{2}, even a small difference between α and β may result in a large difference between the fluxes detected at 30^{o} and 90^{o}. This result would be even more pronounced when comparing the fast neutron flux at 0^{o} and 90^{o}.

Subsection A.3. Positioning of the Copper, Indium, or Teflon Flux Foils

In designing and constructing a support assembly for the foils it was necessary to consider an assembly which would allow for maximum flexibility in positioning the foils, yet allow a rapid, accurate means of determining the position in three-dimensional space. It was also necessary to construct the assembly from materials that would not easily become activated from the neutron beam. Another consideration dealt with minimizing neutron scattering from the support assembly.

The assembly consisted of three arc-shaped pieces of wood. When these were rigidly fixed together by metal clamps they formed a semi-circular arc with an inside radius of 42 inches. On the top side of the assembled pieces grooves were cut so they pointed toward the center of the arc. These grooves were 10^{o} apart. Small, triangular-shaped wooden rods were then fastened in the grooves by metal strips screwed into the arc-shaped wooden assembly. These rods were then marked so that the distance from the end of the rod to the center of the arc was known. The metal strips were easily loosened so that the wooden rods could quickly and easily be adjusted closer or further from the imaginary center of the arc. One-half inch quarter round wooden rods were used. This size was chosen because it was the smallest diameter rod that would remain rigid, even on being extended toward the center of the arc at a distance of three feet.

Eye screws were then placed in the arc so that the assembly could be suspended from the ceiling by nylon cord. When suspended from the ceiling by the nylon cord the arc could easily be adjusted so that it lay in a plane perpendicular to the plane of the target and in the same plane as the center of the beam.

The foils were then positioned at the end of the wooden rods with scotch tape and thumb tacks.

A wooden support assembly was chosen over a metal one because of lower cost, easier construction, less total weight, more easily transported, and less activated by the neutron beam. The arc-rod design was chosen so that the large bulk of the assembly would be removed from the foils. Also by using nylon strings for support of the assembly less backscatter and easier mobility was achieved than if permanent metal or wooden frames had been built.

Subsection A.4. Neutron Scattering from the Surroundings

Neutrons with large energies of the order of 12.3 MeV will undergo many scatterings before they are absorbed. The number of scatterings will depend upon the scattering material and can be represented by

$$N = \frac{\ell n \frac{E}{E_o}}{\xi}$$

where

$E \equiv$ final energy before being absorbed

$E_o \equiv$ initial energy of neutrons

$\xi \equiv$ average energy loss per collision

This means that the foils will be activated not only by neutrons traveling directly from the target, but also by neutrons scattered from the floor, walls, and ceiling. It is therefore necessary to know the number of scattered neutrons reaching the foil or at least be assured that a uniform scattered flux exists at each foil position. As the former is hard to detect and not accurately calculated one must try to achieve uniform scatter.

Uniform scatter is most easily achieved by removing the foils from scattering materials. In the experiments run the foils were kept as far from scattering material as possible. The center of the tritium target was thirty-nine inches above a level concrete floor. The accelerator was in a large room in which a concrete block sand wall five feet thick had been built around three sides of the accelerator. The fourth side was an open door which looked onto an empty field. The ceiling was over twenty feet from the floor and made of transite sheets. The accelerator was placed so that the target was nine feet from either side wall, and so that the beam of neutrons produced would be in the direction of the open field (See figure 10).

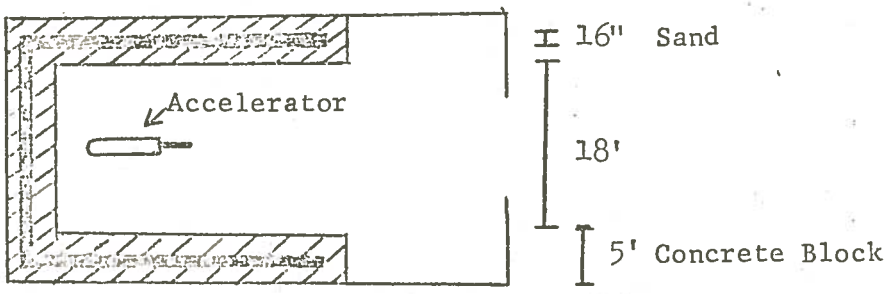

Figure 10

Top View of Experimental Room

All extraneous scattering media were removed during the activation of the foils.

Subsection A.5. Time Delay Considerations

One must not only consider the time that the target was irradiated, but the time delay before counting the foil becomes important depending upon the foil material.

As the foil is being irradiated, it is also decaying. This relationship is expressed by

$$N = C(e^{-\lambda t_1} - e^{-\lambda t_2})$$

where

$N \equiv$ number of neutrons at time of final observation

$C \equiv$ number of neutrons at initial observation

$\lambda \equiv$ decay constant of isotope

$t_1 \equiv$ time delay from end of irradiation to final observation

$t_2 \equiv$ time delay from initial observation to end of irradiation

It is therefore important to know the time of irradiation and the time delay from end of irradiation to beginning of counting. If one counts the activated foil over different lengths of time one must also account for this difference for the same reason as above.

In the experiments run in the first series both copper and teflon foils were used. Copper foils contain both Cu^{63} and Cu^{65}. The possible reactions and the threshold energy for each, when the foil is activated by neutrons, are

Reaction	Threshold	Reaction	Threshold
$Cu^{63}(n,2n)Cu^{62}$	11.01	$Cu^{65}(n,2n)Cu^{64}$	10.06
$Cu^{63}(n,p)Ni^{63}$	0.00	$Cu^{65}(n,p)Ni^{65}$	1.31
$Cu^{63}(n,np)$	6.22	$Cu^{65}(n,np)$	7.56
$Cu^{63}(n,d)$	3.96	$Cu^{65}(n,d)$	5.30
$Cu^{63}(n,t)$	8.36	$Cu^{65}(n,t)$	8.75
$Cu^{63}(n,He^3)Co^{61}$	9.65	$Cu^{65}(n,He^3)Co^{63}$	——
$Cu^{63}(n,He^4)Co^{60}$	0.00	$Cu^{65}(n,He^4)Co^{62}$	0.09
$Cu^{63}(n,nHe^4)$	5.88	$Cu^{65}(n,nHe^4)$	6.85

Since Cu^{63} makes up approximately 70% of the copper, reaction with this isotope will generally dominate the reactions with Cu^{65}. Of particular interest are the reactions of $Cu^{63}(n,2n)Cu^{62}$ and $Cu^{65}(n,2n)Cu^{64}$. Both Cu^{62} and Cu^{64} decay by positron emission. These positrons lose energy generally by elastic collisions and are annihilated by the electrons; the result being two emitted photons, each with energy of 0.511 MeV. Therefore if one detects the 0.511 MeV photons with a NaI(Tl) scintillation counter, he gets indistinguishable counts from both reactions. However, within 10-20 minutes from the end of activation a vast majority of the counts will be from the $Cu^{63}(n,2n)Cu^{62}$ reaction. This results from the fact (1) that there is more than twice as much Cu^{63} as there is Cu^{65} in a copper foil, and (2) the total absorption cross section of Cu^{63} is twice as great as that of

Cu^{65} (i.e., 4.5 barns versus 2.2 barns). However, for a longer elapsed time before counting, the greater the per cent of the total counts come from the $Cu^{65}(n,2n)Cu^{64}$ reaction. This is explained by examining the half-lifes of Cu^{62} and Cu^{64}. Cu^{62} has a half-life of 9.9 minutes and Cu^{64} is 12.9 hours. Thus in only 20 minutes the counts from Cu^{62} have decreased approximately 75% while those of Cu^{64} have decreased very little.

The importance of being able to distinguish between Cu^{62} and Cu^{64} decay is in analyzing the data and comparing experiments in a series. This will be discussed in more detail in Chapter V.

When using teflon foils one is interested in the

$$F^{19}(n,2n)F^{18}$$

reaction. Since fluorine has only one stable isotope (i.e., F^{19}) one does not have the problem discussed above. However, the smaller activation cross section of F^{19} (i.e., 0.09 barns) means one will get fewer counts from F^{18} than from Cu^{62} if both are activated with the same total flux. This is not much of a disadvantage because of the large fast neutron flux from the accelerator (1×10^9 n/sec-cm^2). The $F^{19}(n,2n)F^{18}$ reaction is also excellent since the threshold energy is high, 10.99 MeV. Another desireable characteristic of this reaction is the 110 minute half-life of F^{18}. Again the photons are counted. Therefore the teflon foils will be activated primarily by unscattered neutrons from the target. This reduces the error due to non-uniform

neutron scattering which would also activate the foil if the threshold was lower. Dr. Edgar L. Steele reports that the primary disadvantage to using teflon strips is the non-uniformity of F^{19} content within teflon strips. He stated that the content will vary significantly from batch to batch of the same manufacturer.[36] All teflon foils used in this research came from the same sheet.

Subsection A.6. Background Count Considerations

If the NaI(Tl) scintillation crystal is not well shielded from the neutrons produced from the accelerator, it too may be activated. In particular the sodium might be activated by the following reactions.

$$^{23}Na(n,\gamma)^{24}Na$$

$$^{23}Na(n,\alpha)^{20}F$$

$$^{23}Na(n,p)^{20}Ne$$

$$^{23}Na(n,2n)^{22}Na$$

All the nuclides decay by modes producing counts in the 0.51 MeV single channel analyzer window. Therefore an activated crystal would add counts to those being detected from the foils.

This problem was encountered in some of the earlier experiments run which will be discussed in more detail in Chapter V. However the $Na^{23}(n,2n)Na^{22}$ reaction has a threshold of 12.98 MeV. Therefore by shielding the crystal with lead, concrete blocks, water, etc. one

---

[36]Steele, E.L., Private Communication on September 9, 1969.

may reduce the neutron activation of the crystal, particularly in the case of the high energy threshold reactions.

B. Determination of Slow (< 0.041 eV) Neutrons About the Target of a Low Voltage Accelerator

As before, the accelerator is allowed to "warm up", the foils are placed on the rods, and then the deuterium beam is turned on to produce the fast neutrons. The primary differences in this series of experiments was the use of a different foil technique.

Since F^{19} and Cu^{63} have a threshold of 10.99 MeV and 11.01 MeV respectively, for a (n,2n) reaction, foils of the materials would not be activated by a 0.041 eV neutron. It is therefore necessary to choose an element whose threshold energy for a particular reaction is less than 0.041 eV, but it is also necessary to be able to discriminate from neutrons with energy greater than 0.041 eV. The foil technique most commonly employed is a cadmium and indium combination (See figure 11).

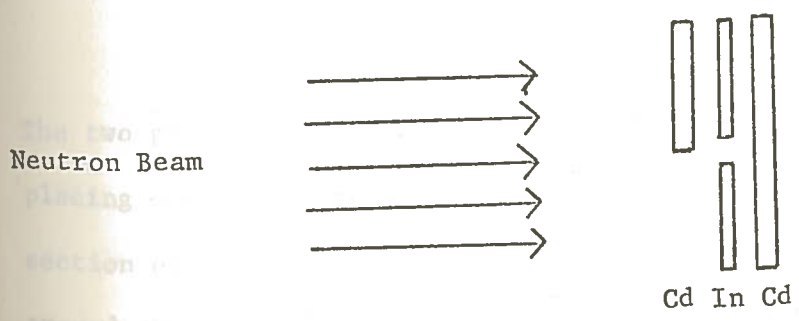

Figure 11
Foil Arrangement for Detecting Thermal Neutrons

The In^{115} is activated by the thermal neutrons in the following reaction.

$$In^{115}(n,\gamma)In^{116m}$$

The isotope In^{116m} then decays by

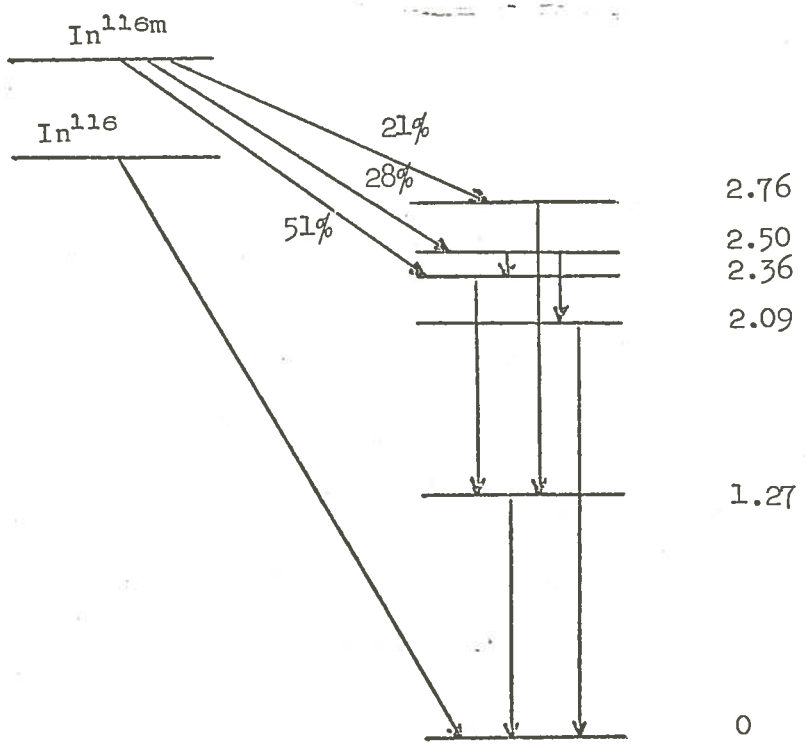

The two principal γ's, 1.09 and 1.27 MeV, are counted. Now by placing a cadmium foil, which has a thermal neutron absorption cross section of 2250-10,000 barns depending on energy of the neutron, around the In foil only neutrons above 0.0411 eV will be able to activate the indium foil. The exposed foil will be activated by the fast and thermal neutrons. One may therefore obtain the number of

neutrons with energy less than 0.041 eV by subtracting the counts obtained from the In foil covered with Cd from the counts obtained from the uncovered In foil.

One problem with using indium foils is the high self-absorption of the released γ rays. Although there are formuli derived to correct this problem

$$f_s = \frac{1}{\mu s}(1 - e^{-\mu s})$$

where

$f_s \equiv$ self-absorption factor

$\mu \equiv$ mass absorption coefficient

$s \equiv$ source thickness

the problem is most easily solved by using foils of uniform thickness. Experiments were run to measure the amount of self-absorption in the indium foils. This is discussed in greater detail in Chapter V.

C. Maximization of Thermal Neutron Flux at a Predetermined Position

The indium foil is placed at the predetermined position. For this series of experiments the foil was placed two feet from the center of the target in the direction normal to the plane of the target. Next a fast flux monitor foil is placed on the target. The target is then irradiated after the moderator is placed around the target.

Three basic moderator designs were employed: (1) slabs, (2) hemispheres, and (3) paraboloids.

Subsection C.1. Paraffin Slabs as Moderators

Household paraffin manufactured by Texaco, Inc. was used in the slab moderator system. These slabs measured 2.5" x 5" x .625". Individual slabs were centered about the target as seen below.

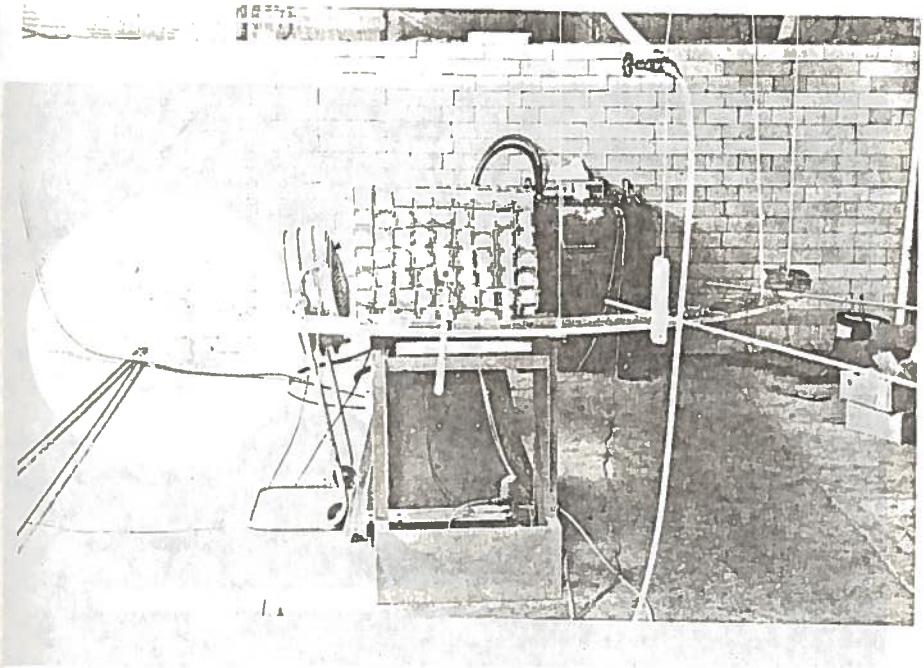

Photograph 3
Slab Moderator System

The first experiment was conducted with only one slab. The number of slabs was increased until a maximum thermal flux as indicated by the number of flux foil counts was obtained.

Subsection C.2. Polyethylene Hemispherical Moderators

Four polyethylene hemispherical moderators were precision carved to have wall thicknesses of 1, 2, 4, and 6 cms. All of the hemispheres had the same internal hollow volume formed by the radius of the target cooling jacket.

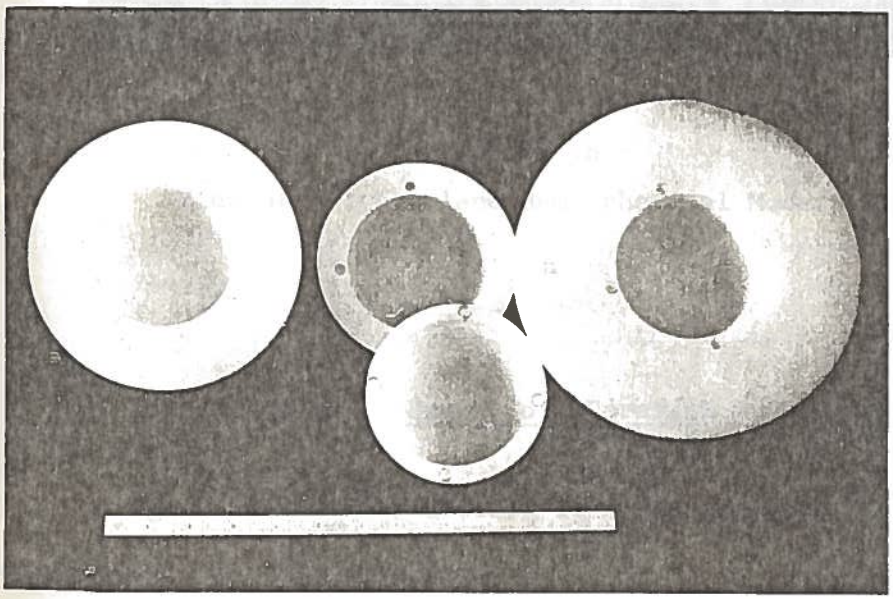

Photograph 4a

Front View of Polyethylene Hemispherical Moderators

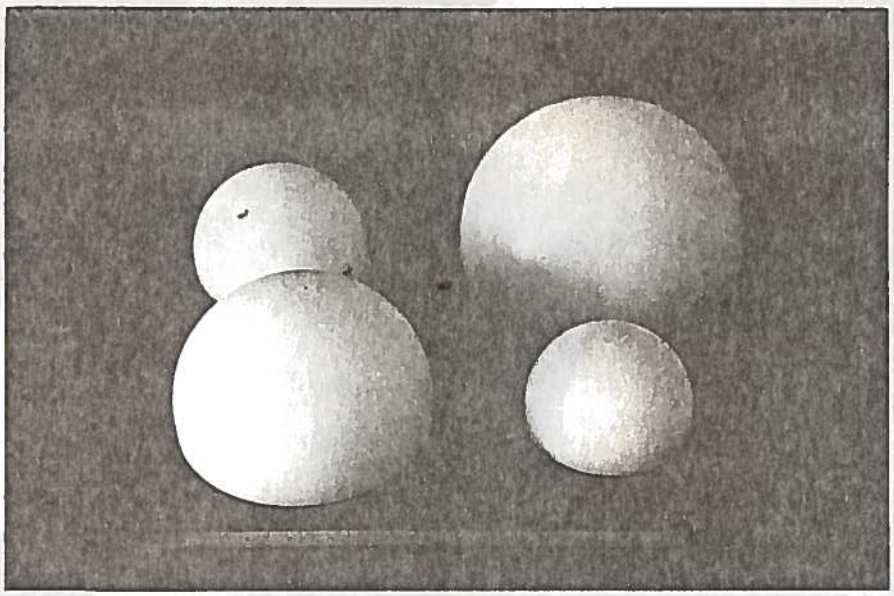

Photograph 4b
View of Polyethylene Hemispherical Moderators

Subsection C.3. Paraboloid Paraffin Moderators

Again the thermal neutron flux was measured at the same predetermined position as before.

The paraboloid-shaped moderator was constructed from a pre-molded "doughnut-shaped" paraffin block and a combination of the paraffin slabs. This combination was varied in order to determine the paraboloid shape that gave the maximum thermal flux at the position two feet from the target. Examples of this combination are shown in Figure 12.

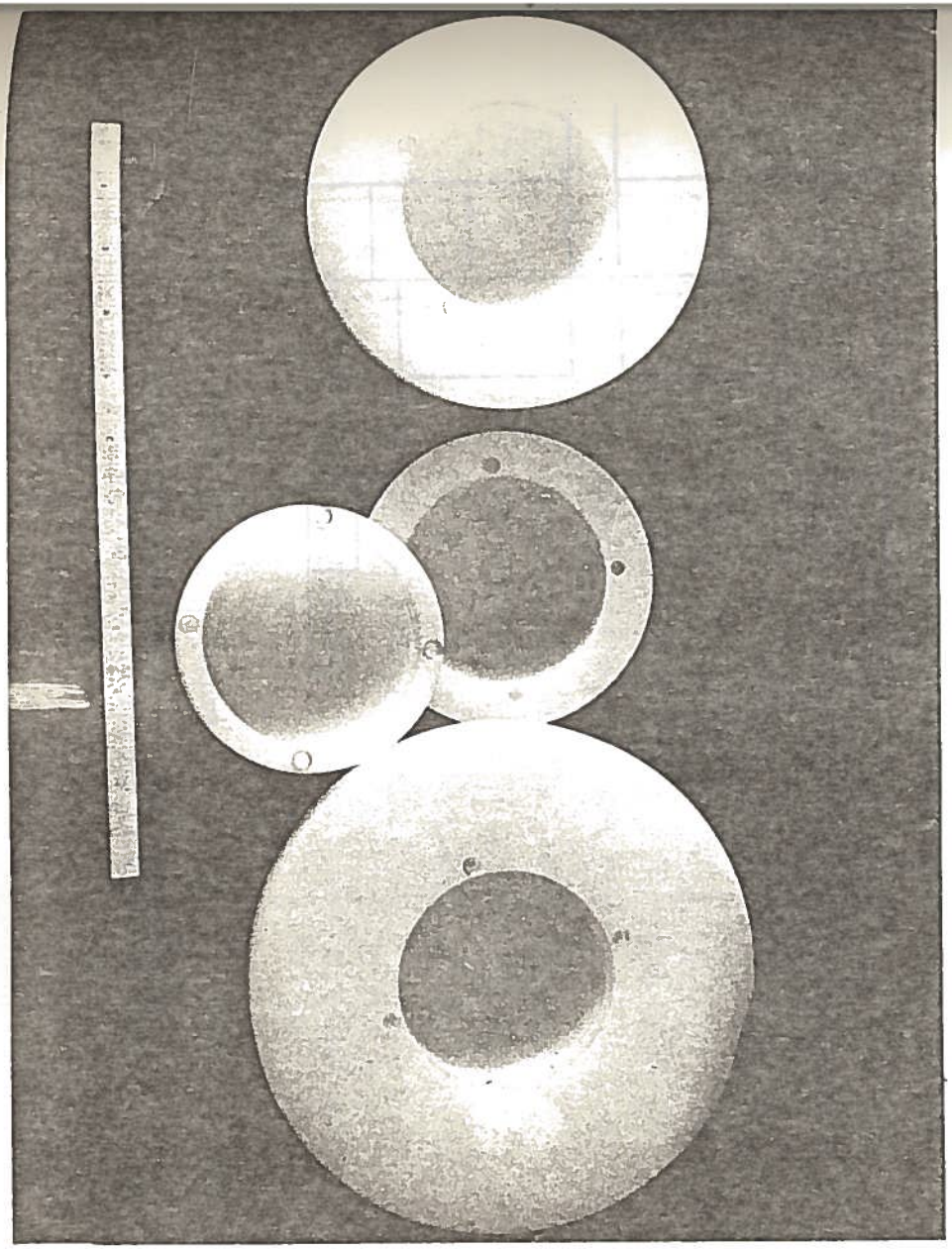

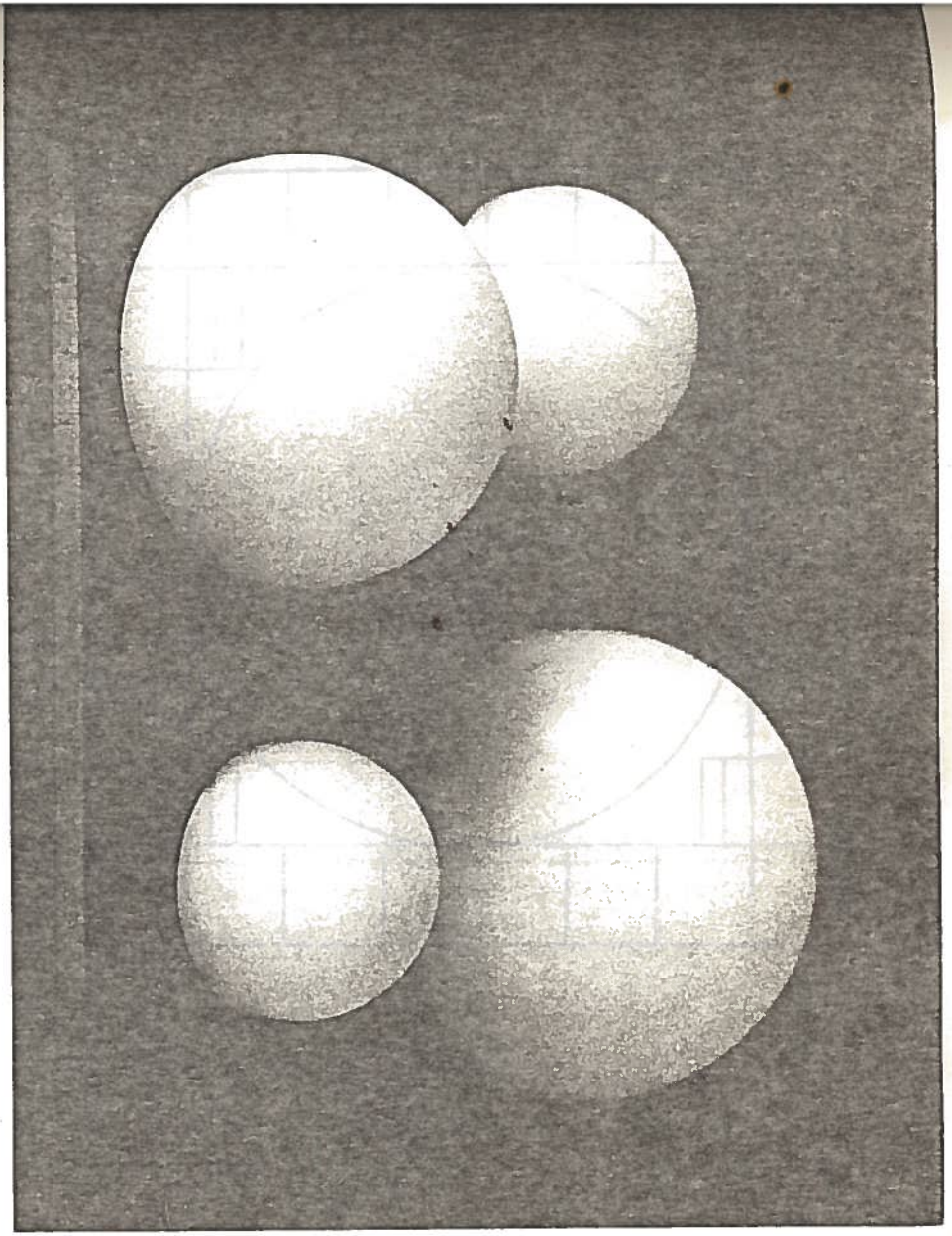

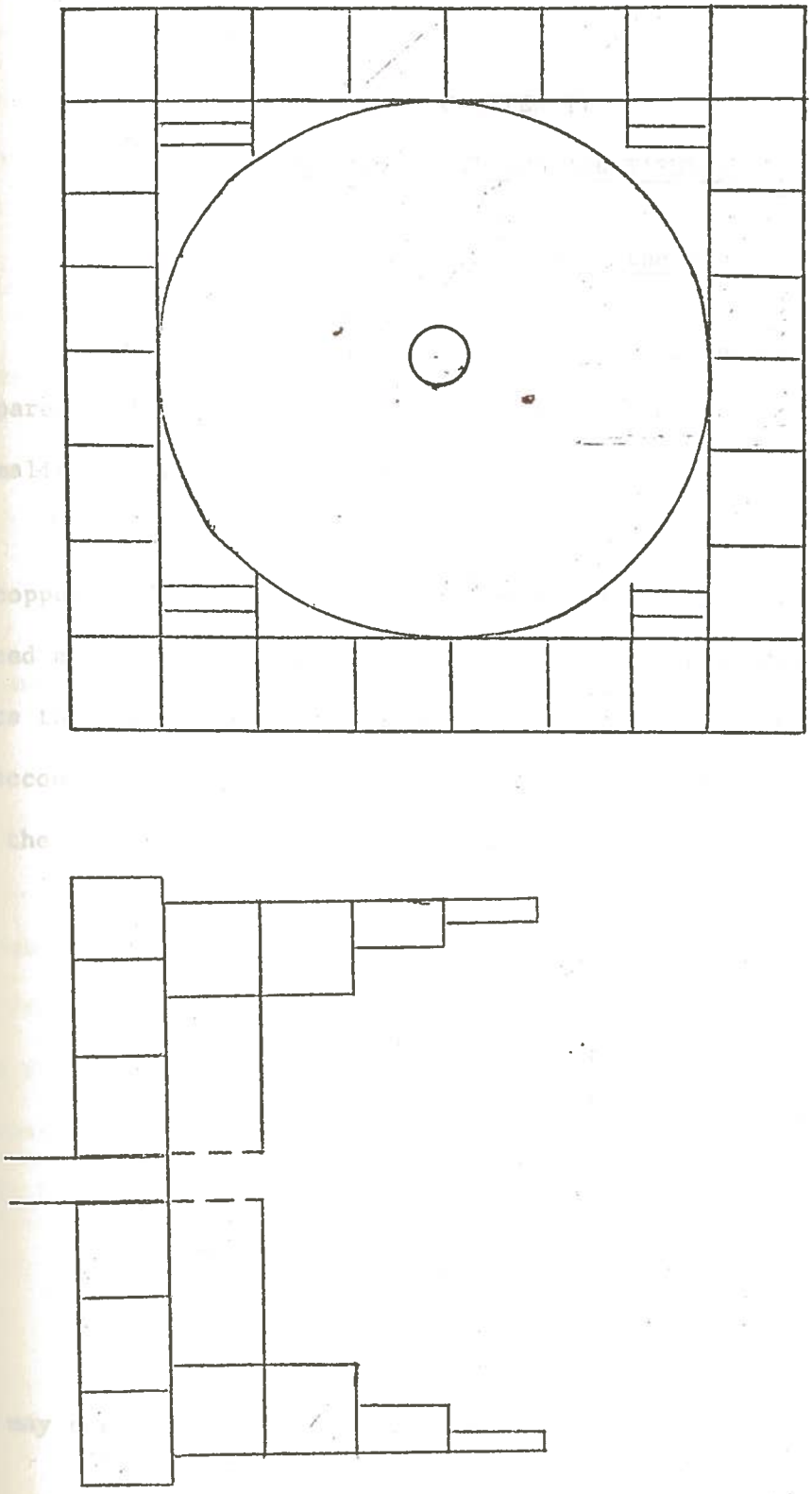

Figure 12

Front and Side Views of the Combinations
of Paraboloid Shaped Moderators

CHAPTER IV

DATA NORMALIZATION AND TABULATION

A. Normalization of the Data

In order that the experiments within a series might be compared with one another the data obtained from the experiments were normalized to conform to a standard experiment.

In the first series of experiments the foils were made of copper pellets and discs or indium squares. There was no foil placed at the target in this series of experiments. For the experiments to conform to the standard experiment, the data was normalized to account for weight and time elapsed between the end of irradiation and the beginning of the counting. This was done as follows:

Letting

C_1 = number of counts/minute obtained from the foil placed at the pre-determined position

W_1 = weight in grams of the foil placed at the pre-determined position

T_1 = time elapsed between the end of the irradiation and the beginning of the counting of the foil placed at the pre-determined position

one may normalize for the weight when the standard weight is one gram by

$$C_1' = \frac{C_1}{W_1},$$

and for the time elapsed when the time elapsed in the standard experiment is zero seconds by

$$C_1'' = C_1' e^{0.693\, T_1/T_{(\frac{1}{2})1}}$$

where

$T_{(\frac{1}{2})1}$ = half-life of the isotope counted which was produced when the foil at the predetermined position was irradiated.

Therefore, the data in the first series of experiments is normalized by the formula

$$C_1'' = \frac{C_1}{W_1} e^{0.693\, T_1/T_{(\frac{1}{2})1}}.$$

In the second series the thermal flux (< 0.41 eV) was measured. As discussed previously, the thermal flux was determined by using a cadmium-indium technique. If the subscripts "a" and "b" are used to denote the indium foil covered one side and on two sides, respectfully, (i.e.; C_{1a} and C_{1b}, W_{1a} and W_{1b}, T_{1a} and T_{1b}, etc.) then the thermal flux may be found by

letting

C_3 = number of counts/minute due to neutrons with thermal energy (< 0.41 eV)

and thus is given by

$$C_3 = C_{1a}'' - C_{1b}''$$

In the third series a foil was placed at the target. This foil was used to indicate the neutron flux of the accelerator during the irradiation. The counts from this foil were normalized as before; i.e.,

letting

C_2 = number of counts/minute obtained from the foil placed at the target

W_2 = weight in grams of the foil placed at the target

T_2 = time elapsed between the end of the irradiation and the beginning of the counting of the foil placed at the target.

the normalized counts may be obtained from the formula

$$C_2'' = \frac{C_2}{W_2} e^{0.693\ T_2/T_{(\frac{1}{2})2}}.$$

Finally, the flux from the accelerator was normalized to a standard number of counts/minute. 1,000,000 counts/minute was selected. The thermal normalized counts/minute for the foil placed at the pre-determined position may be obtained by

letting

C_n = thermal normalized counts/minute for the foil placed at the pre-determined position

and from the formula

$$C_n = 1 \times 10^6 \frac{C_3}{C_2''}$$

$$= 1 \times 10^6 \frac{\frac{C_{1a}}{W_{1a}} e^{0.693\, T_{1a}/T_{(\frac{1}{2})1a}} - \frac{C_{1b}}{W_{1b}} e^{0.693\, T_{1b}/T_{(\frac{1}{2})1b}}}{\frac{C_2}{W_2} e^{0.693\, T_2/T_{(\frac{1}{2})2}}}$$

The fast normalized counts/minute, C_m, for the foil placed at the predetermined position is similarly obtained from the formula

$$C_m = 1 \times 10^6 \frac{C_{1b}''}{C_2''}$$

$$= 1 \times 10^6 \frac{\frac{C_{1b}}{W_{1b}} e^{0.693\, T_{1b}/T_{(\frac{1}{2})1b}}}{\frac{C_2}{W_2} e^{0.693\, T_2/T_{(\frac{1}{2})2}}}$$

B. Data Tabulation

1. Series I - A table for each experiment is given which includes a foil identification number, the position defined by an angle and distance from the target, C_1, T_1, W_1, and C_1''. Following the table for a particular experiment will be found a graph illustrating the relationship between the normalized counts/minute, C_1'', and the position angle.

EXPERIMENT 1

Cu Pellets	Position Angle	Distance	C_1	T_1	W_1	C_1''
1	00	1	105,062	7	1.87	91,708
2	30	1	115,945	10	1.78	131,171
3	60	1	111,236	13	1.79	154,383
4	90	1	98,849	16	1.88	161,148
5	120	1	61,978	19	1.66	141,170
6	150	1	47,658	22	1.88	118,247
7	180	1	20,083	25	--	---

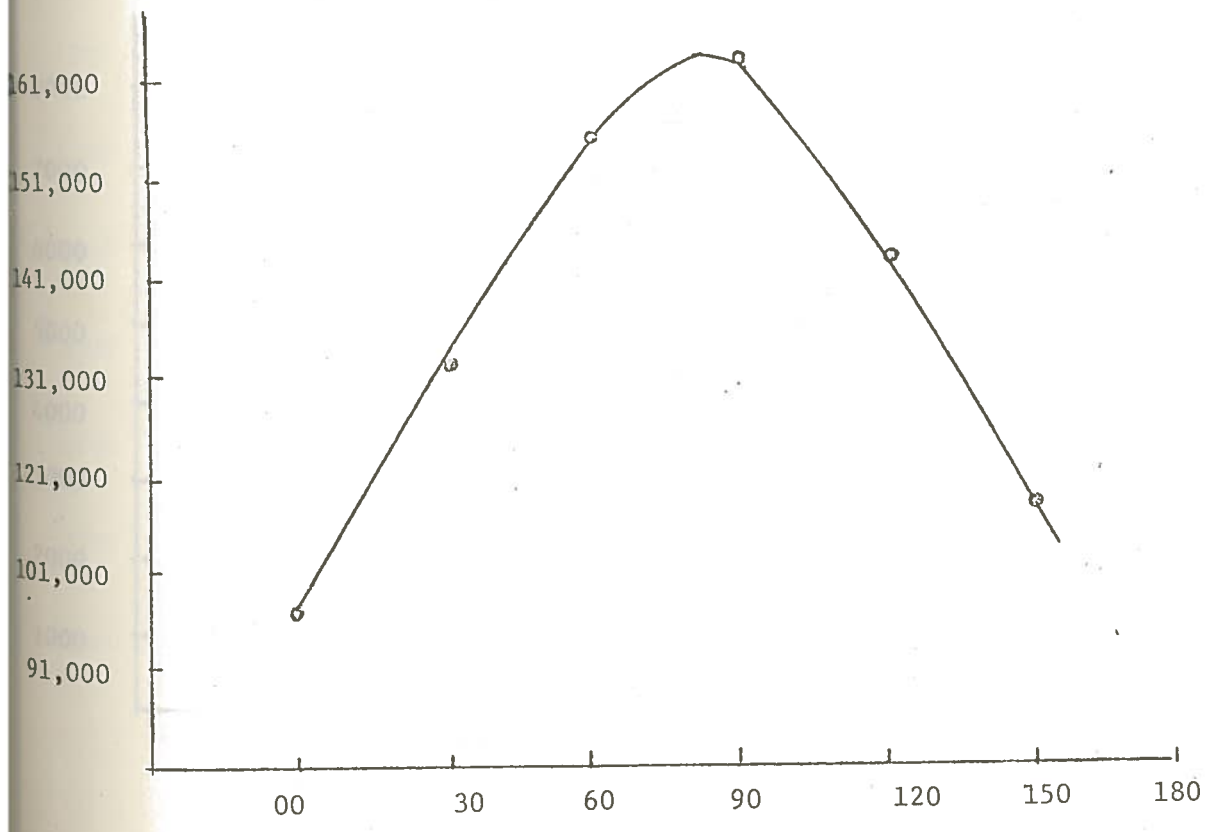

GRAPH 1

Fast Neutron Curve for Experiment 1

EXPERIMENT 2

In Foil	Position Angle	Position Distance	C_1	T_1	W_1	C_1''
10	00	1	2141	11	0.32	7706
12	30	1	1906	21	0.33	7564
14	60	1	1775	31	0.33	8006
16	90	1	1475	41	0.33	7564
18	120	1	1246	51	0.32	7494
20	150	1	1135	61	0.32	7759
22	180	1	990	71	0.32	7694

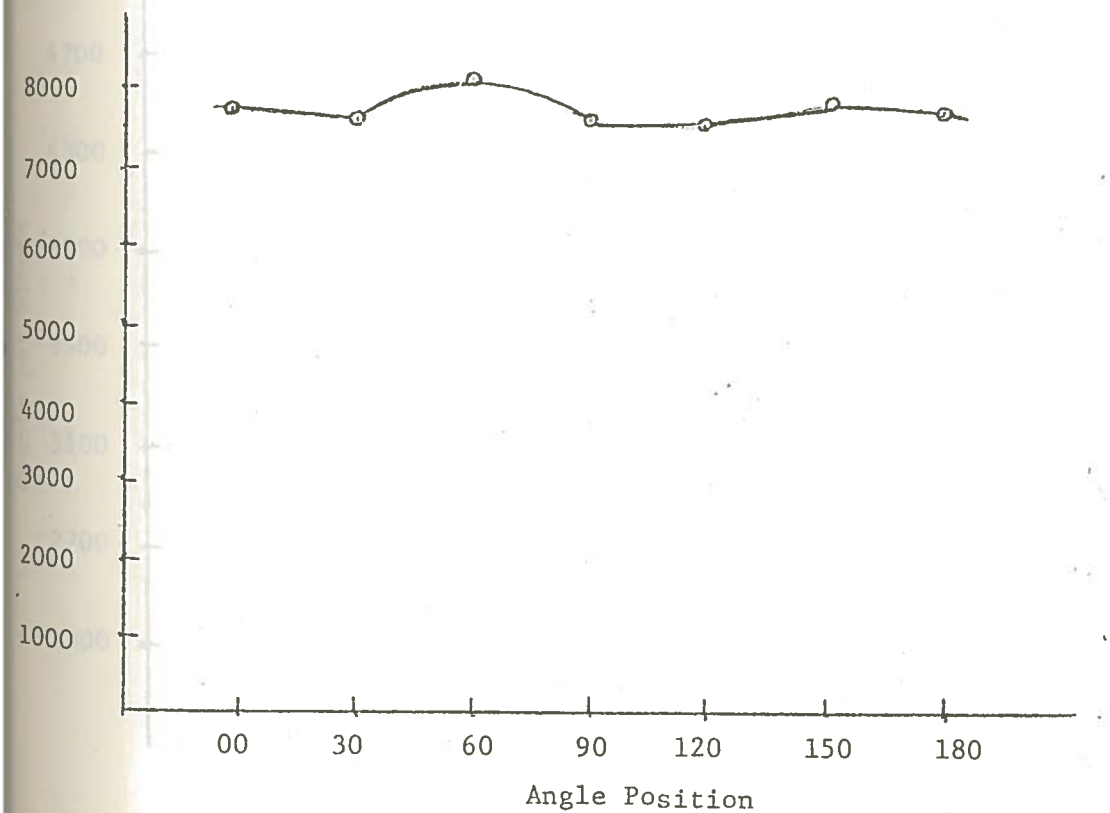

GRAPH II

Fast Neutron Curve for Experiment 2

EXPERIMENT 3

Cu Foil	Position Angle	Position Distance	C_1	T_1	W_1	C_1''
18	00	2	2233	8	1.48	2641
19	30	2	2757	10	1.62	3427
20	60	2	2756	12	1.66	3362
21	90	2	2511	14	1.80	3717
22	120	2	2483	16	1.61	4727
10	150	2	1705	18	1.72	3495
9	180	2	994	20	1.74	2317

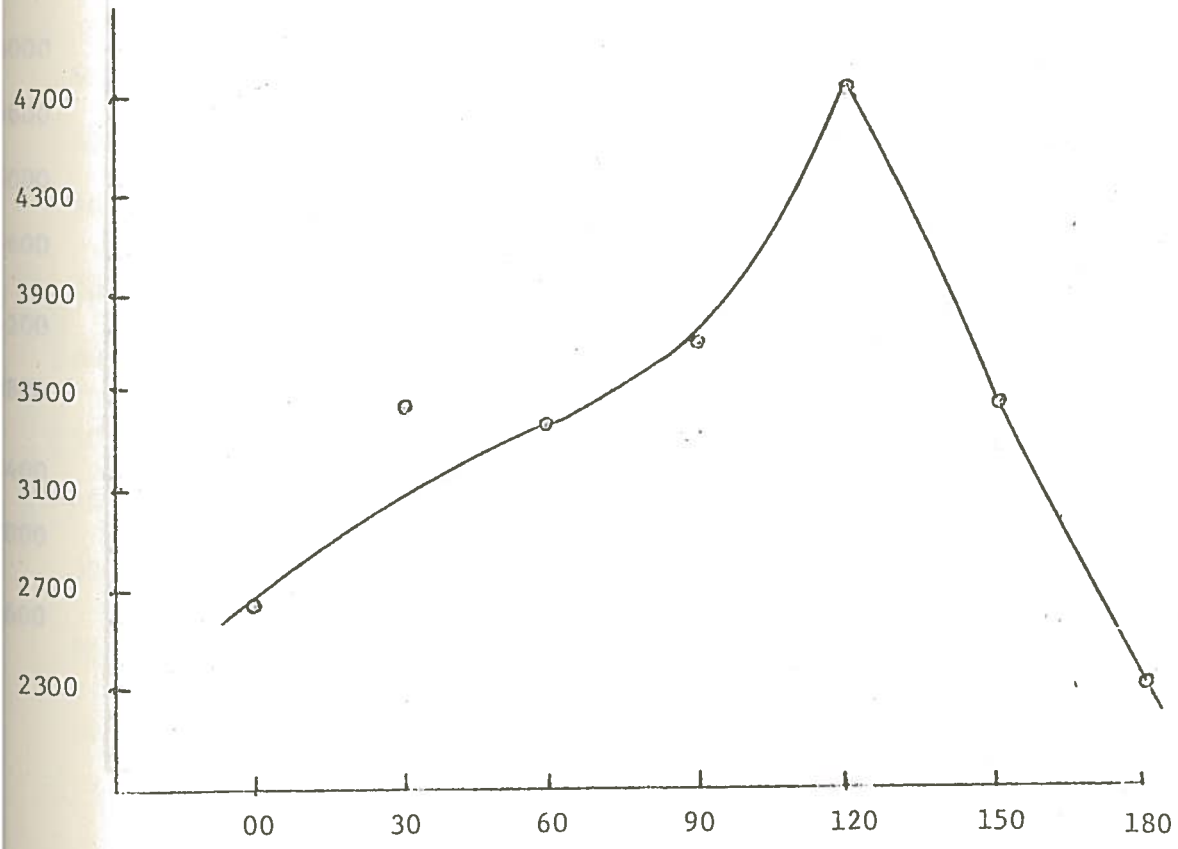

GRAPH III

Fast Neutron Curve for Experiment 3

EXPERIMENT 4

Cu Foil	Position Angle	Position Distance	C_1	T_1	W_1	C_1''
18	00	2	749	24	1.48	2716
19	30	2	916	26	1.62	3490
20	60	2	852	28	1.66	3644
21	90	2	882	30	1.80	4002
22	120	2	1095	32	1.61	6389
10	150	2	598	34	1.72	3756
9	180	2	365	36	1.74	2607

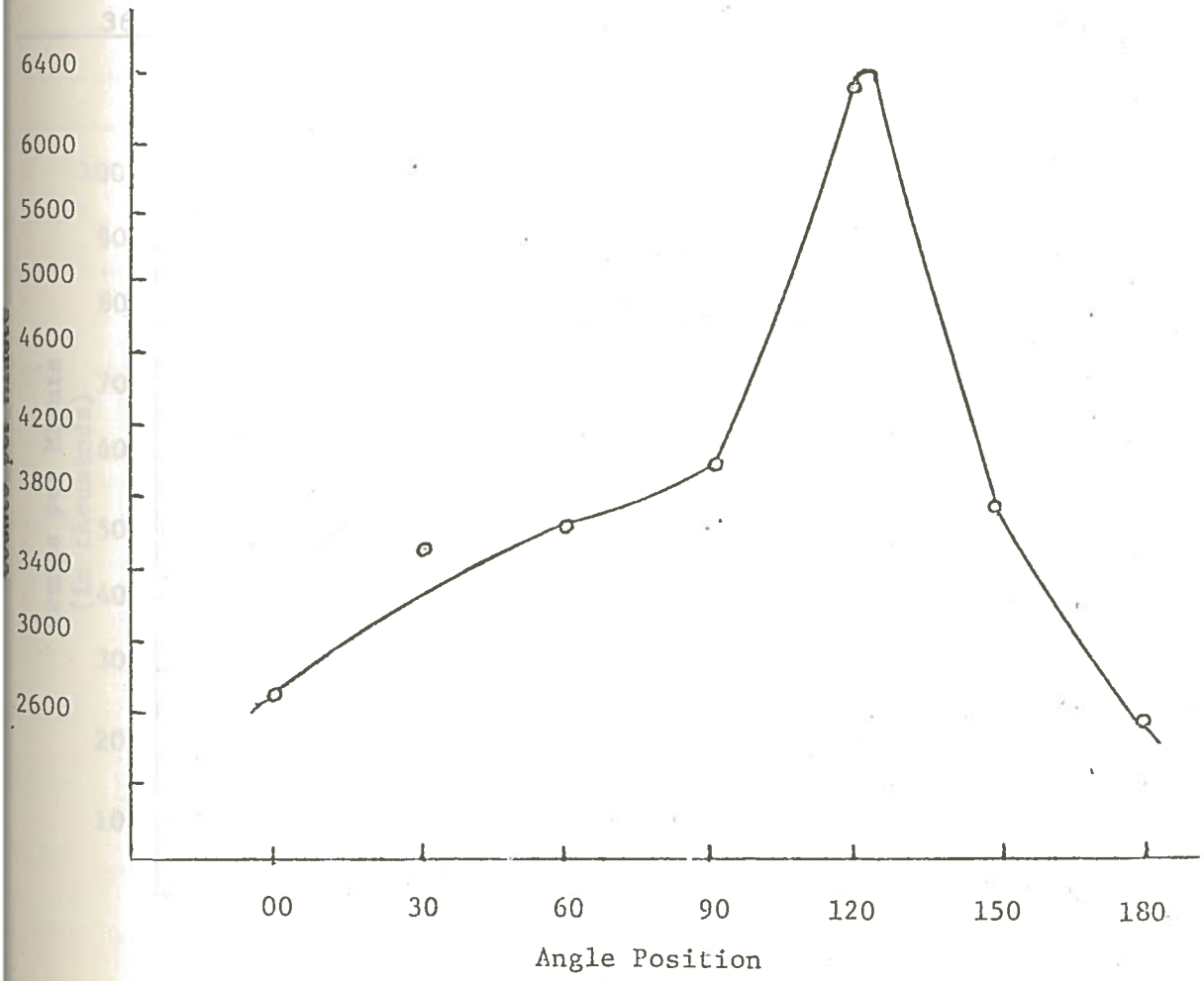

GRAPH IV

Fast Neutron Curve for Experiment 4

EXPERIMENT 5

In Foil	Position Angle	Position Distance	C_1	T_1	W_1	C_1''
24	00	1	12,590	13	0.33	45,079
26	30	1	15,398	23	0.34	60,838
28	60	1	15,932	33	0.32	76,041
30	90	1	14,669	43	0.32	79,600
32	120	1	11,973	53	0.32	73,866
34	150	1	9,615	63	0.34	63,474
36	180	1	5,443	73	0.30	46,800

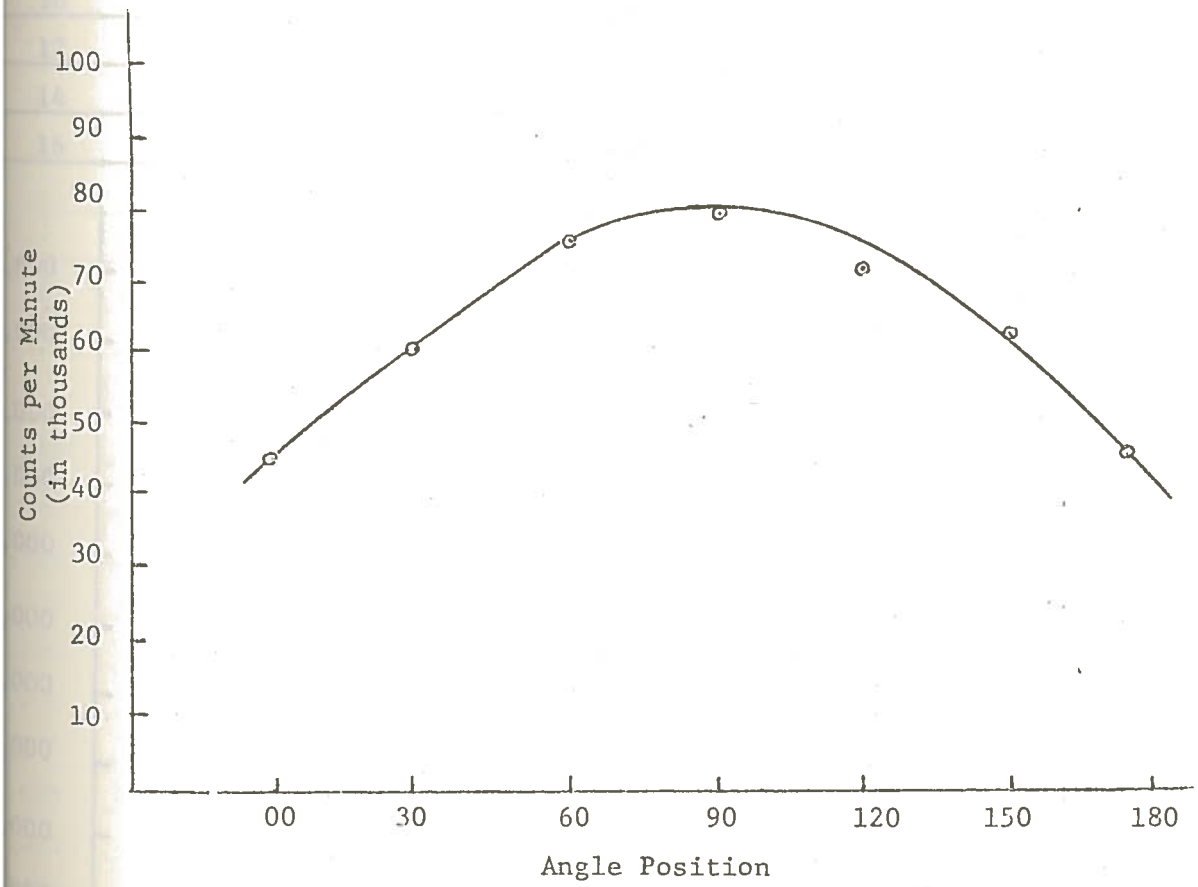

GRAPH V

Fast Neutron Curve After Moderation
By 6 cm Polyethylene Hemisphere,
Experiment 5

EXPERIMENT 6

In Foil	Position Angle	Position Distance	C_1	T_1	W_1	C_1''
2	00	3	3977	13	0.32	14,684
4	20	3	3807	23	0.32	15,981
6	30	3	3411	33	0.32	16,281
8	40	3	1049	138	0.32	19,263
38	60	3	3031	53	0.33	18,133
40	80	3	2669	63	0.31	19,326
42	90	3	2397	73	0.32	19,116
44	100	3	2074	83	0.32	18,803
46	120	3	1779	93	0.32	18,338
10	140	3	1478	103	0.32	17,322
12	150	3	1321	113	0.33	17,070
14	160	3	1210	123	0.33	17,776
16	180	3	928	133	0.33	15,500

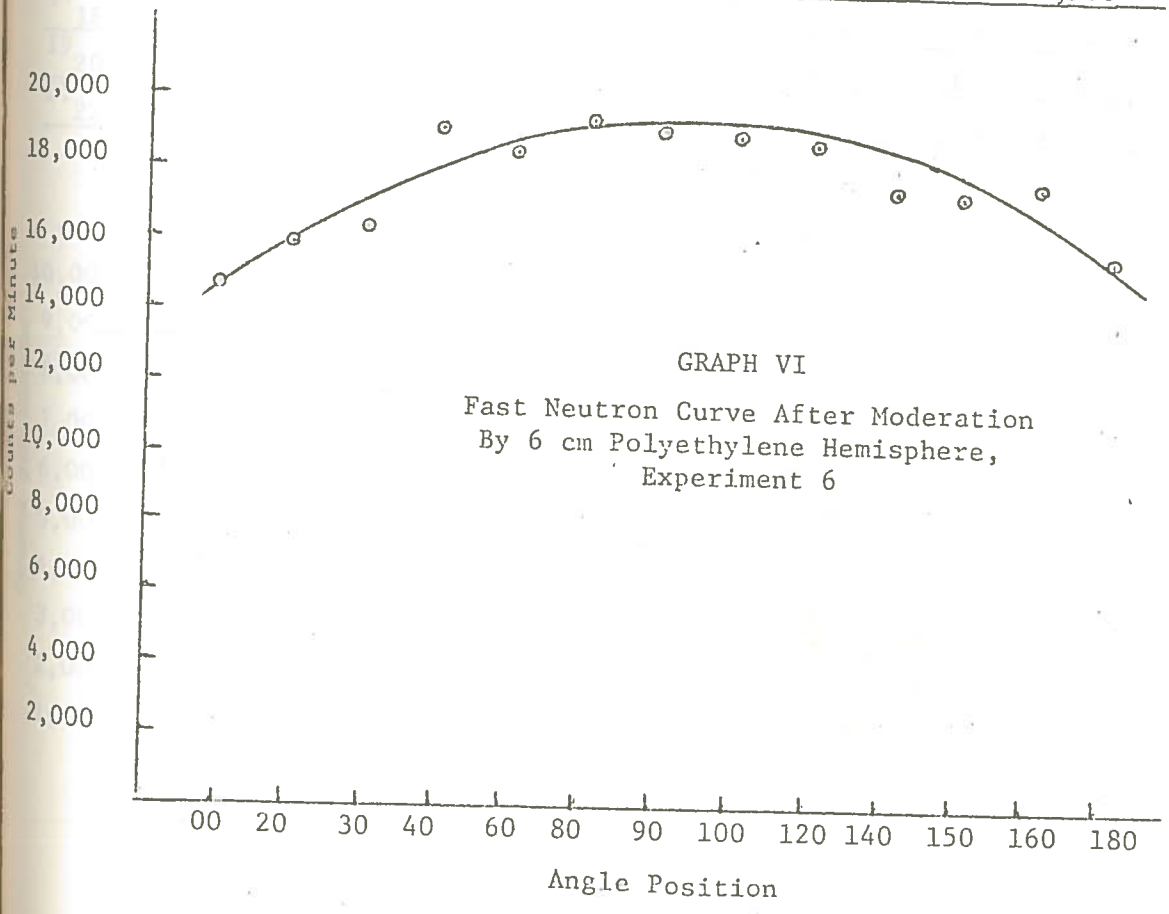

GRAPH VI

Fast Neutron Curve After Moderation
By 6 cm Polyethylene Hemisphere,
Experiment 6

2. Series II

A table for each experiment is given which includes a foil identification number, the position defined by an angle and distance from the target, C_{1a}, T_{1a}, W_{1a}, C_{1b}, T_{1b}, W_{1b}, and C_3. Following the table for each experiment will be a graph illustrating the relationship between C_3 and the position angle.

EXPERIMENT 7

In Foil	Position Angle	Position Distance	C_{1a}	T_{1a}	W_{1a}	C_{1b}	T_{1b}	W_{1b}	C_3
9 10	00	1	3920	6	0.31	2141	11	0.32	5952
11 12	30	1	3654	16	0.32	1906	21	0.33	6458
13 14	60	1	2972	26	0.31	1775	31	0.33	5378
15 16	90	1	2716	36	0.32	1475	41	0.33	5908
17 18	120	1	2509	46	0.33	1246	51	0.32	6227
19 20	150	1	2035	56	0.31	1135	61	0.32	5709
21 22	180	1	1857	66	0.32	990	71	0.32	5844

GRAPH VII

Thermal Neutron Curve for Experiment 7;

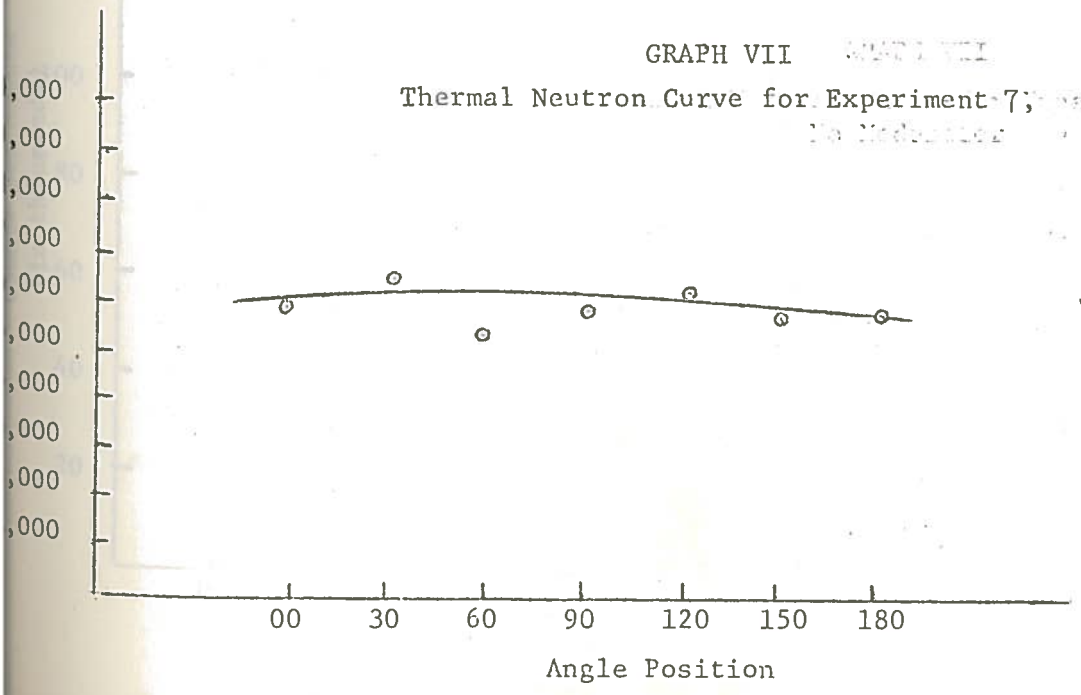

EXPERIMENT 8

Position Angle	Distance	C_{1a}	T_{1a}	W_{1a}	C_{1b}	T_{1b}	W_{1b}	C_3
00	1	35,855	8	0.32	12,590	13	0.33	79,084
30	1	47,350	18	0.32	15,398	23	0.34	125,581
60	1	53,500	28	0.31	15,932	33	0.32	171,159
90	1	49,749	38	0.32	14,669	43	0.32	173,578
120	1	38,780	48	0.30	11,973	53	0.32	165,471
150	1	29,452	58	0.32	9,615	63	0.34	130,270
180	1	16,811	68	0.32	5,443	73	0.30	79,431

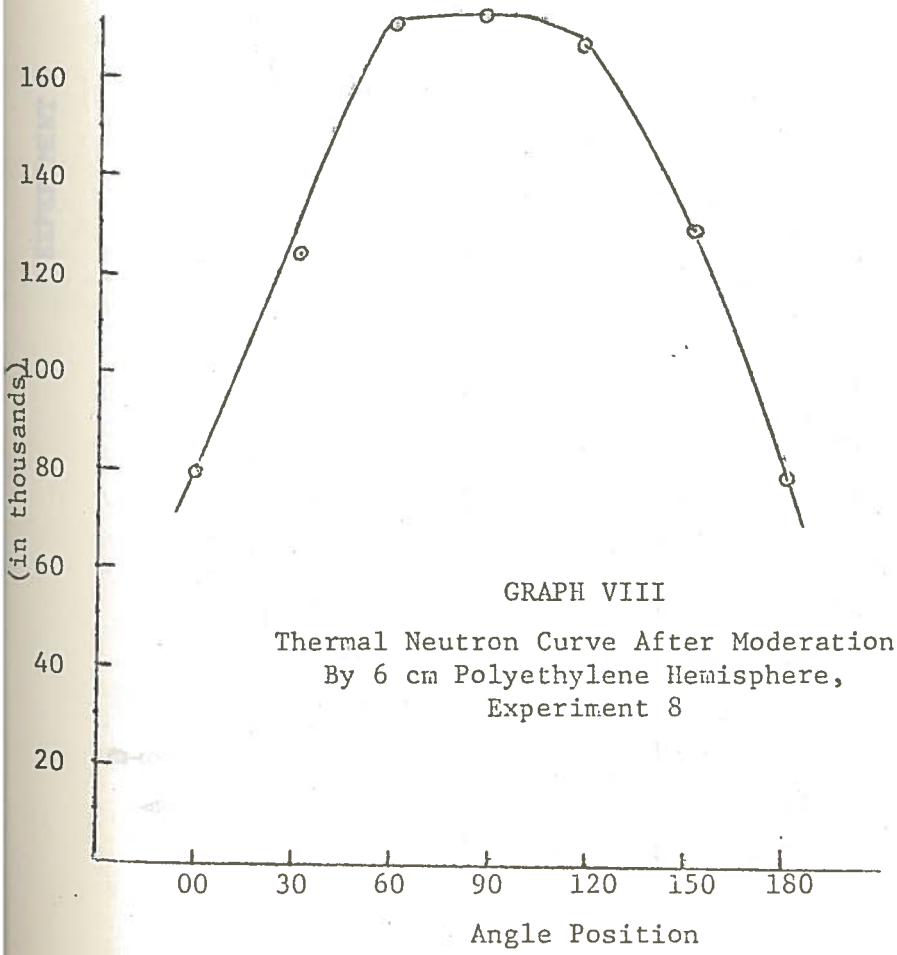

GRAPH VIII

Thermal Neutron Curve After Moderation
By 6 cm Polyethylene Hemisphere,
Experiment 8

ANGLE	DISTANCE	C_{1a}	W_{1a}	T_{1a}	C_{1b}	W_{1b}	T_{1b}	C''_{Ta}	C''_{1b}	C_3
00	3	10,970	0.33	8	3,977	0.32	13	36,836	14,684	22,152
20	3	10,618	0.34	18	3,807	0.32	23	39,344	15,981	23,363
30	3	9,708	0.32	28	3,411	0.32	33	43,453	16,281	27,172
40	3	8,334	0.31	38	1,049	0.32	138	43,781	19,263	24,518
60	3	8,407	0.31	48	3,303	0.33	53	50,213	18,133	32,080
80	3	7,858	0.32	58	2,669	0.31	63	51,691	19,326	32,365
90	3	6,990	0.32	68	2,397	0.32	73	52,278	19,116	33,162
100	3	5,860	0.32	78	2,074	0.32	83	49,828	18,803	31,025
120	3	5,324	0.32	88	1,779	0.32	93	51,469	18,338	33,131
140	3	4,301	0.31	98	1,478	0.32	103	48,797	17,322	31,475
150	3	3,565	0.32	108	1,321	0.33	113	44,550	17,070	27,480
160	3	2,771	0.31	118	1,210	0.33	123	40,639	17,776	22,863
180	3	2,353	0.32	128	928	0.33	133	38,009	15,500	22,509

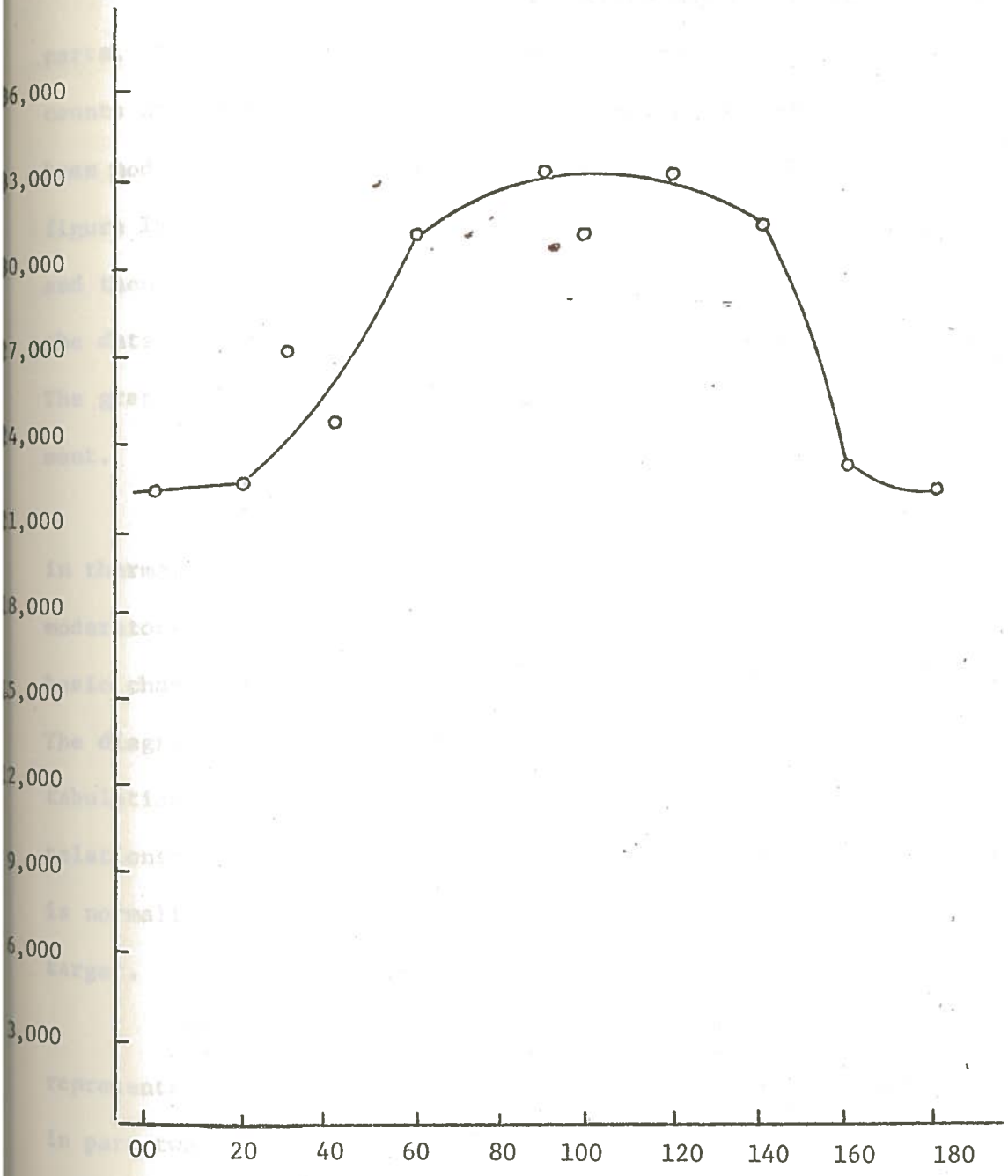

GRAPH IX

Thermal Neutron Curve After Moderation
By 6 cm Polyethylene Hemisphere,
Experiment 9

3. Series III - The third series may be divided into three parts. The first part dealt with determining the thermal neutron counts at various positions about the accelerator target, which has been moderated by different size polyethylene hemispheres (See Figure 14). Data tables for the four experiments in this part given, and then followed by graphs for the data. It should be noted that the data is corrected for a standard copper disc placed at the target. The graphs also contrast the fast and thermal counts for each experiment.

The experiments in the second part illustrate the change in thermal flux detected when the size and shape of the paraffin moderators is altered. Four subseries of experiments representing basic changes in paraffin moderator shape are included in this part. The diagrams for each subseries experiments are followed by data tabulation and a graphical representation of the thermal count relationship among the experiments in the subseries. Again the data is normalized to the counts of a standard copper disc placed at the target.

Six subseries are included in part three. Each subseries represents a basic moderator design. Some of the series included in part two are repeated, except that a Teflon strip is used to normalize all the data. This is in contrast to the copper disc. One of the subseries illustrates the change in thermal counts after the thermal neutron beam has been collimated. As before, diagrams of each experiment in a subseries are presented, followed by tabulation

of the data, and a graph illustrating the neutron count changes among the experiments.

Finally data representing a duplicated experiment is presented. A graph comparing the identical experiments run at different days is shown in order that the reproducibility of the experiments might be determined.

SERIES III

Subsection 1.

Different Dimension of Hemispherical

Polyethylene Moderator

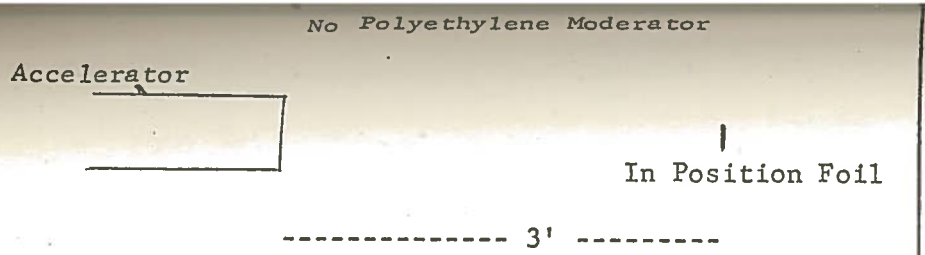

Figure 13
Experiment 10

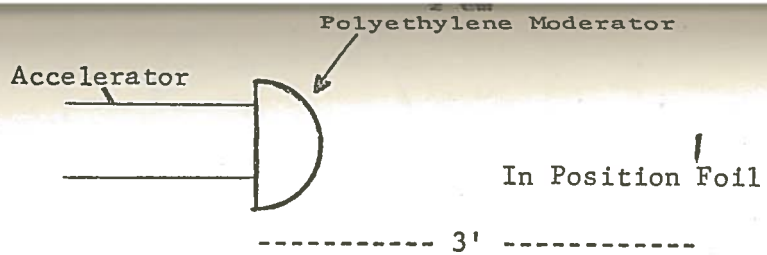

Figure 14
Experiment 11

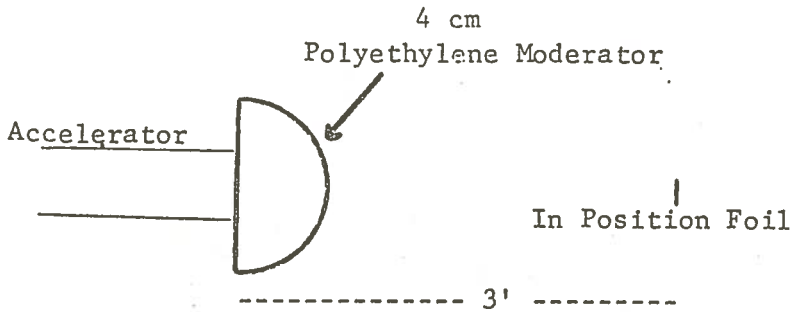

Figure 15
Experiment 12

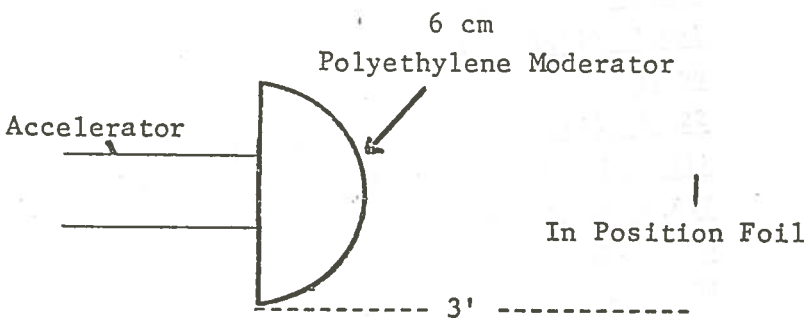

Figure 16
Experiment 13

EXPERIMENTS 10 - 13

Experiment Number	Position Angle	Position Distance	C_{1a}	W_{1a}	T_{1a}	C_{1b}	W_{1b}	T_{1b}	C''_{1a}	C''_{1b}	C_3	C_2	W_2	T_2	C''_2	Thermal C_n	Fast C_m
10	00	3	3,753	0.31	6	2,122	0.33	4	13,075	6,306	6,306	288,693	1.60	53	7.376	855	918
10	30	3	3,775	0.32	10	1,965	0.31	8	13,412	7,024	6,388	288,693	1.60	53	7.376	866	952
10	60	3	3,551	0.32	14	1,834	0.32	12	13,281	6,685	6,595	288,693	1.60	53	7.376	894	906
10	90	3	3,375	0.32	18	1,744	0.32	16	13,288	6,692	6,596	288,693	1.60	53	7.376	894	907
11	00	3	4,594	0.33	6	2,285	0.32	4	15,035	7,517	7,518	295,200	1.72	53	7.012	1,072	1,072
11	30	3	4,663	0.34	10	2,214	0.32	8	15,593	7,667	7,926	295,200	1.72	53	7.012	1,130	1,093
11	60	3	4,162	0.32	14	2,098	0.32	12	15,566	7,648	7,918	295,200	1.72	53	7.012	1,129	1,091
11	90	3	3,785	0.31	16	2,077	0.32	18	14,993	8,177	6,816	295,200	1.72	53	7.012	972	1,166
12	00	3	5,152	0.31	9	2,505	0.32	8	18,774	8,675	10,099	238,979	1.60	53	6.102	1,655	1,422
12	30	3	5,046	0.32	21	2,384	0.33	19	20,646	9,219	11,427	238,979	1.60	53	6.102	1,873	1,511
12	60	3	5,274	0.31	25	2,453	0.33	23	23,448	9,986	13,462	238,979	1.60	53	6.102	2,206	1,637
12	90	3	6,422	0.32	14	2,890	0.33	12	24,019	10,216	13,803	238,979	1.60	53	6.102	2,262	1.674
13	00	3	4,993	0.33	7	1,950	0.32	5	16,552	6,498	10,054	151,525	1.63	53	3.802	2,644	1,709
13	30	3	5,716	0.31	11	2,179	0.32	9	21,234	7,643	13,591	151,525	1.63	53	3.802	3,575	2,010
13	60	3	6,279	0.32	15	2,207	0.32	13	23,787	8,149	15,638	151,525	1.63	53	3.802	4,113	2,143
13	90	3	5,948	0.32	19	2,394	0.33	17	23,720	9,023	14,697	151,525	1.63	53	3.802	3,866	2,373

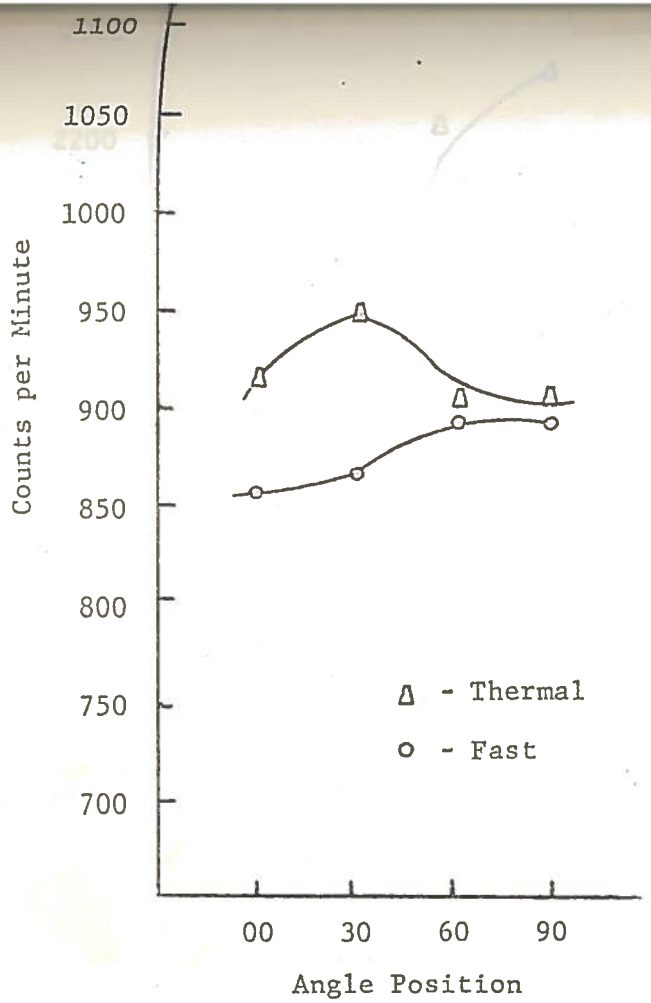

GRAPH X

Fast and Thermal Neutron Curves
of Experiment 10

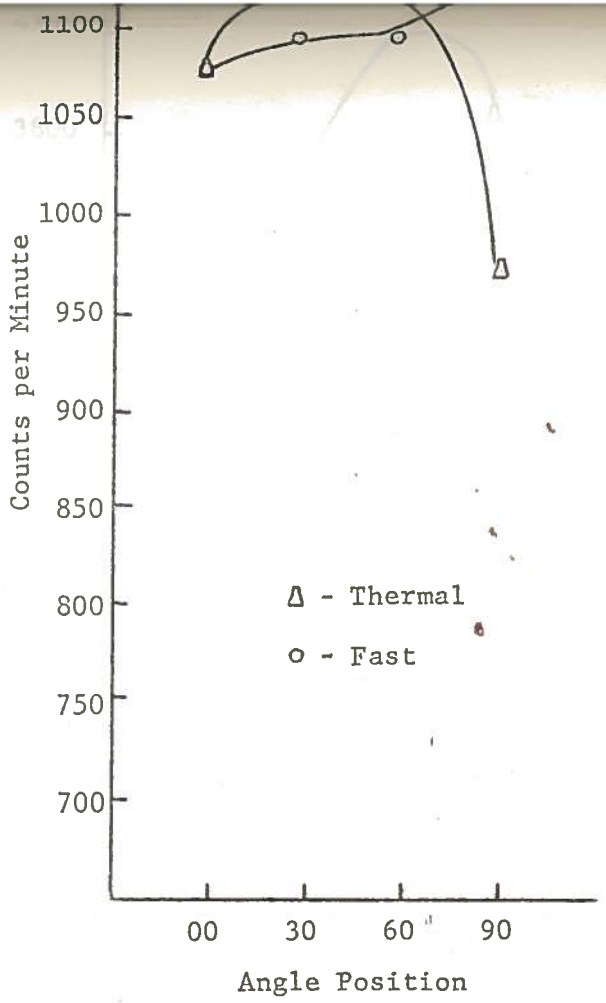

GRAPH XI

Fast and Thermal Neutron Curves
of Experiment 11

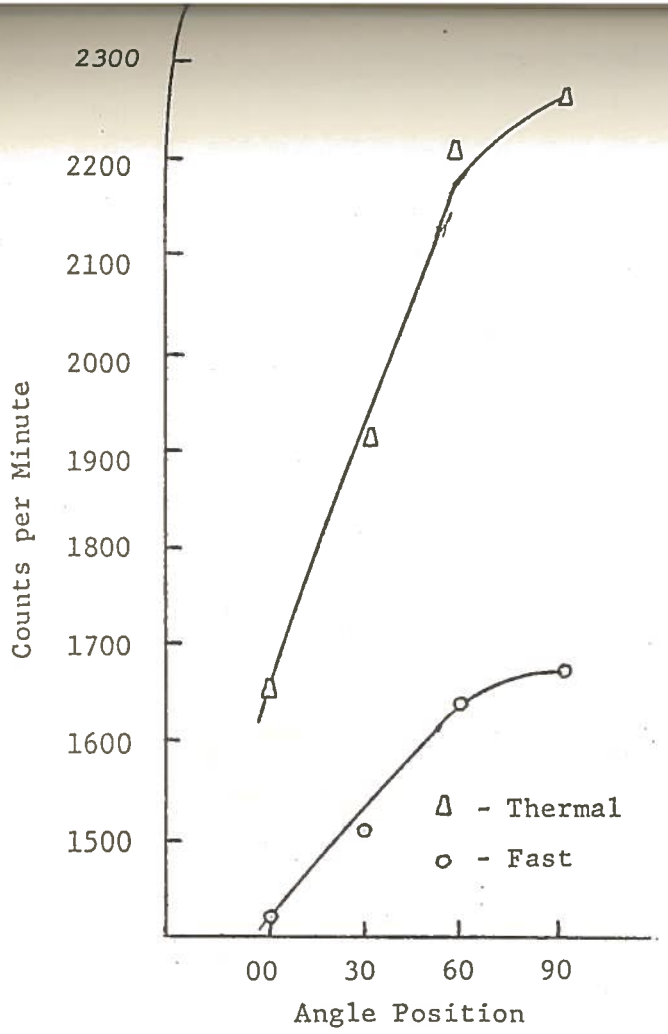

GRAPH XII

Fast and Thermal Neutron Curves
of Experiment 12

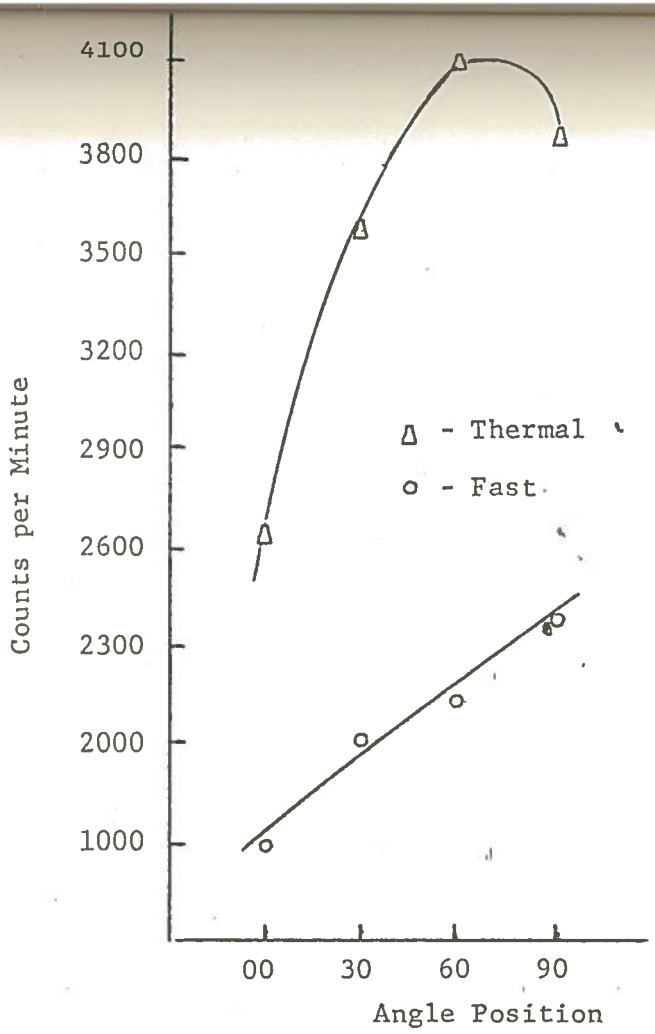

GRAPH XIII

Fast and Thermal Neutron Curves
of Experiment 13

SERIES III

Subseries 2

Part a

EXPERIMENTS 14-20

EXPERIMENTS 14 - 18

Experiment Number	Position Angle	Position Distance	C_{1a}	W_{1a}	T_{1a}	C_{1b}	W_{1b}	T_{1b}	C_2	W_2	T_2	C''_{1a}	C''_{1b}	C''_2	C_3	C_n	C_m
14	90	2	8,130	0.33	9	3,595	0.32	4	170,975	1.62	47	27,652	11,825	2.840	16,827	5,925	4,186
15	90	2	47,668	0.34	8	13,462	0.32	3	78,148	1.48	54	155,359	43,719	2.322	111,640	48,079	18,828
16	90	2	82,658	0.32	5	16,618	0.32	10	52,289	1.76	58	275,425	59,044	1.723	216,381	125,584	34,268
17	90	2	79,946	0.31	10	20,233	0.32	5	43,971	1.62	55	293,203	67,419	1.274	225,784	177,224	52,919
18	90	2	100,522	0.31	10	22,704	0.32	5	24,876	1.62	68	368,668	75,653	1.798	293,105	162,967	42,076

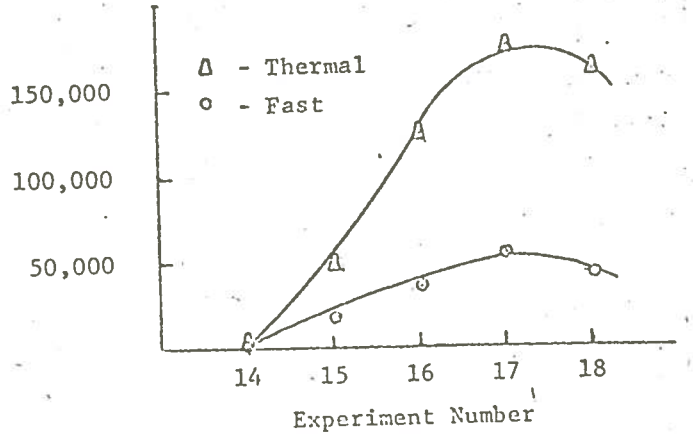

GRAPH XIV

Fast and Thermal Neutron Count
Comparisons of Experiments 14-18

Figure 17
Experiment 14

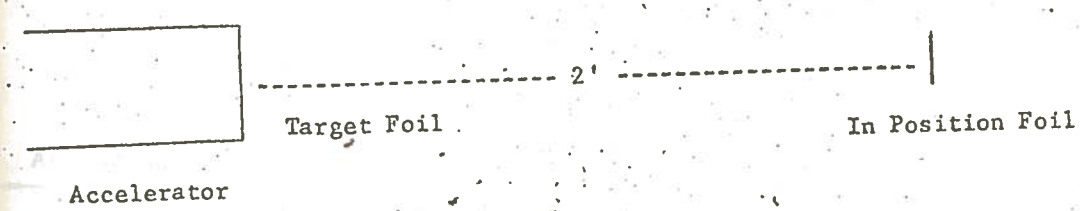

Figure 18
Experiment 15

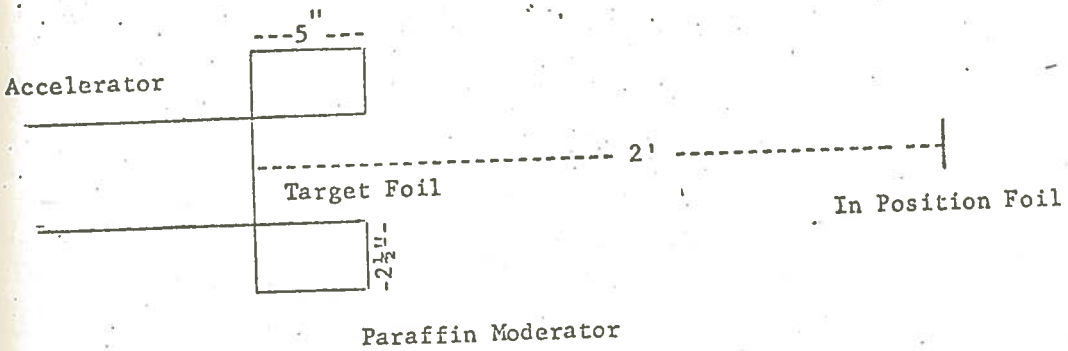

Figure 19
Experiment 16

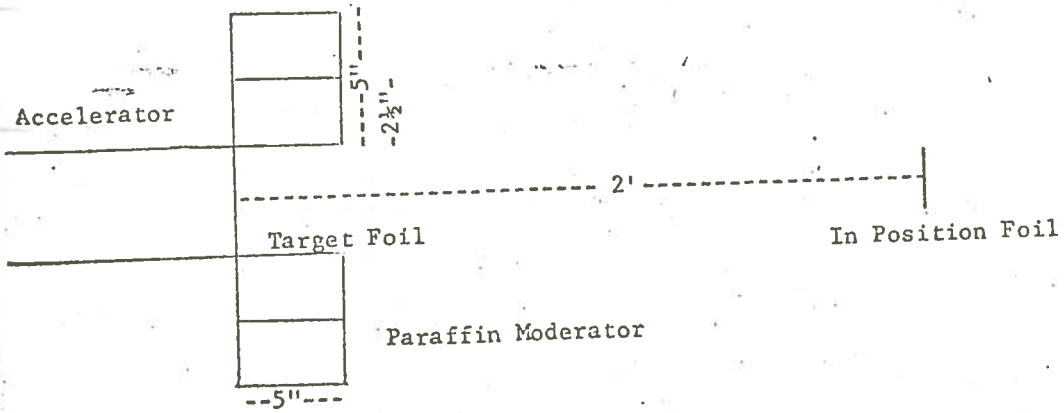

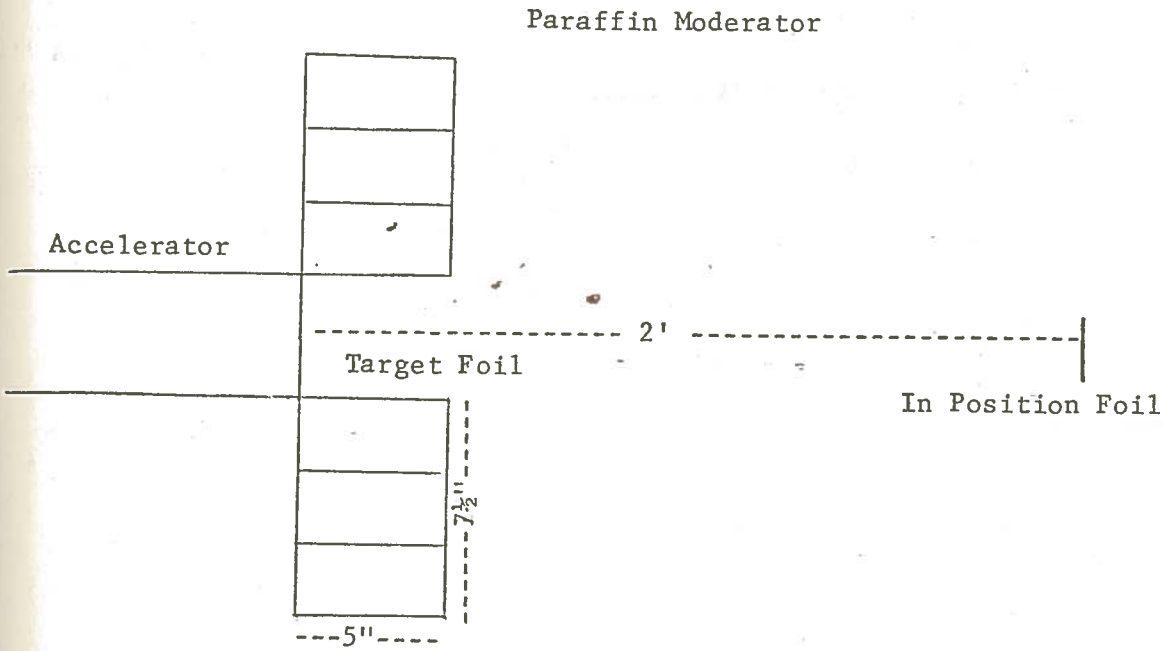

Figure 20
Experiment 17

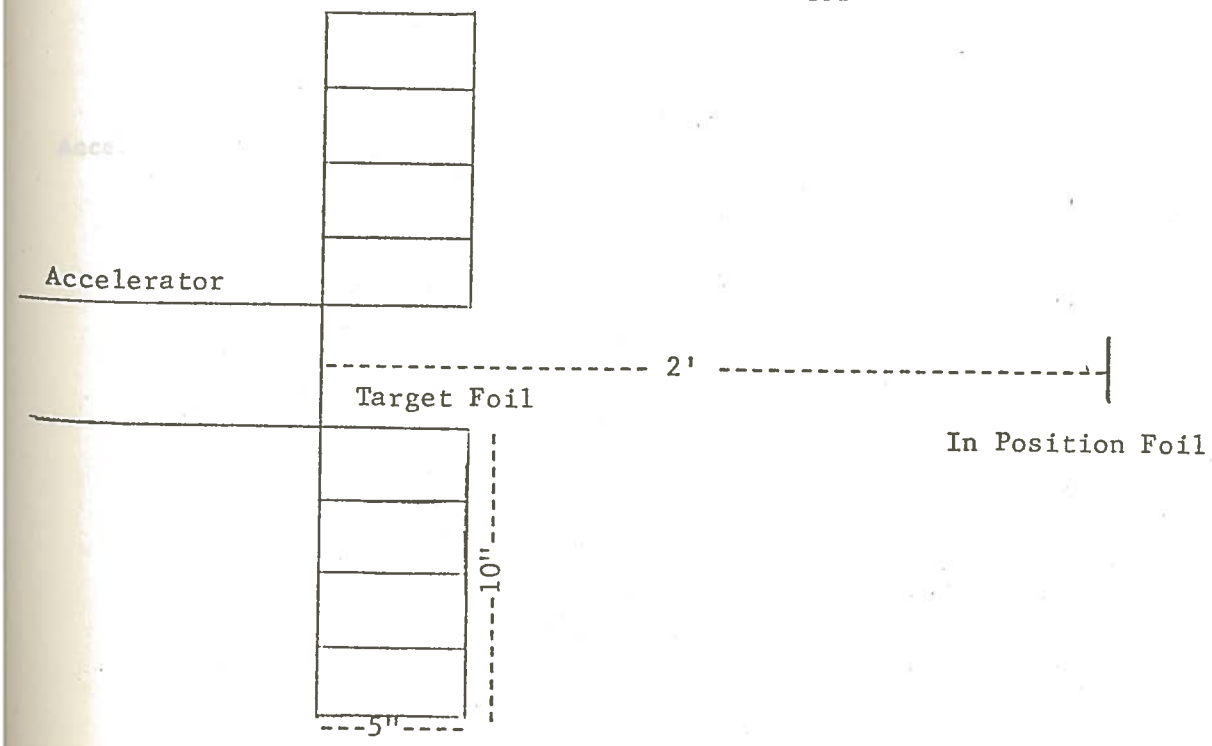

Figure 21
Experimant 18

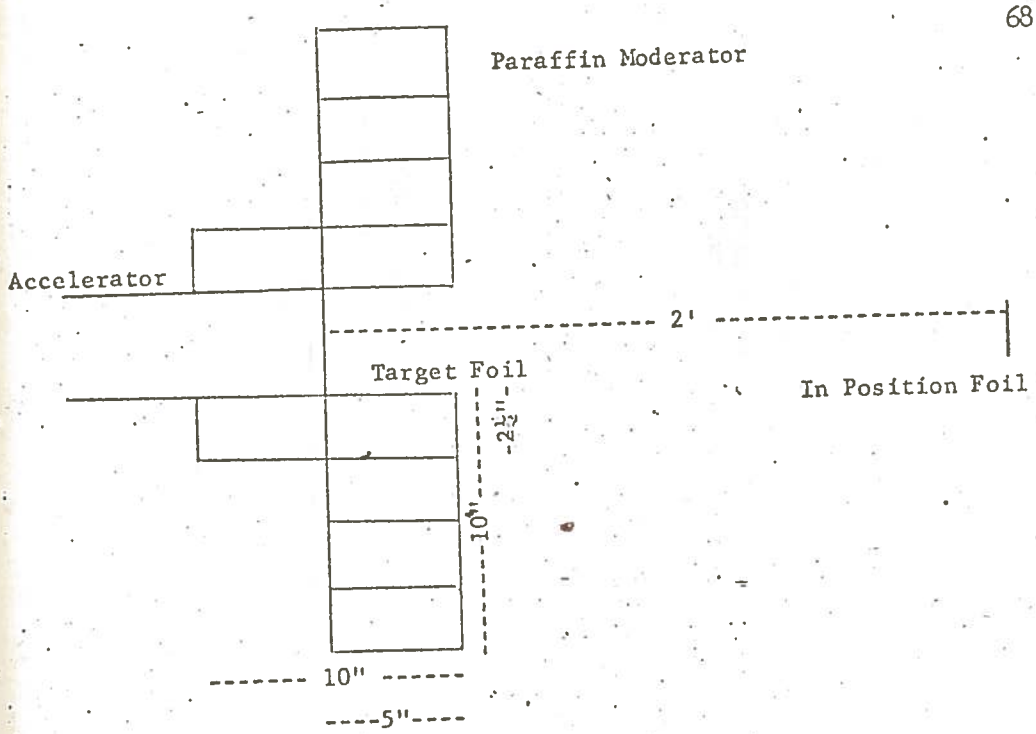

Figure 22
Experiment 19

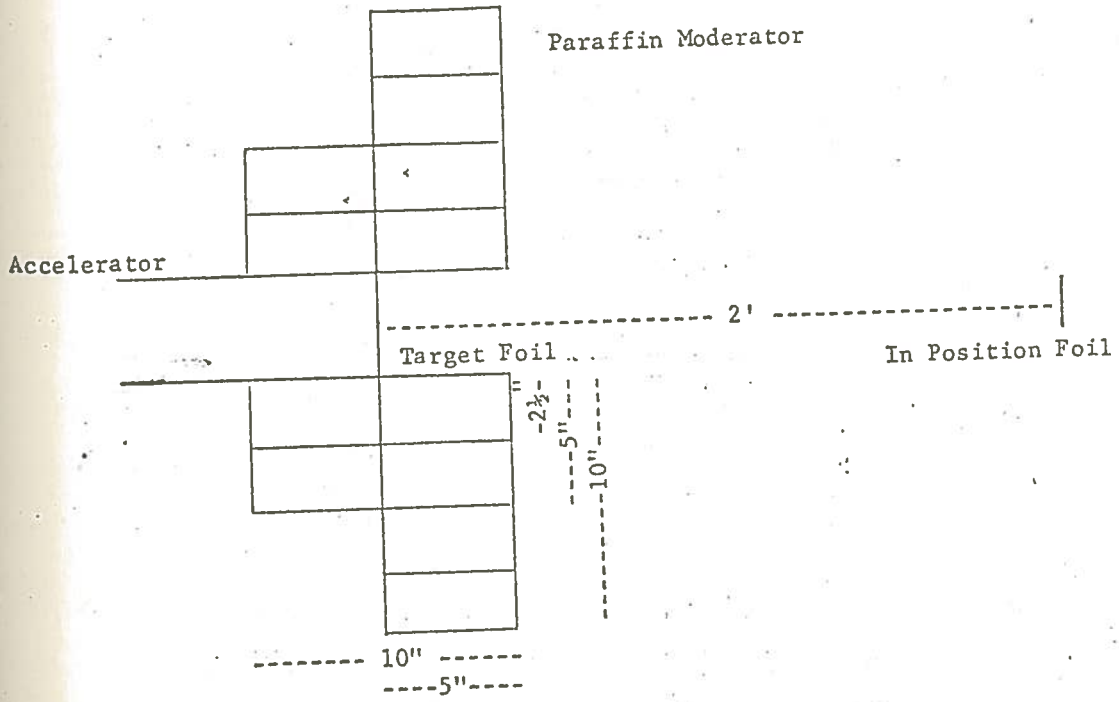

Figure 23
Experiment 20

EXPERIMENTS 19 - 20

EXPERIMENT NUMBER	Position ANGLE	Position DISTANCE	C_{1a}	W_{1a}	T_{1a}	C_{1b}	W_{1b}	T_{1b}	C_2	W_2	T_2	C''_{1a}	C''_{1b}	C_3	C''_2	C_n	C_m
19	90	2	95,530	0.32	25	25,600	0.33	4	95,290	1.63	47	411,459	81,661	329,798	1.574	209,529	51,881
20	90	2	110,212	0.31	10	24,739	0.33	5	95,094	1.75	47	404,206	79,333	324,873	1.459	222,668	54,375

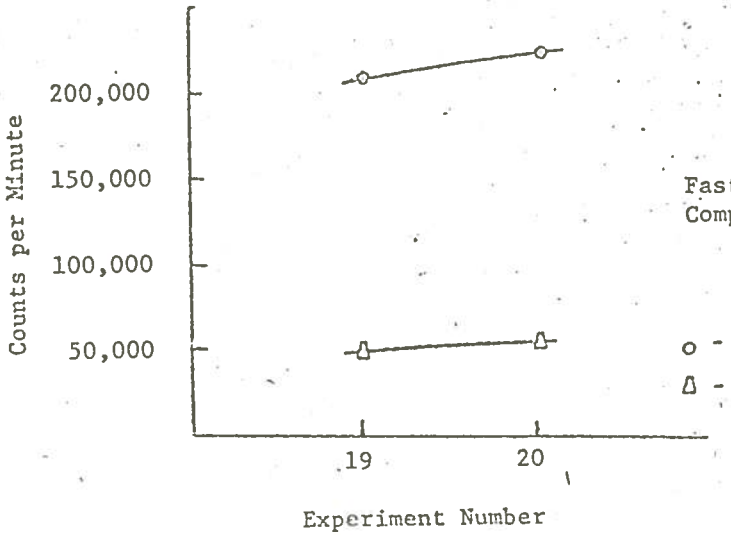

GRAPH XV

Fast and Thermal Neutron Count Comparisons of Experiments 19-20

SERIES III

Subsection 2

Part b

EXPERIMENTS 25-26

EXPERIMENTS 25 - 26

EXPERIMENT NUMBER	ANGLE	DISTANCE	C_{1a}	W_{1a}	T_{1a}	C_{1b}	W_{1b}	T_{1b}	C_2	W_2	T_2	C''_{1a}	C''_{1b}	C_3	C''_2	C_n	C_m
25	90	2	8,597	0.31	6	2,838	0.34	4	71,976	1.60	44	29,952	8,787	21,165	44,873	471,664	195,819
26	90	2	5,250	0.31	6	1,913	0.32	4	266,214	1.57	27	18,291	6,293	11,998	169,671	70,713	37,089

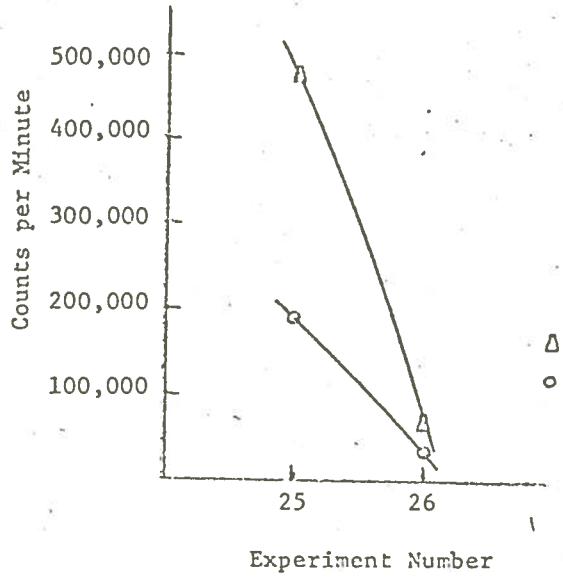

GRAPH XVI

Fast and Thermal Neutron Counts
Comparisons of Experiments 25-26

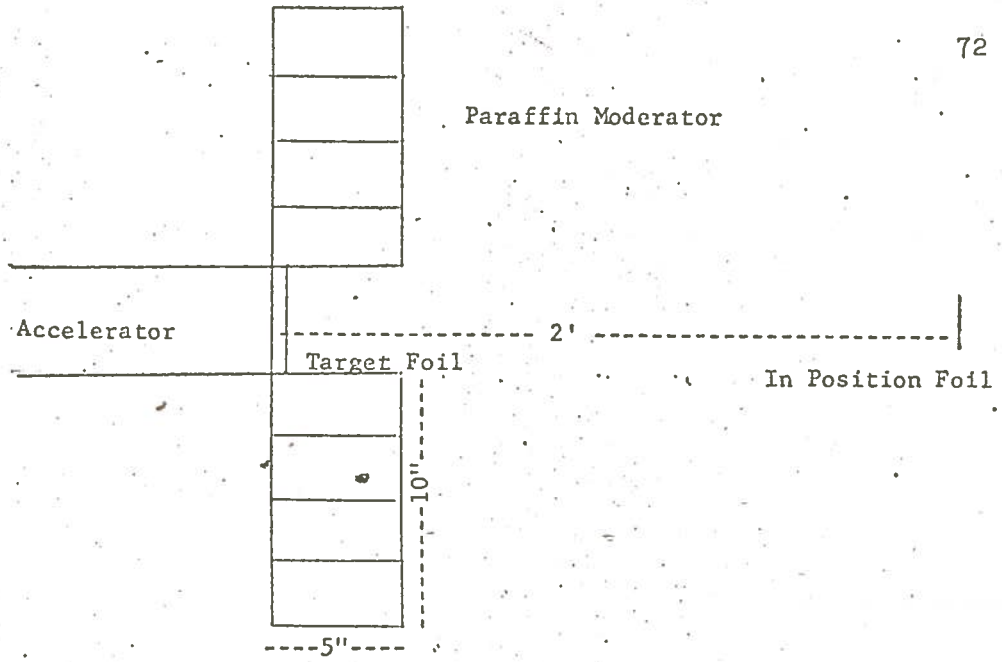

Figure 24
Experiment 25

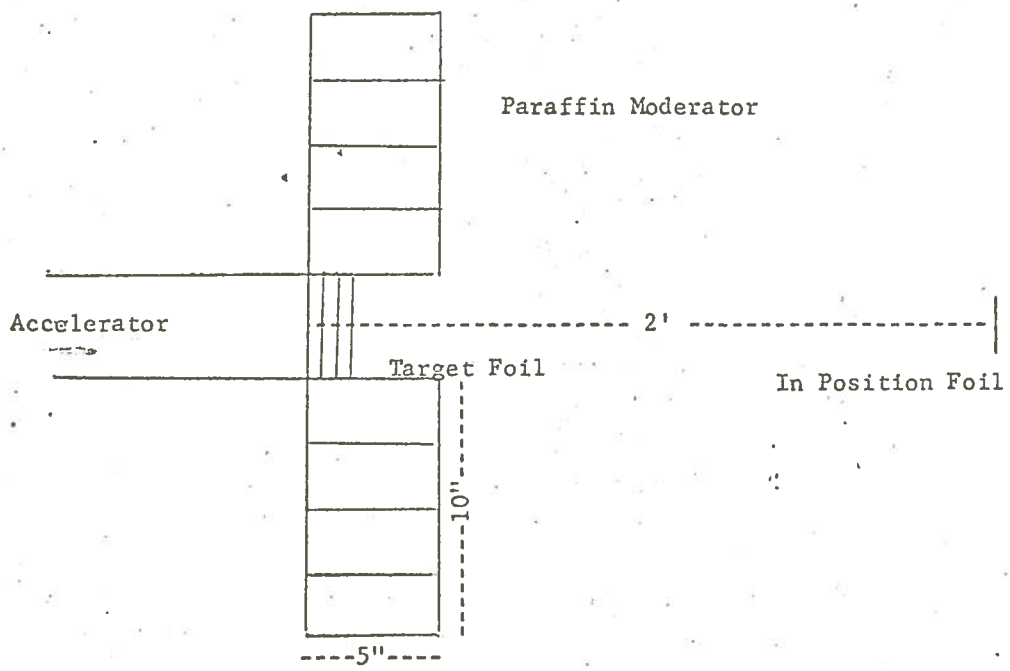

Figure 25
Experiment 26

SERIES III

Subsection 2

Part C

EXPERIMENTS 21-24

EXPERIMENTS 21 - 24

Experiment Number	Position: Angle	Position: Distance	C_{1a}	W_{1a}	T_{1a}	C_{1b}	W_{1b}	T_{1b}	C_2	W_2	T_2	C''_{1a}	C''_{1b}	C_3	C''_2	C_n	C_m
21	90	2	146,800	0.33	6	22,932	0.32	4	85,137	1.63	49	480,455	75,438	405,017	1.613	251,095	46,769
22	90	2	29,454	0.31	6	4,907	0.32	4	48,562	1.72	54	102,619	16,141	86,478	1.237	69,909	13,049
23	90	2	27,617	0.32	5	4,666	0.32	3	196,001	1.74	36	92,022	15,154	76,868	1.400	54,913	10,824
24	90	2	19,407	0.32	7	3,443	0.33	5	34,379	1.61	57	64,542	11,125	53,417	1.156	46,208	9,624

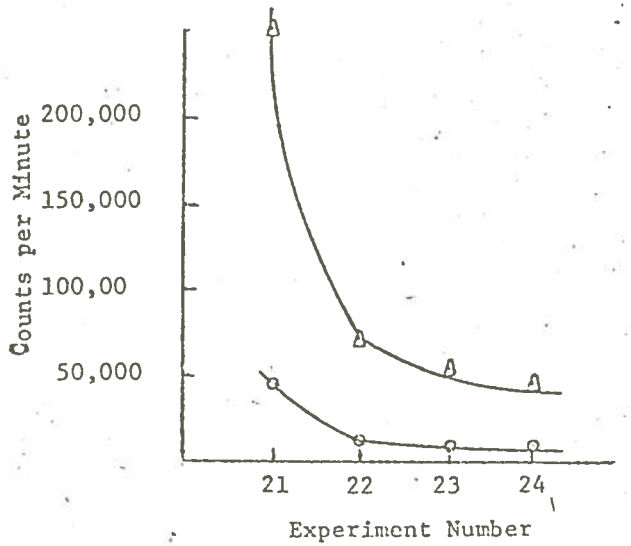

GRAPH XVII

Fast and Thermal Neutron Counts
Comparisons of Experiments 21-24

Δ - Thermal

o - Fast

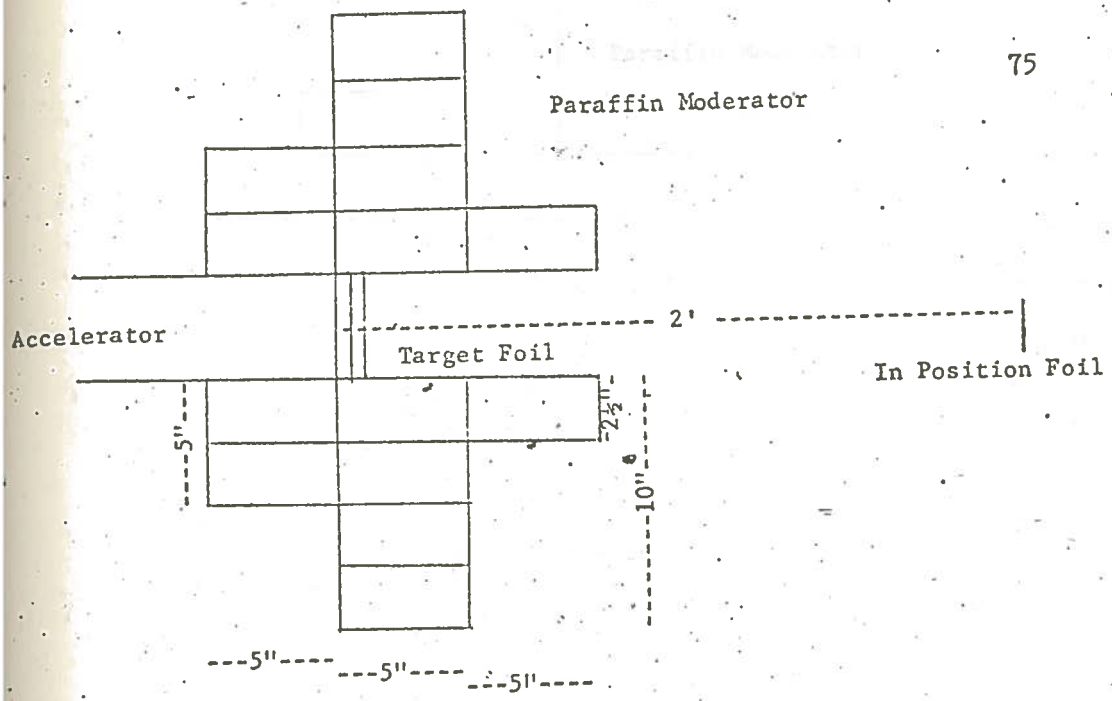

Figure 26
Experiment 21

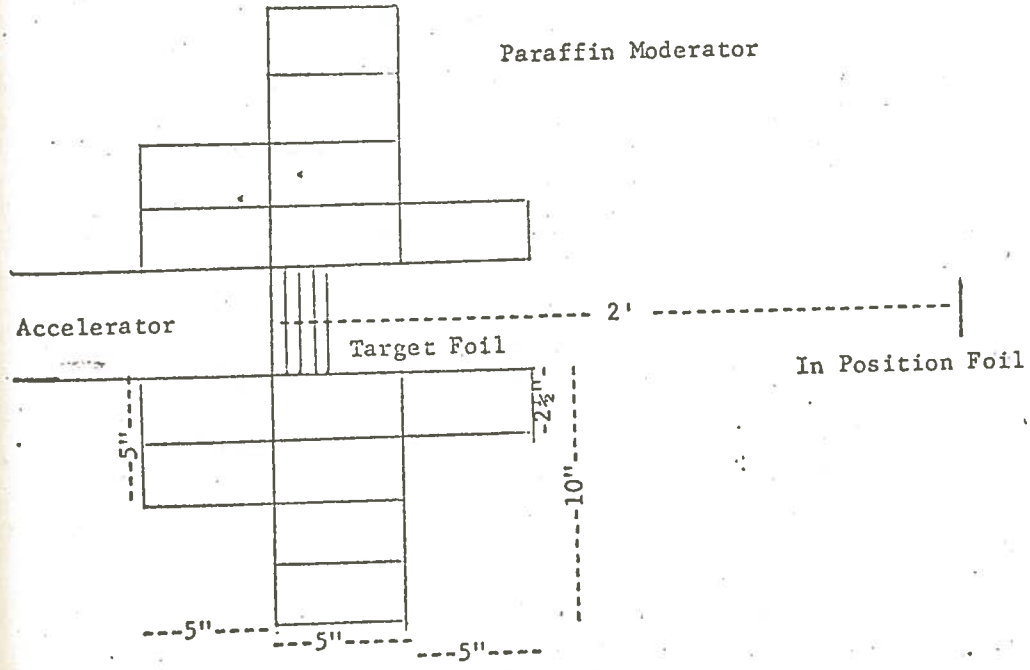

Figure 27
Experiment 22

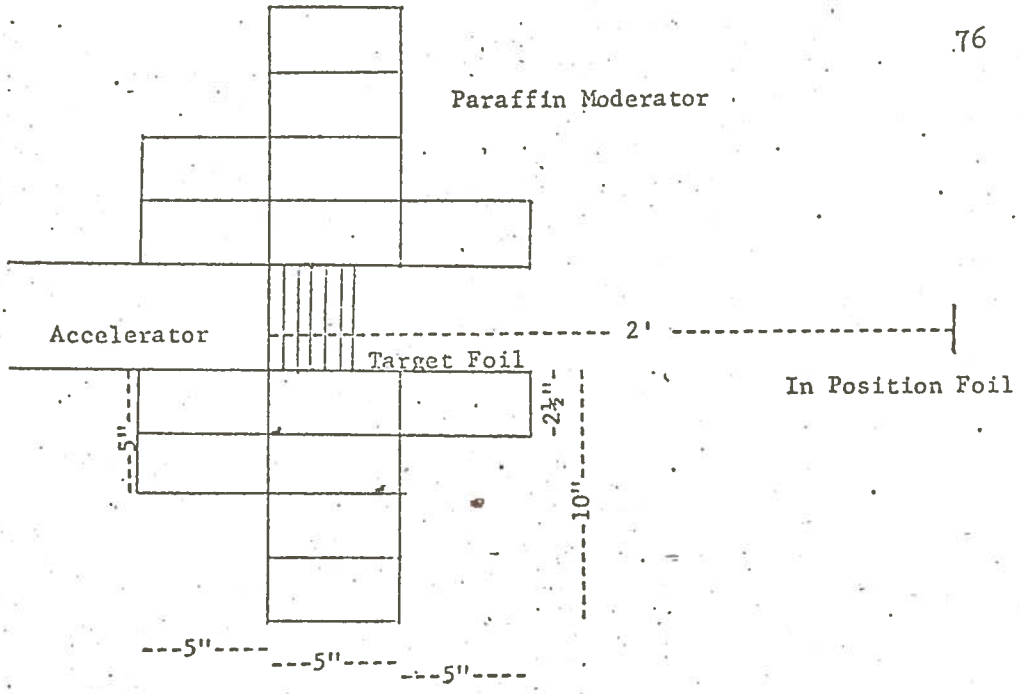

Figure 28
Experiment 23

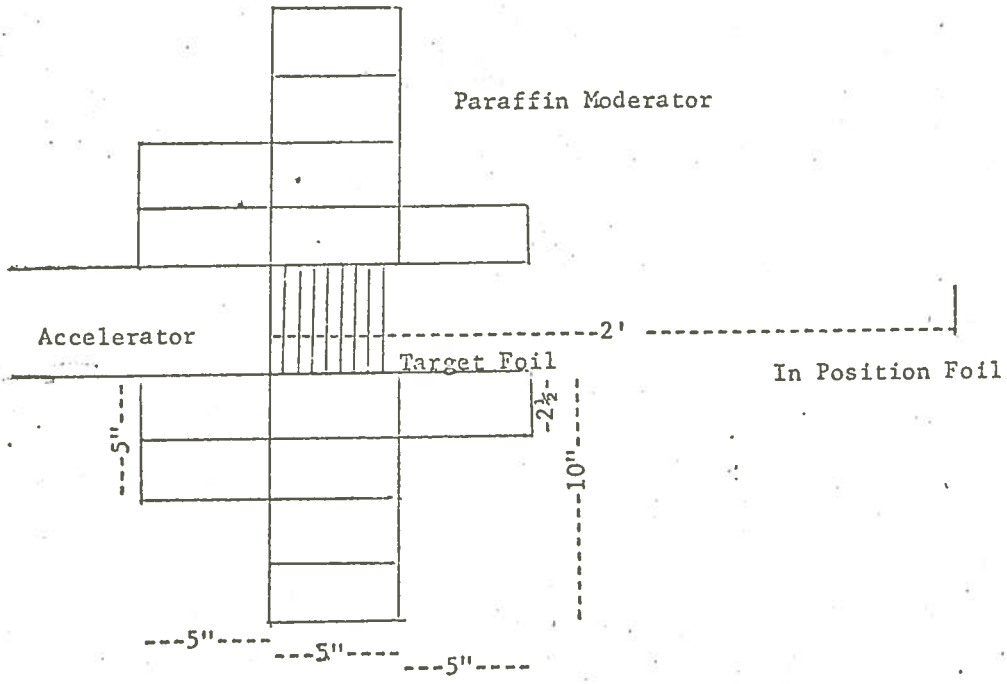

Figure 29
Experiment 24

SERIES III

Subseries 3

Part a

EXPERIMENTS 27-33

EXPERIMENTS 27 - 33

EXPERIMENT	Position ANGLE	Position DISTANCE	C_{1b}	W_{1b}	T_{1b}	C_{1a}	W_{1a}	T_{1a}	C_2	W_2	T_2	C''_{1a}	C''_{1b}	C_3	C''_2	C_n	C_m
27	90	2	10,399	0.31	3	13,988	0.31	8	56,515	2.22	17	50,700	35,210	15,490	28,690	539,909	1,227,257
28	90	2	18,652	0.29	3	57,070	0.29	8	41,204	2.23	15	222,800	69,280	153,520	20,280	7,570,020	3,416,174
29	90	2	24,460	0.31	3	77,238	0.34	8	41,326	2.07	15	253,300	86,130	167,170	22,000	7,598,636	3,915,000
30	90	2	14,679	0.32	3	43,125	0.30	8	25,458	2.13	15	157,500	47,750	109,750	13,160	8,339,666	3,628,419
31	90	2	24,066	0.31	3	74,253	0.31	8	39,884	2.09	15	268,500	88,000	180,500	20,970	8,607,535	4,196,471
32	90	2	20,085	0.31	3	70,562	0.34	8	33,953	2.17	15	227,100	71,150	155,950	17,170	9,082,702	4,143,856
33	90	2	14,720	0.30	3	47,868	0.30	8	23,434	2.14	15	176,600	52,000	124,600	12,000	10,331,675	4,311,774

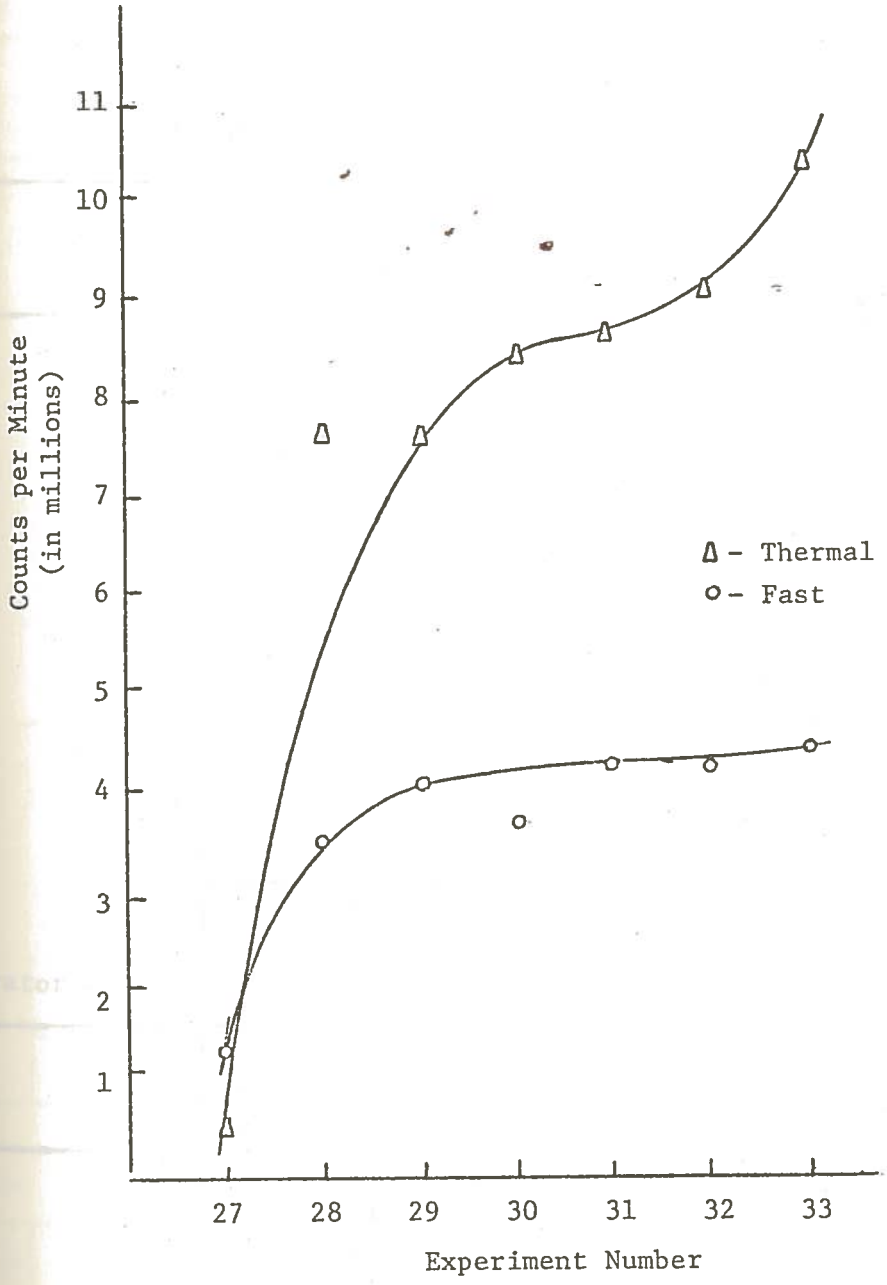

GRAPH XVIII

Fast and Thermal Neutron Count
Comparisons of Experiments 27-33

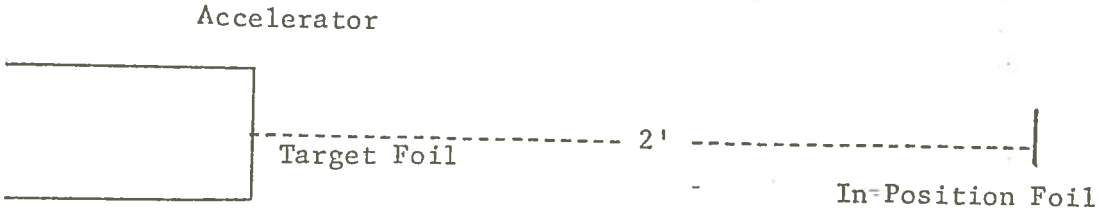

Figure 30
Experiment 27

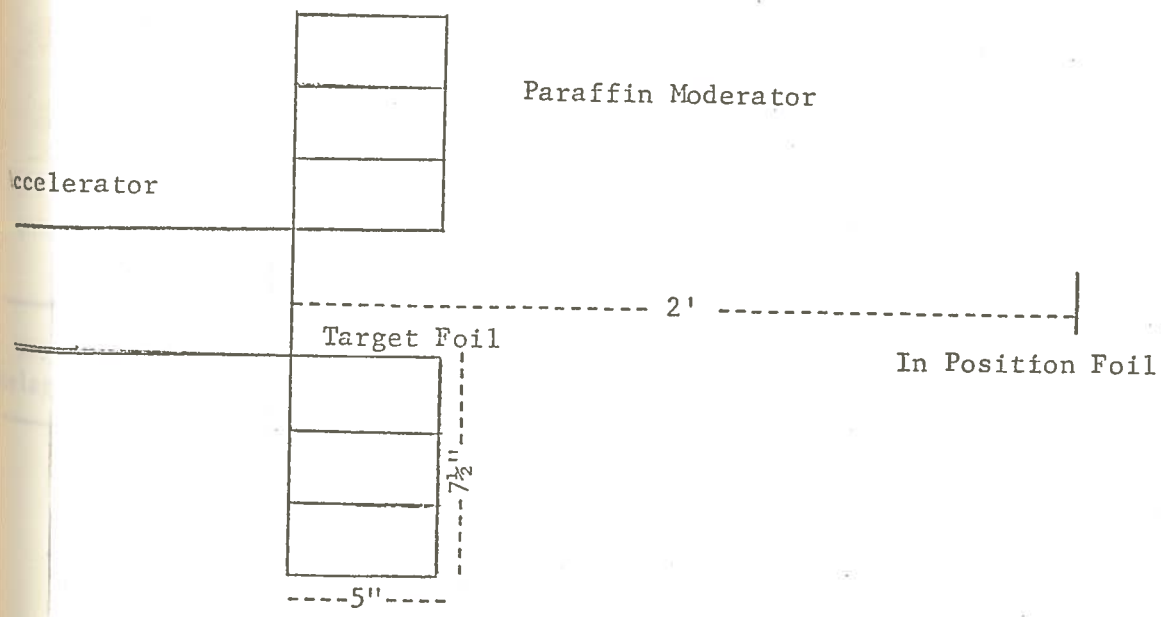

Figure 31
Experiment 28

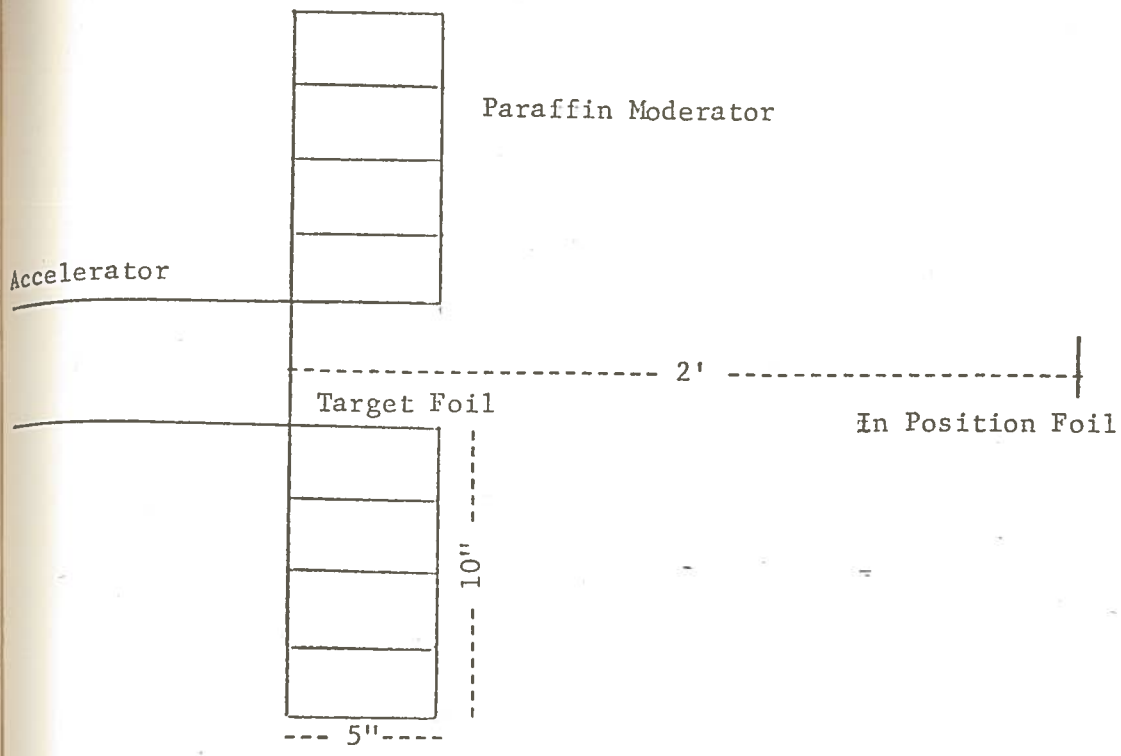

Figure 32
Experiment 29

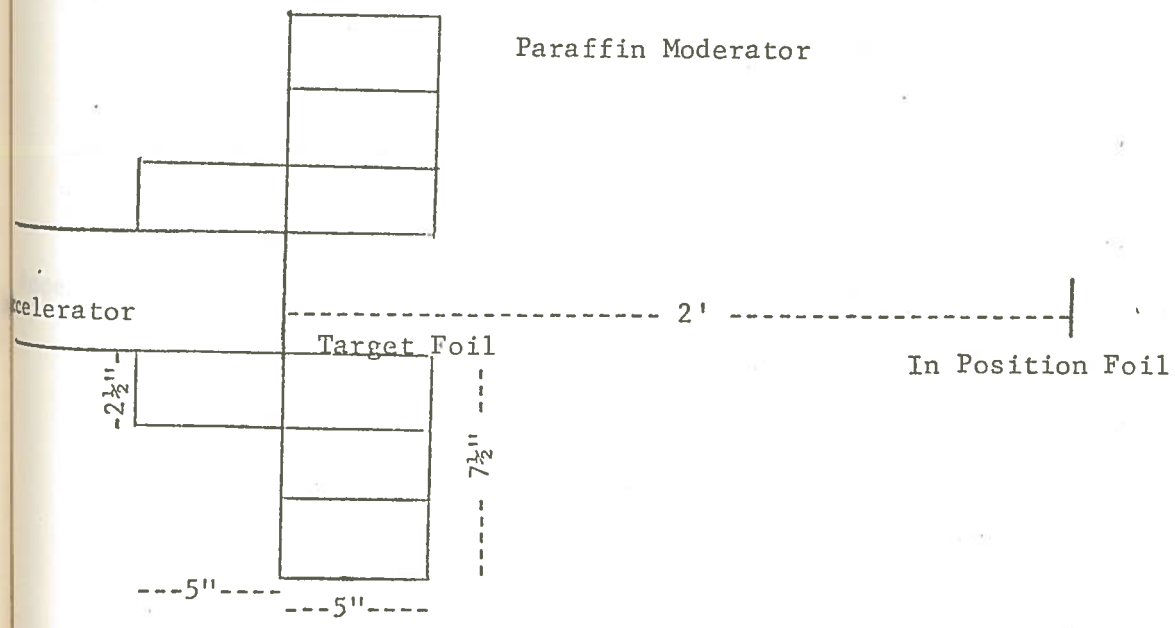

Figure 33
Experiment 30

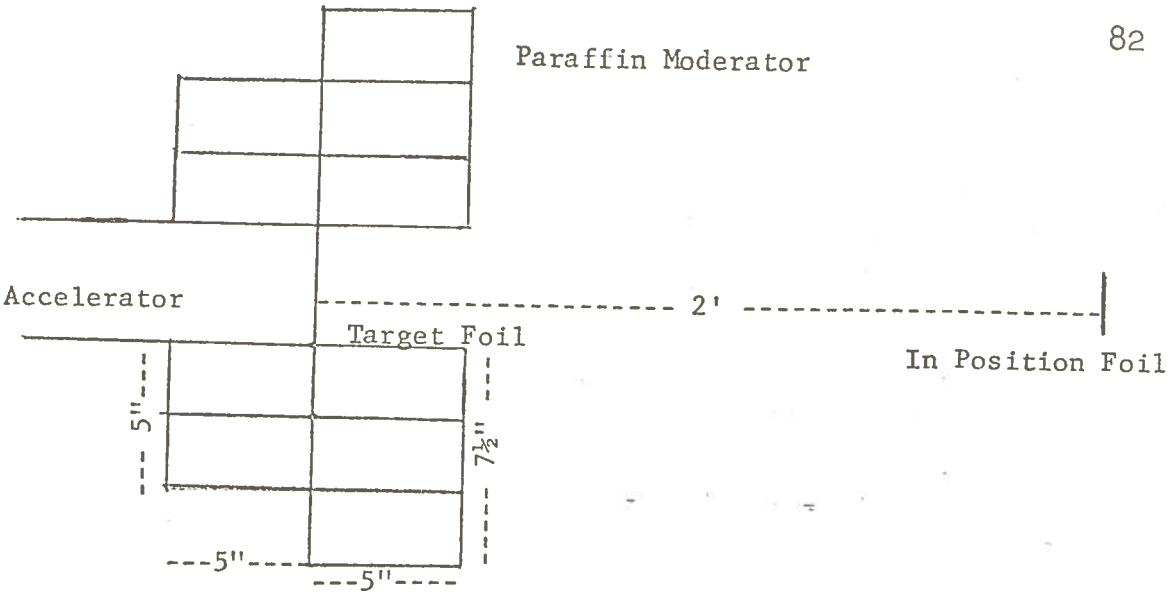

Figure 34
Experiment 31

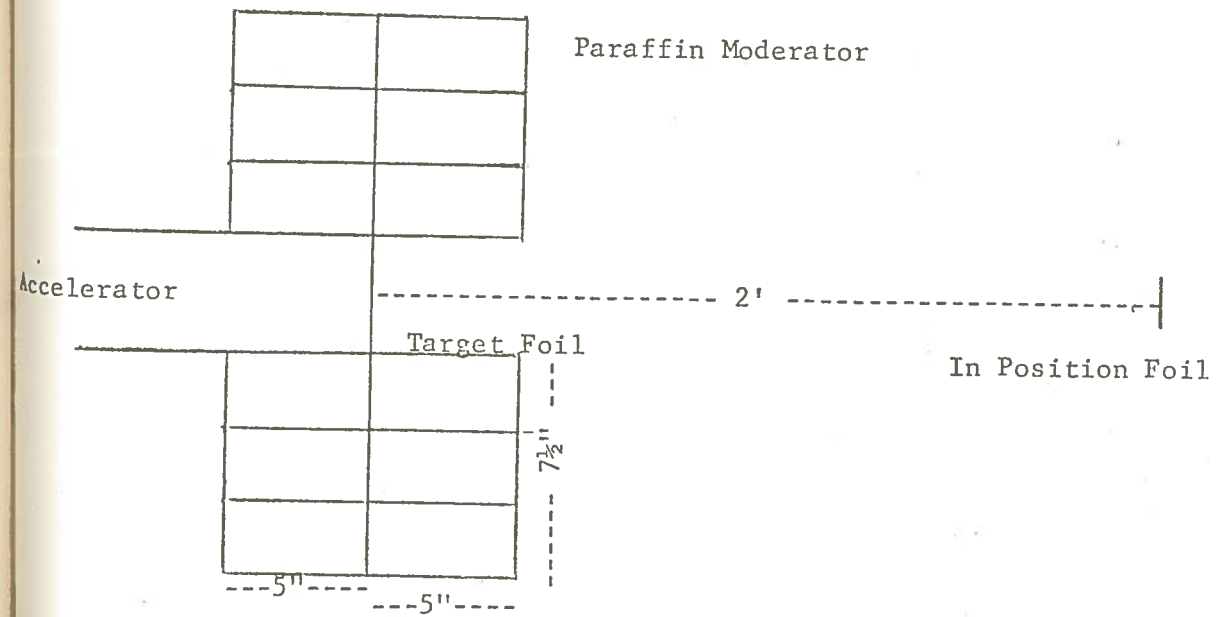

Figure 35
Experiments 32 and 33

SERIES III

Subseries 3

Part b

EXPERIMENTS 34-37

EXPERIMENTS 34 - 37

EXPERIMENT NUMBER	ANGLE	DISTANCE	C_{1a}	W_{1a}	T_{1a}	C_{1b}	W_{1b}	T_{1b}	C_2	W_2	T_2	C''_{1a}	C''_{1b}	C_3	C''_2	C_n	C_m
34	90	2	46,796	0.30	8	14,714	0.30	3	32,575	2.06	15	172,500	50,900	121,600	17,400	6,938,506	2,925,287
35	90	2	43,280	0.28	8	13,968	0.30	3	30,811	2.04	15	186,300	49,100	137,200	16,600	8,257,030	2,957,831
36	90	2	61,288	0.29	8	19,779	0.31	3	34,705	2.10	15	231,000	66,600	164,400	18,050	9,108,033	3,689,751
37	90	2	46,621	0.31	8	12,363	0.33	3	25,570	2.10	15	156,800	41,600	115,200	13,370	8,616,305	3,111,444

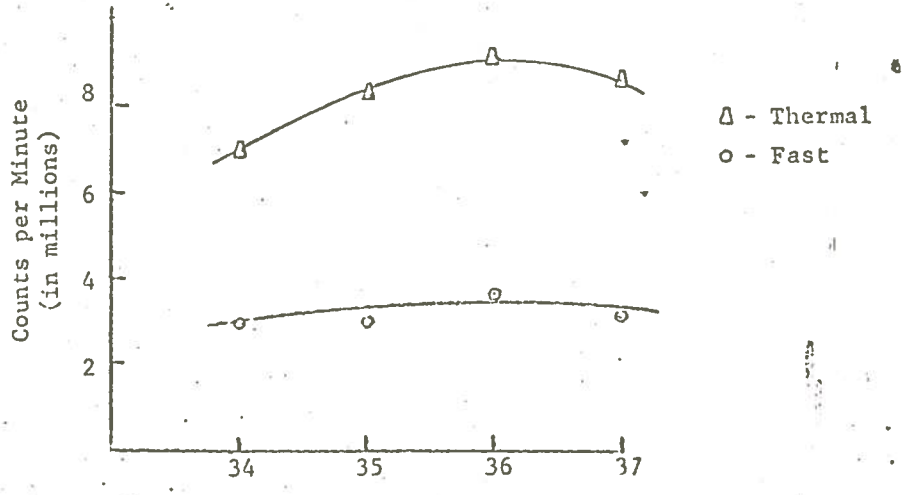

GRAPH XIX

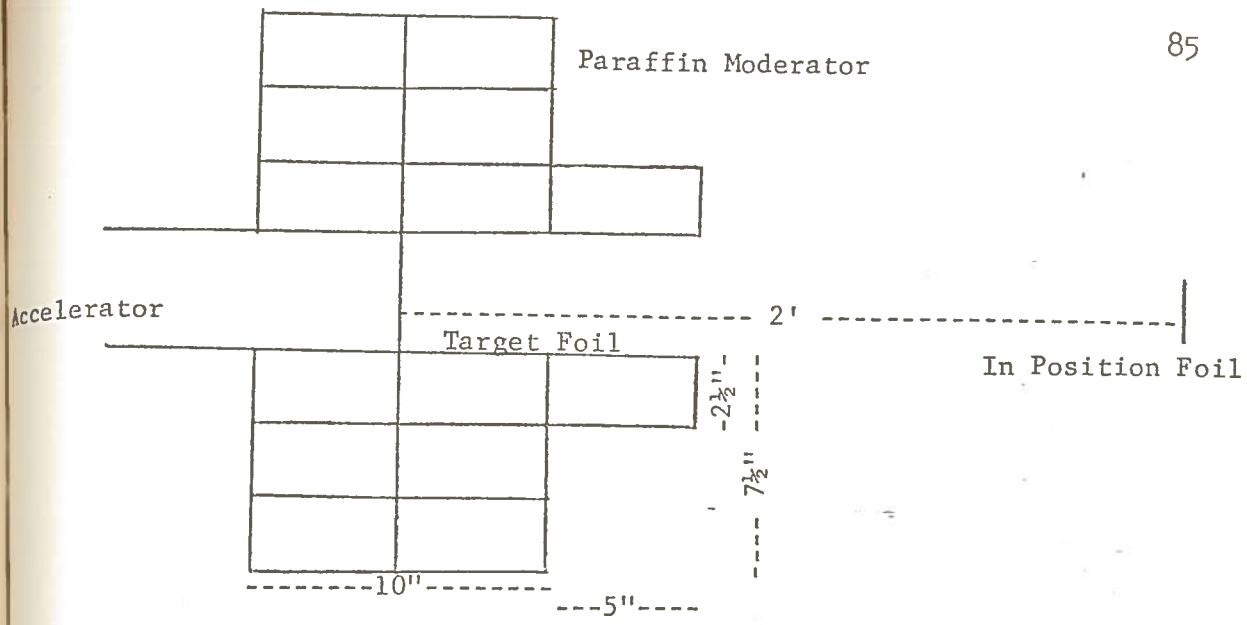

Figure 36
Experiment 34

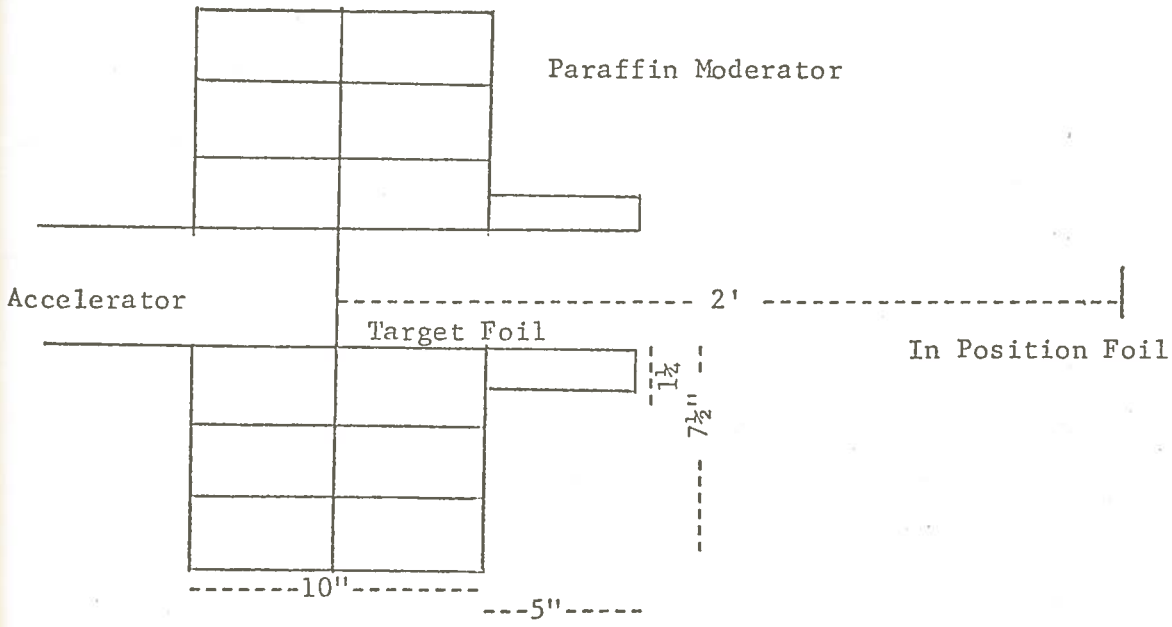

Figure 37
Experiment 35

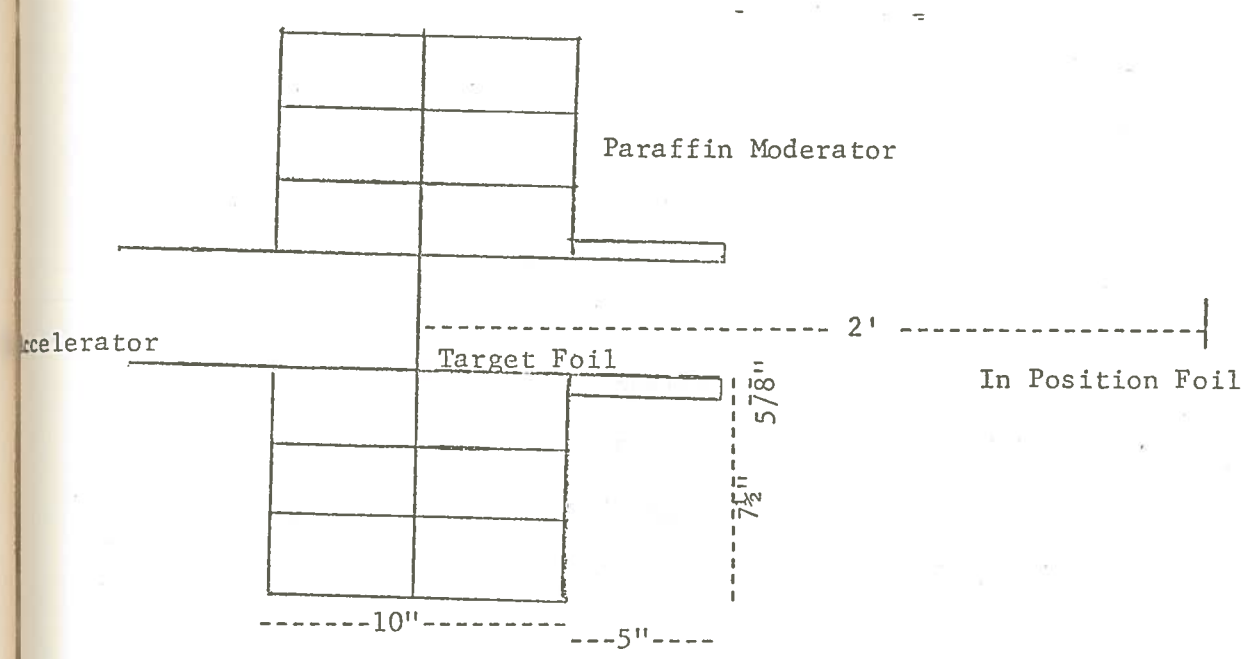

Figure 38
Experiments 36 and 37

SERIES III

Subseries 3

Part c

EXPERIMENTS 41-45

EXPERIMENTS 41 - 45

EXPERIMENT NUMBER	ANGLE	DISTANCE	C_{1a}	W_{1a}	T_{1a}	C_{1b}	W_{1b}	T_{1b}	C_2	W_2	T_2	C''_{1a}	C''_{1b}	C_3	C''_2	C_n	C_m
41	90	2	50,446	0.29	8	15,125	0.28	3	29,323	2.17	15	194,700	56,000	138,700	14,840	9,346,361	3,773,585
42	90	2	75,600	0.32	8	22,201	0.32	3½	36,460	2.12	15	259,000	72,170	186,830	18,920	9,874,736	3,814,482
43	90	2	51,131	0.30	8	14,000	0.30	3	23,969	2.09	16	187,300	48,820	138,480	12,660	10,938,389	3,856,240
44	90	2	68,786	0.33	8	17,520	0.31	3	28,940	2.24	15	234,000	59,390	174,610	14,220	12,279,184	4,176,512
45	90	2	59,138	0.30	8	16,881	0.30	3	28,544	2.03	15	218,100	58,200	159,900	15,475	10,332,795	3,760,905

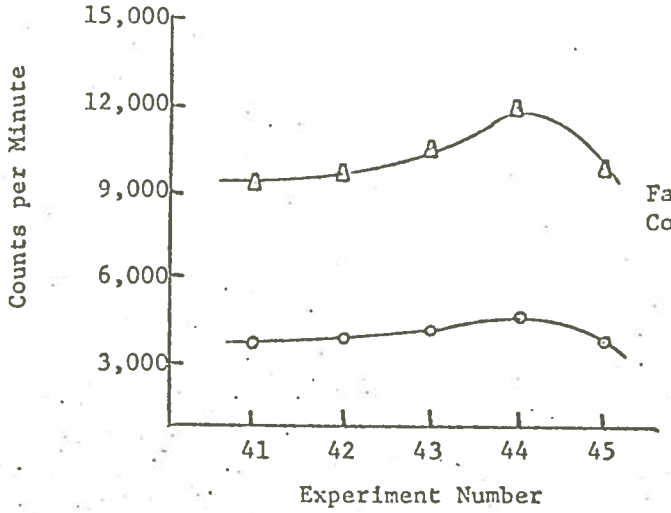

GRAPH XX

Fast and Thermal Neutron Counts
Comparisons of Experiments 41-45

Δ - Thermal

o - Fast

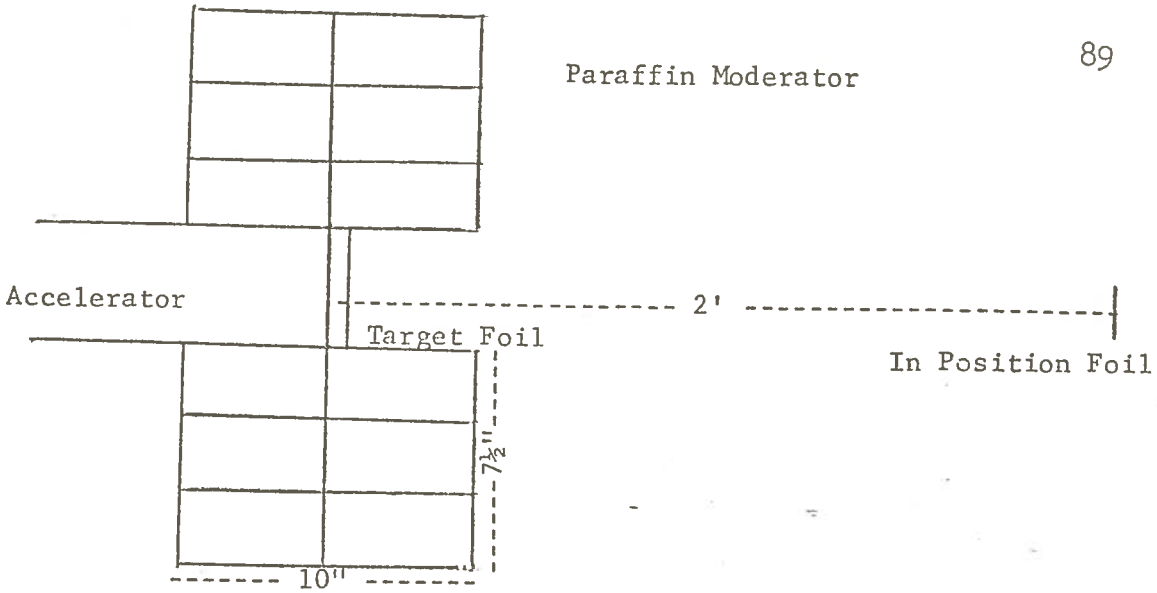

Figure 39
Experiment 41

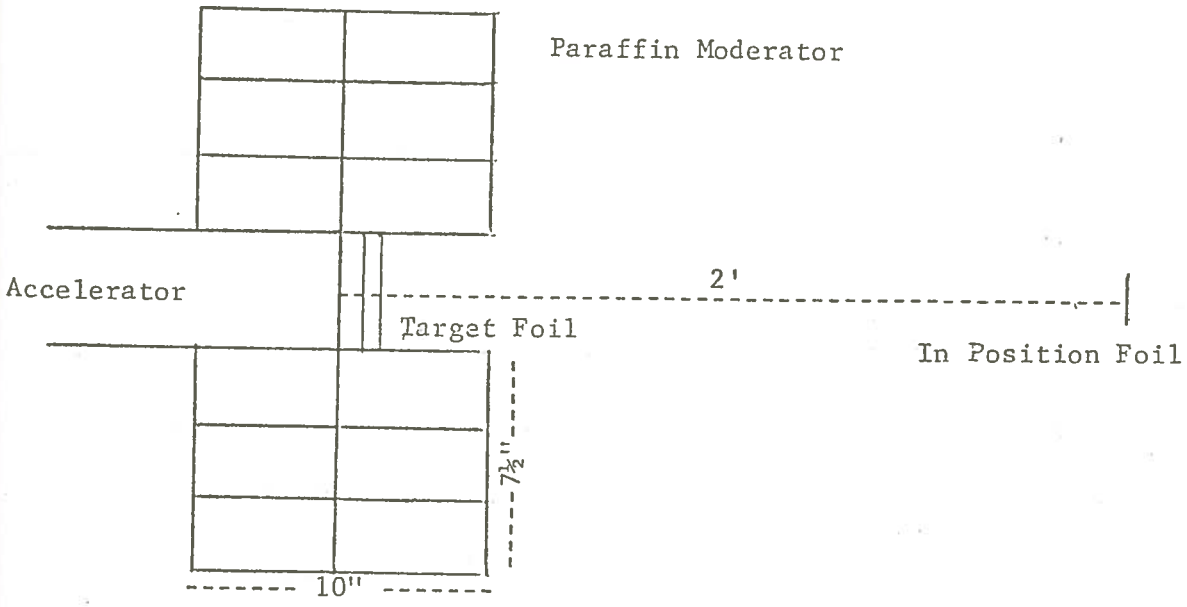

Figure 40
Experiments 42 - 43

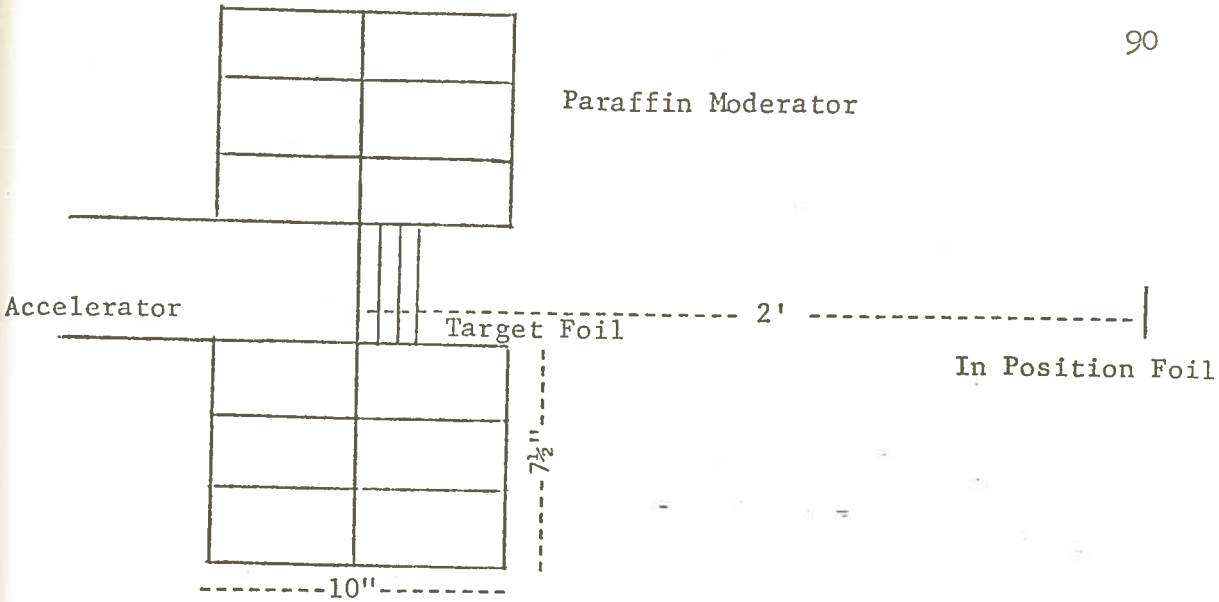

Figure 41
Experiment 44

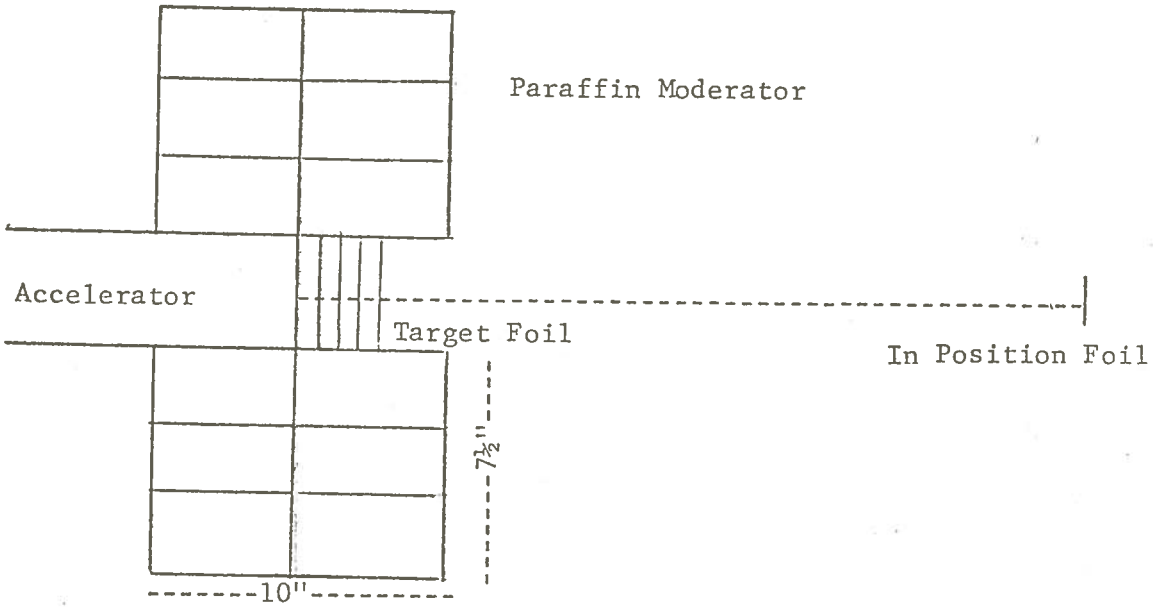

Figure 42
Experiment 45

SERIES III

Subseries 3

Part d

EXPERIMENTS 38-40

EXPERIMENTS 38 - 40

EXPERIMENT NUMBER	ANGLE	DISTANCE	C_{1a}	W_{1a}	T_{1a}	C_{1b}	W_{1b}	T_{1b}	C_2	W_2	T_2	C''_{1a}	C''_{1b}	C_3	C''_2	C_n	C_m
38	90	8	5,610	0.31	14	2,312	0.31	3	72,395	2.14	25	21,980	7,660	14,320	39,530	362,257	193,777
39	90	8	5,519	0.31	14	2,374	0.33	3	70,249	2.11	25	21,240	7,580	13,660	39,050	349,808	194,110
40	90	8	3,936	0.30	14	1,888	0.33	3	57,007	2.11	25	15,870	5,935	9,935	31,700	313,407	187,224

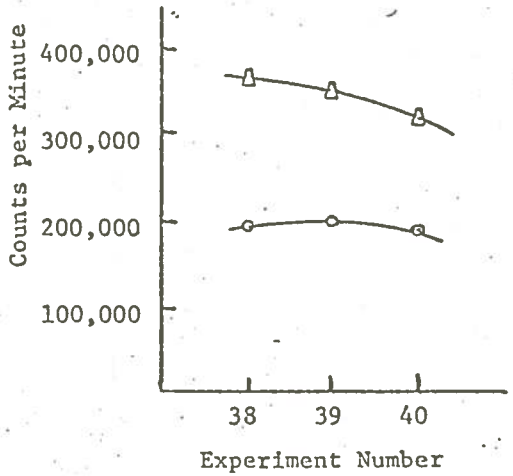

GRAPH XXI

Fast and Thermal Neutron Counts
Comparisons of Experiments 38-40

Δ - Thermal

o - Fast

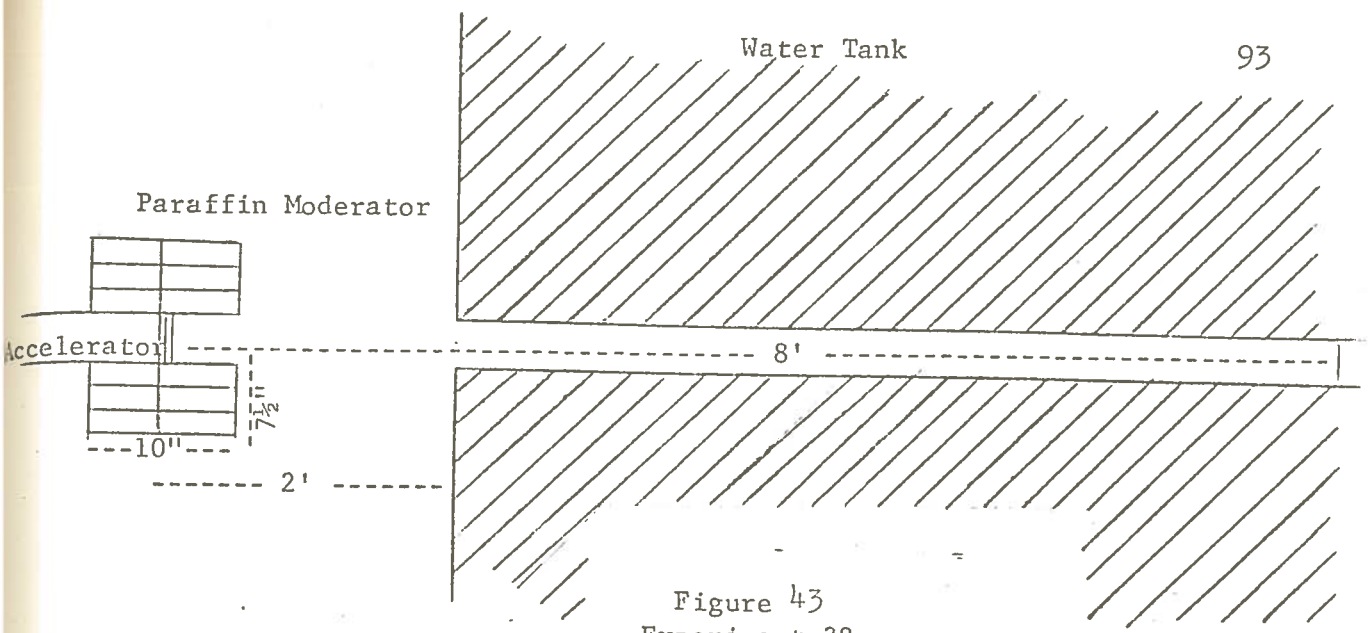

Figure 43
Experiment 38

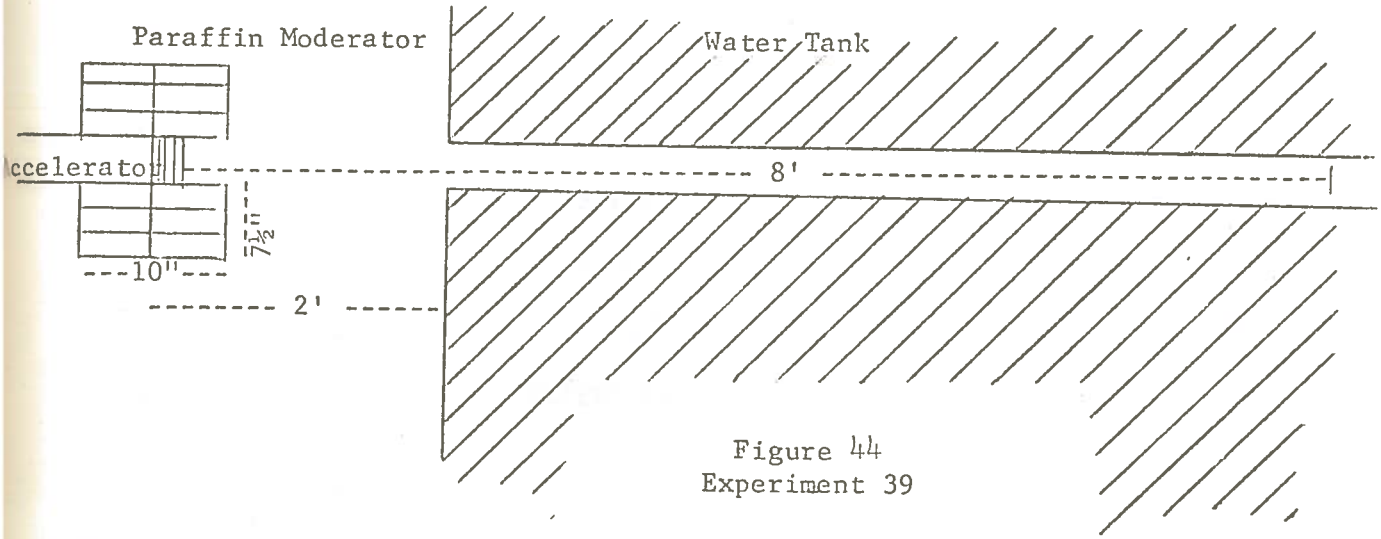

Figure 44
Experiment 39

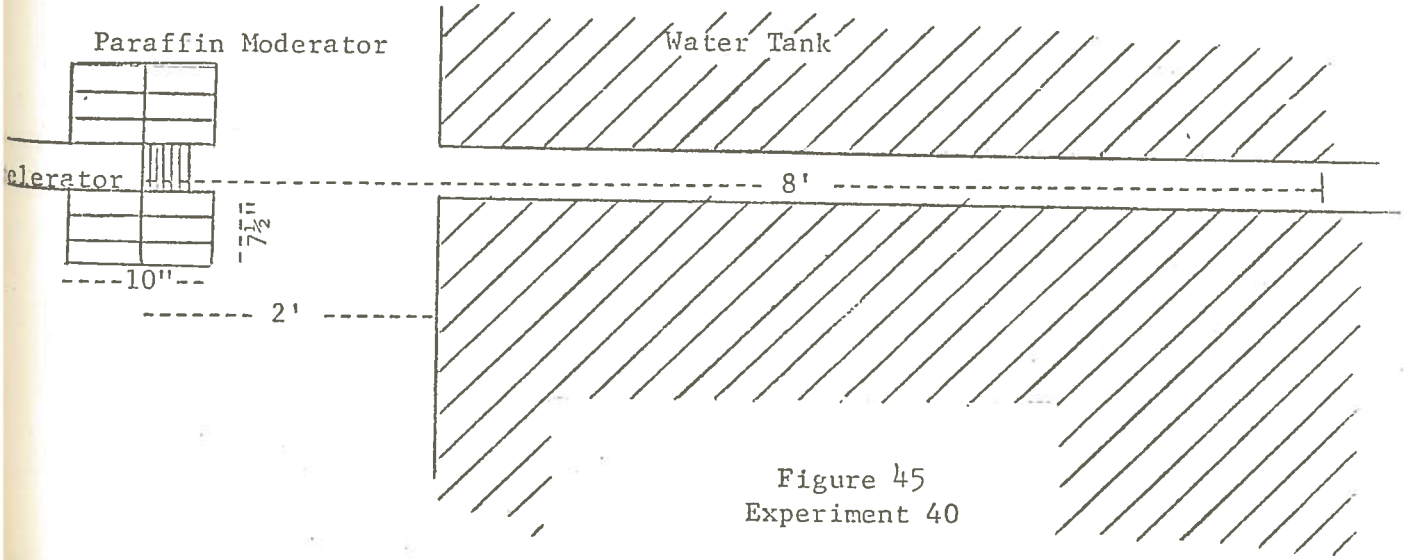

Figure 45
Experiment 40

SERIES III

Subseries 3

Part e

EXPERIMENTS 46-49

EXPERIMENTS 46 - 49

EXPERIMENT	ANGLE	DISTANCE	C_{1a}	W_{1a}	T_{1a}	C_{1b}	W_{1b}	T_{1b}	C_2	W_2	T_2	C''_{1a}	C''_{1b}	C_3	C''_2	C_n	C_m
46	90	2	23,302	0.30	8.0	9,975	0.30	3.0	27,648	2.09	16.0	85,900	34,150	51,750	14,600	13,544,521	2,339,041
47	90	2	60,151	0.30	10.0	12,772	0.31	5.0	22,696	2.22	15.0	192,000	44,050	147,950	11,240	13,162,811	3,919,039
48	90	2	60,151	0.30	10.0	13,134	0.30	5.0	21,906	2.23	15.0	228,000	47,500	180,500	10,780	16,743,970	4,406,308
49	90	2	64,029	0.30	10.5	13,012	0.30	5.5	19,999	2.07	15.5	243,800	46,320	197,480	10,680	18,490,637	4,337,079

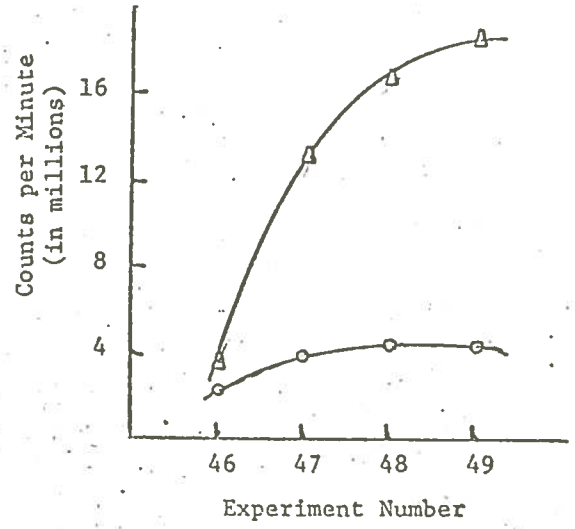

GRAPH XXII

Fast and Thermal Neutron Counts
Comparisons of Experiments 46-49

Δ - Thermal

o - Fast

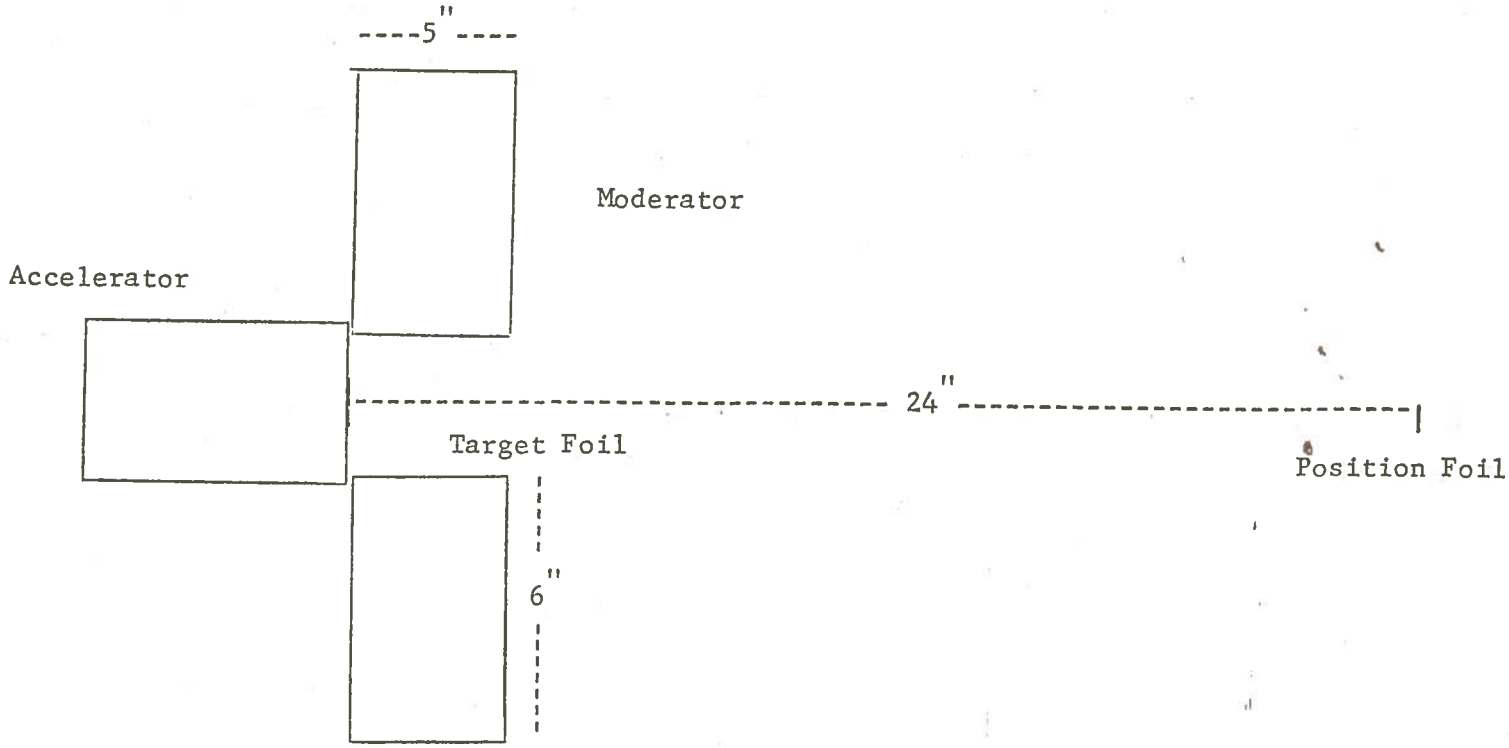

Figure 46
Experiment 46

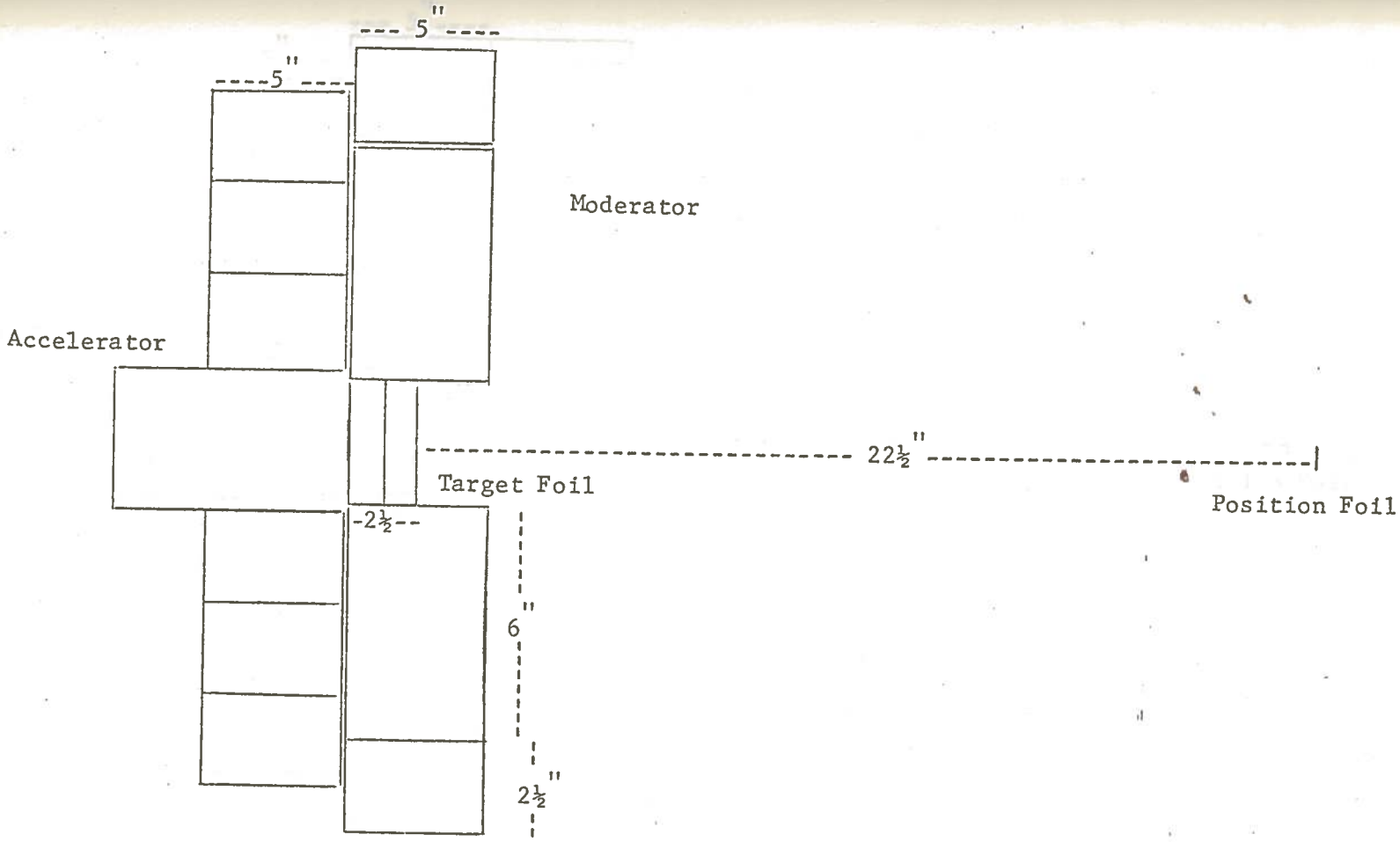

Figure 47
Experiment 47

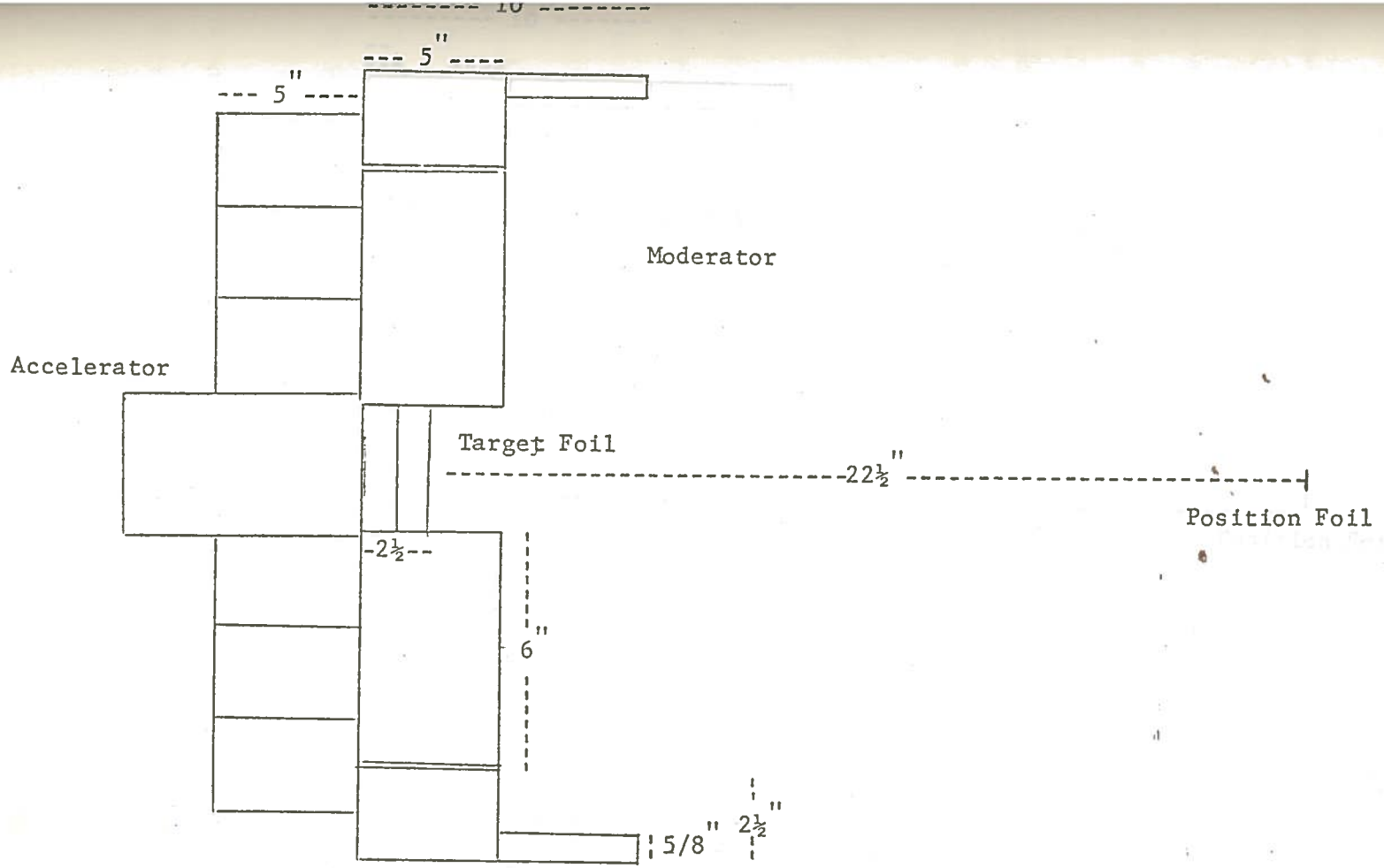

Figure 48
Experiment 48

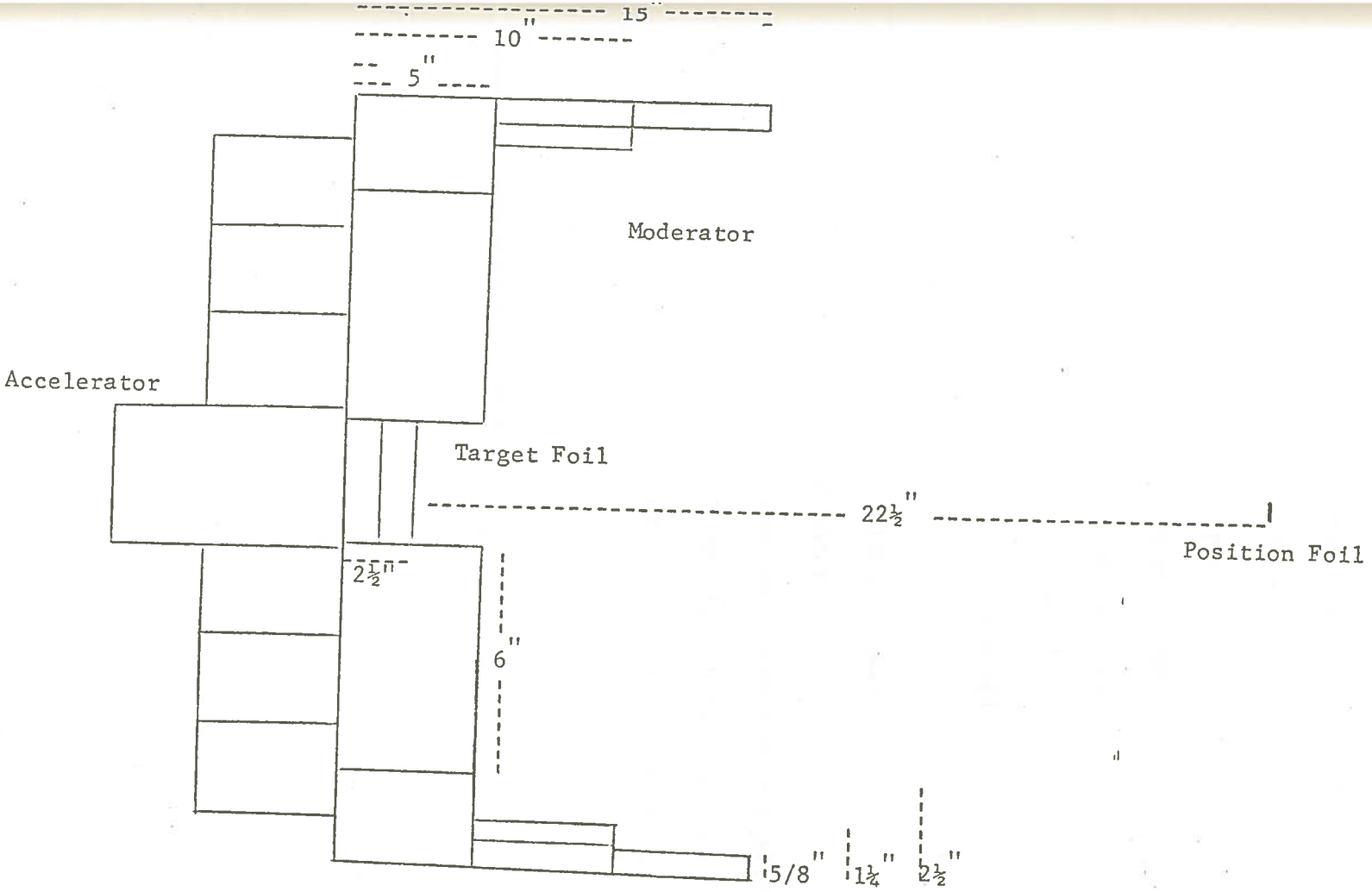

Figure 49
Experiment 49

CHAPTER V

DATA ANALYSIS

As stated previously, three series of experiments were run. The first series had three objectives:

(1) to determine the importance of the deuterium beam positioning on the tritium target with regard to fast neutron distribution produced by the irradiation of the target.

(2) to obtain the fast neutron distribution before any moderating media, other than the target assembly, was placed around the target.

(3) to determine the effect on fast neutron distribution by hemispherical hydrocarbon moderators.

The second series of experiments dealt with similar considerations as the first series, except that thermal neutrons (neutrons with energy less than 0.41 eV) were considered. The objectives included:

(1) to obtain the thermal neutron distribution before any moderating media, other than the target assembly, was placed around the target.

(2) to determine the effect on thermal neutron distribution by hemispherical hydrocarbon moderators.

Finally, the third series of experiments dealt with developing a moderator design that maximized the thermal neutron counts at a predetermined position about the target. The third series has been

divided into three subseries. The first two subseries make use of a copper disc as the target foil, while the final subseries uses a Teflon strip.

The positioning of the indium foils was predicated on the considerations of:

(a) statistical accuracy in number of counts obtained from the irradiated foil,

(b) need for space to place different sized moderator designs, and

(c) reduction in geometry errors introduced in determining the center of the deuterium beam striking the target and the positioning of the indium foils.

As a result of these considerations the position selected in the first subseries was three feet from the target in the direction of a normal from the center of the irradiated target. In the second and third subseries, the position was two feet from the target in the direction of the normal described above. The only exception was Part d of the third subseries in which fast and thermal neutron distribution after collimation of the neutron beam was studied. In that part the position was eight feet from the target in the direction of the same normal.

A. Consideration of Target Foil Material

1. Copper Foils - As discussed in Chapter III the particular reactions of interest when irradiating the copper foil are:

$Cu^{63}(n,2n)Cu^{62}$ and $Cu^{65}(n,2n)Cu^{64}$. Both Cu^{62} and Cu^{64} are unstable and decay by position emission. Then emitted positions annilate producing two 0.511 MeV photons. It is these photons which are detected by the NaI(Tl) scintillation counter. With such a counter it is not possible to distinguish between the photons produced by the Cu^{62} and Cu^{64}. However for delay times less than thirty minutes, it can be assumed that the majority of the photons are produced from the $Cu^{63}(n,2n)Cu^{63}$ reaction.

This assumption is based on the fact that the copper disc contains 70% Cu^{63} and only 30% Cu^{65}. Also, the total absorption cross-section of Cu^{63} is 4.5 barns, and that of Cu^{65} only 2.2 barns. Finally, the Cu^{62} decays at a more rapid rate (halflife of 9.9 minutes) than Cu^{64} (halflife of 12.9 hours).

This relationship between the number of photons produced by Cu^{62} versus Cu^{64} is important because the normalization of the data is based on the assumption that all the photons were produced by the decay of Cu^{62}. Therefore, when the assumption loses validity the normalized data must be suspect. The longer the delay time the less valid the assumption. This fact must be considered in analyzing the data.

For an example illustrating the interference caused by the decay of Cu^{64} compare Experiment 3 with Experiment 4. These are identical experiments except for the increase in delay time in Experiment 4.

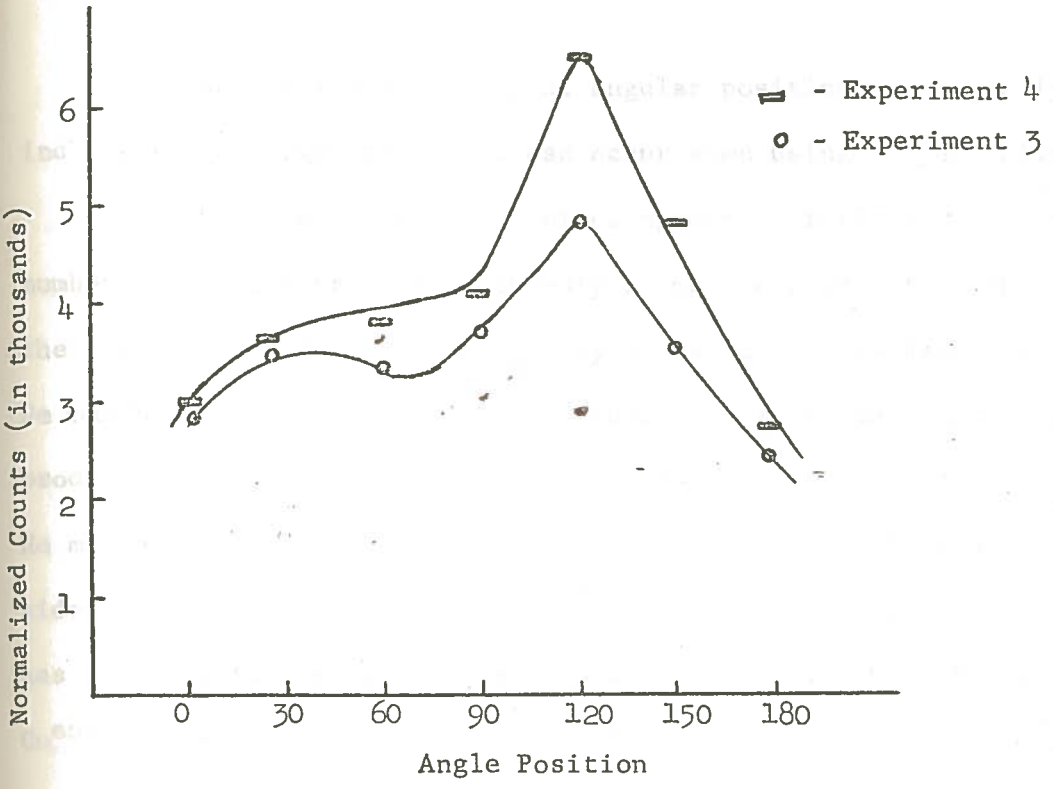

Figure 50
The Importance of Delay Time When Using Copper Foils as Illustrated by Comparison of Experiment 3 with Experiment 4.

The foils were irradiated at the same time. Then the foils were counted, starting with the foil at angular position 0 and ending at position 180. After the foils were counted once, the foils were counted again in the same order as before. This second count comprises the data in Experiment 4.

The normalized data is statistically within two standard deviations for angular positions 0 and 30. However the deviation is greater for all other angular positions. The amount of deviation is expressed more clearly in the following table.

ANGULAR POSITION	0	30	60	90	120	150	180
DIFFERENCE IN σ	1.5	1.4	4.9	4.6	24.1	4.4	6.0

The great discrepancy at angular position 120° clearly indicates the large error that can occur when using copper foils.

The primary advantage of using copper foils is the large number of photons produced with only a small copper foil. This allows the experimenter greater flexibility in designing his experiments. He may place the foils at great distances from the source and still produce enough photons so that statistical error is not a problem. He may also make use of small foils. This will aid if geometry considerations are important. In fast neutron detection, the copper foil has the advantage of a high threshold energy (11.01 MeV) for the $Cu^{63}(n,2n)Cu^{62}$ reaction. This fact implies that there will be few photon produced by scattered neutrons activating the copper foil. Therefore, non-uniform scatter introduces little error in fast neutron determinations.

2. Fluorine Containing Foils - The reaction of primary interest is $F^{19}(n,2n)F^{18}$. As do the Cu^{62} and Cu^{64}, F^{18} decays by positron emission. The resulting photons are then counted. The advantage of using fluorine containing materials is that there is only one stable isotope of fluorine. Therefore, there is no interference in the photon counts by the decay of other isotopes, provided the other materials in the foil don't result in photon production upon decay.

As for copper, the threshold of the $F^{19}(n,2n)F^{18}$ reaction is high (threshold of 10.99 MeV). Thus, primarily only photons produced by unscattered neutrons will be detected. As stated before, this reduces the error due to non-uniform neutron scattering.

The fluorine containing material selected was Teflon. This material was selected because of ready availability and it contained an appreciable amount of fluorine. Teflon had another advantage in that it could be easily cut to the size desired.

The primary disadvantage to Teflon is the inconsistency of the chemical composition from batch to batch and from one manufacturer to another. For this reason care must be taken to use Teflon from the same manufacturer and from the same batch. This was done in selecting the Teflon for the experiments run.

The use of Teflon has other disadvantages. The total neutron absorption cross-section for fluorine is 0.09 barns. This means that fewer photons will be produced than with copper foils of the same size. Also the amount of fluorine in the Teflon strip is less than 70% of the amount of Cu^{63} in a copper foil. This too would result in fewer photons produced than a copper foil. Therefore, the flexibility in designing the experiments is restricted. These disadvantages can be overcome because of the long half-life of F^{18} (half-life of 110 minutes). The long half-life allows one to take long photon counts without having to worry about interference in the photon counts, as occurs when using copper foils.

3. Conclusions As to Foil Use - Copper foils are desirable when the fast neutron flux produced by the accelerator is small at the point where the foil is placed. This would mean at distances far from the accelerator target. This advantage is overshadowed, if the time delay before counting is greater than thirty minutes (about

three half-lifes of Cu^{62}), by the interference caused by the Cu^{64} decay. In this case fluorine containing materials result in more accurate normalized data. Teflon is not the best fluorine containing material available because of the inconsistency in its production.

B. Consideration of Series I Objectives

1. Importance of Deuterium Beam Position - In Experiment 1 the deuterium beam was not centered on the target. The exact position is seen in photograph 5 .

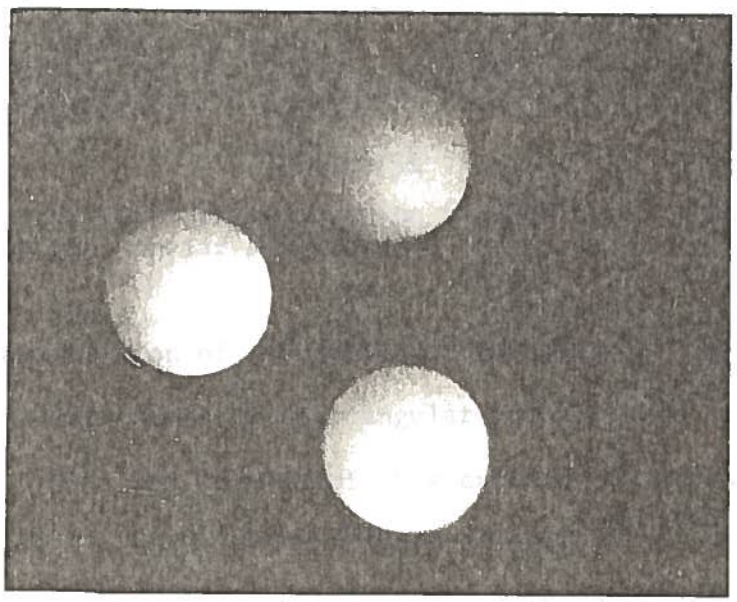

Photograph 5

Neutron Radiographs Taken with 30, 60, and 120 Second Exposures Indicating the Position of the Deuterium Beam on the Target in Experiment 1

From the photograph it appears that the deuterium beam was below and to the right (when facing the target) of the center of the target. The relationship of the beam to the angular position of the copper foils is seen in figure 51 below:

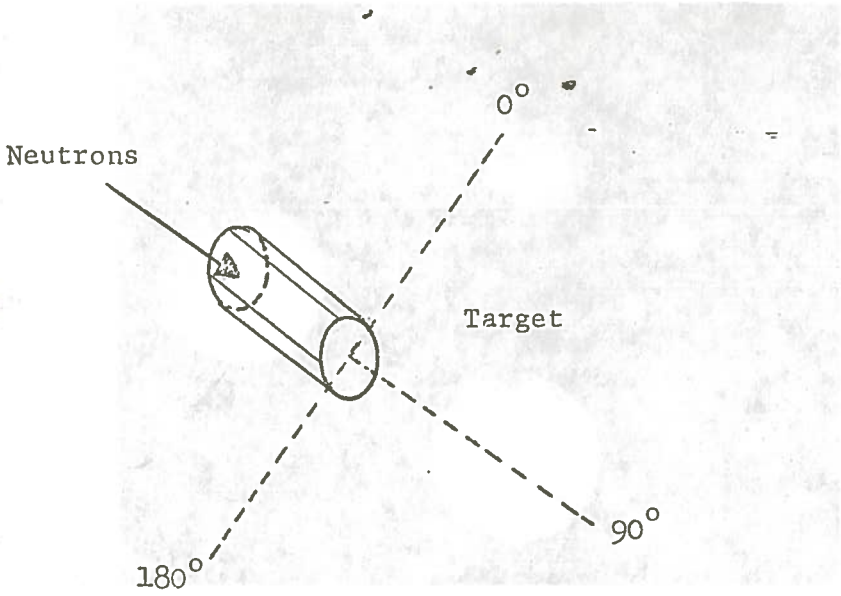

Figure 51

Spacial Relationship Between the Deuterium Beam and the Angular Positions of the Copper Foils

An examination of the graph for Experiment 1 indicates more fast neutrons were detected from angular positions 30° to 90°, than from 90° to 150°. The results of this experiment indicate the importance of the positioning of the deuterium beam.

It should be noted that in none of the data obtained was the time delay greater than thirty minutes. In fact the largest time delay was at position 150° and it was for only 22 minutes. Thus, the interference from Cu^{64} decay should not be a factor.

The data from Experiment 2 is in accord with Experiment 1. In this experiment the deuterium beam was focused closer to the center of the target as seen in photograph 6 below

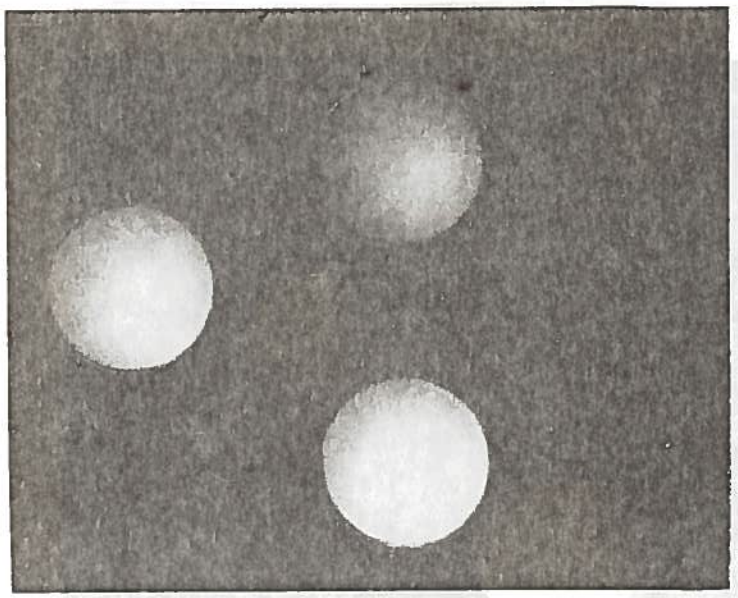

Photograph 6

Neutron Radiographs Taken with 30, 60, and 120 Second Exposures Indicating the Position of the Deuterium Beam on the Target in Experiment 2

There is very little change in the fast neutron distribution, but perhaps slightly more fast neutrons detected in the 30° to 90° region, than the 90° to 120° region.

Experiments 3 and 4 again amplify the proposition that the positioning of the deuterium beam is important in the fast neutron

distribution. In these experiments the deuterium beam has been focused above and to the left of the target center as seen in photograph 7 below.

1 min. 30 sec.

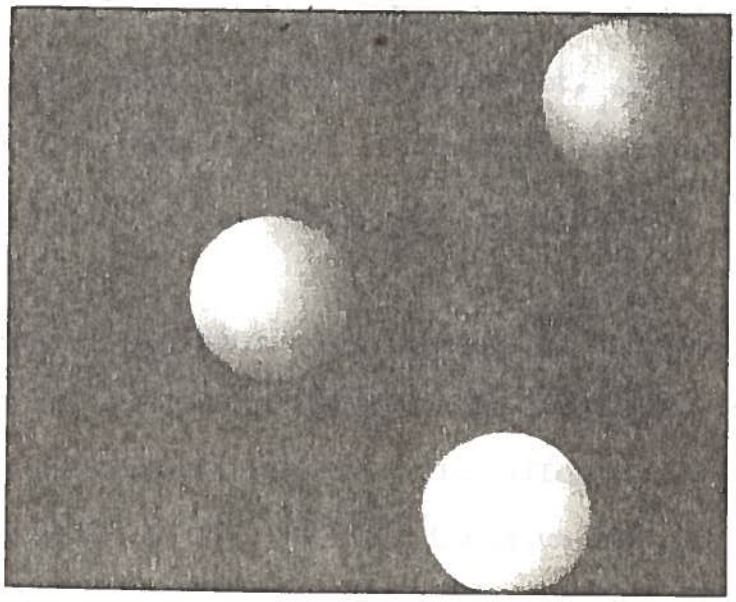

2 min.

Photograph 7

Neutron Radiograph Taken with 30, 60, and 120 Second Exposures Indicating the Positions of the Deuterium Beam on the Target in Experiments 3 and 4

As expected more fast neutrons were detected in the 90° - 150° region, than in the 30° - 90° region. This is clearly seen from the graph of Experiment 3.

From these four experiments this author concludes the positioning of the deuterium beam is important. This merely reinforces a similar conclusion by E.G. Andresen.[34]

2. Preferred Angle Considerations when No Moderator Present - As stated in Chapter II, earlier authors have concluded that there is no preferred angle when no moderator is present. In particular Kenna and Conrad[35] noted the fast neutron flux was lower at angular positions 0^{o} and 180^{o}, due to absorption, scattering by the target assembly.

An examination of the normalized counts in Experiment 2 would indicate that the earlier literature is correct. There was very little change in fast neutron distribution. The difference that does exist can be explained by the fact that the deuterium beam was not centered.

3. Effect of Hemispherical Hydrocarbon Moderator on the Fast Flux Distribution Moderation - In light of the results obtained in the first four experiments the dueterium beam was centered on the target as seen in photograph 8

---

[34]Andresen, Ibid., p. 83.

[35]Kenna, B.T., and F.J. Conrad, Ibid., p. 564-6.

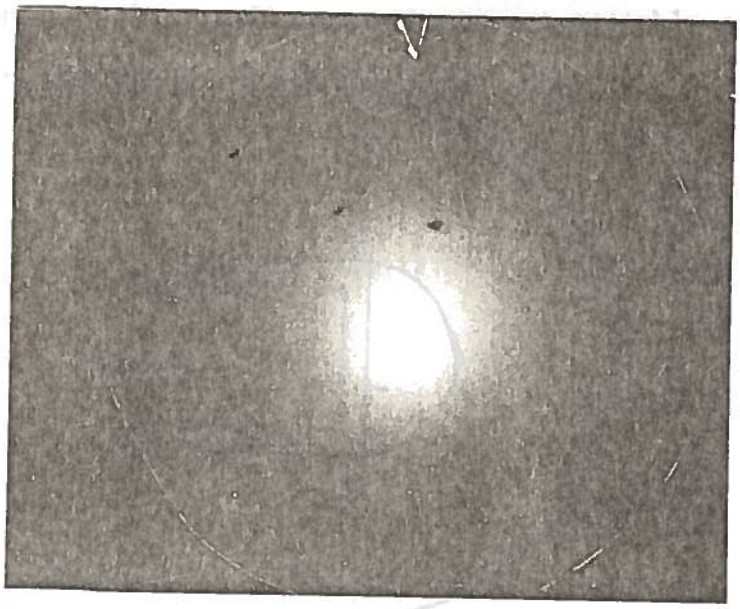

Photograph 8

Neutron Radiograph Taken with 10 Minute Exposure Indicating the Position of the Deuterium Beam on the Target in Experiments 5 and 6

(30 second irradiation; 10 min. exposure)

Another change was made in the next two experiments. Indium foils, instead of copper foils were used. This eliminates the time delay problems experienced with the copper foils.

The difference between Experiment 5 and 6 is the distance of the indium foils from the target. In Experiment 5 they were placed

one foot away, but three feet in Experiment 6. In both experiments a six centimeter polyethylene hemisphere was used on a moderator. It was shaped so that it fit over the target assembly and aligned its edge with the target plane (see figure 52).

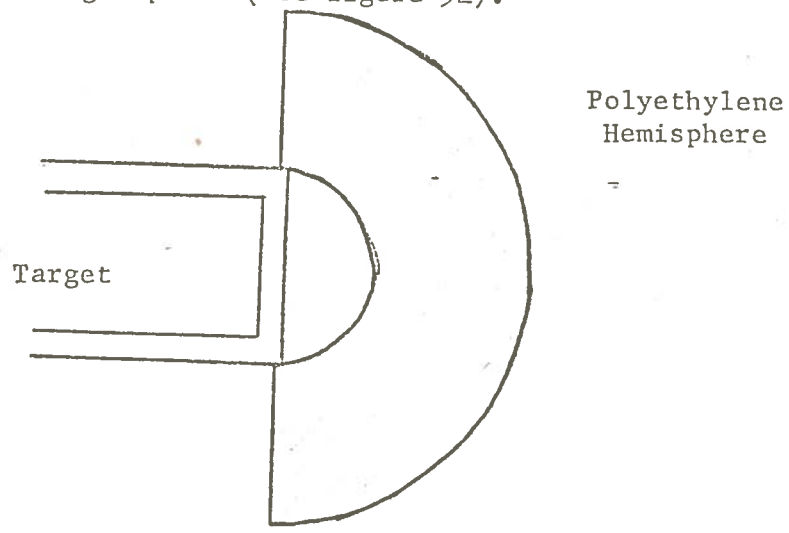

Figure 52

The Position of the Six Centimeter Polyethylene Hemisphere Moderator on the Target Assembly With Relationship to the Target

The decrease in fast neutrons at angle positions 0° and 180° and the rather flat curve from 60°-120° indicate, when contrasting with the flat curve of Experiment 2, that fast neutrons have been deflected from 0-30° to 60°-90° and from 150°-180° to 90°-120°. The symmetrical curves of both Experiment 5 and 6 indicate the scatter from the polyethylene was uniform.

C. Consideration of Series II Objectives

1. Thermal Neutron Distribution Without Moderator - Experiment 7 is the thermal neutron distribution obtained at the same time as the fast neutron distribution in Experiment 2. As in the former experiment no moderator, other than the target assembly, was used.

As seen from the graph of Experiment 7 the thermal neutron distribution curve is relatively flat. This indicates that the target assembly does not effect the fast neutrons to any great extent. The data may also be taken as an indication that backscatter from the floor, walls, and other material near the accelerator is not a serious problem in thermal neutron distribution determinations.

2. Thermal Neutron Distribution With 6 cm Hemispherical Polyethylene Moderator - Experiment 8 is the thermal counterpart of Experiment 5, as is Experiment 9 of Experiment 6. As in both former experiments the six centimeter hemispherical polyethylene moderator was employed.

Comparisons between the fast and thermal neutron distribution curves of the counterpart experiments (see graph XXIII and graph XXIV) reveal several interesting facts.

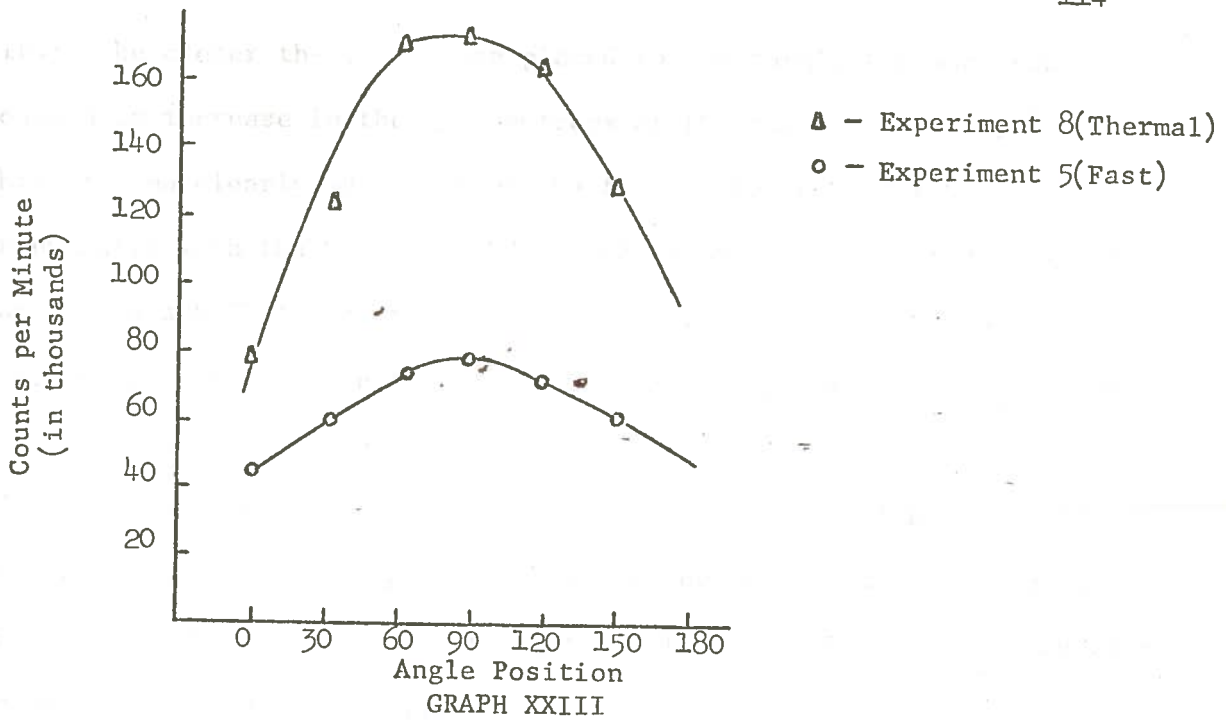

GRAPH XXIII

Comparison Between Thermal and Fast
Neutron Distribution From Experiments 8 and 5

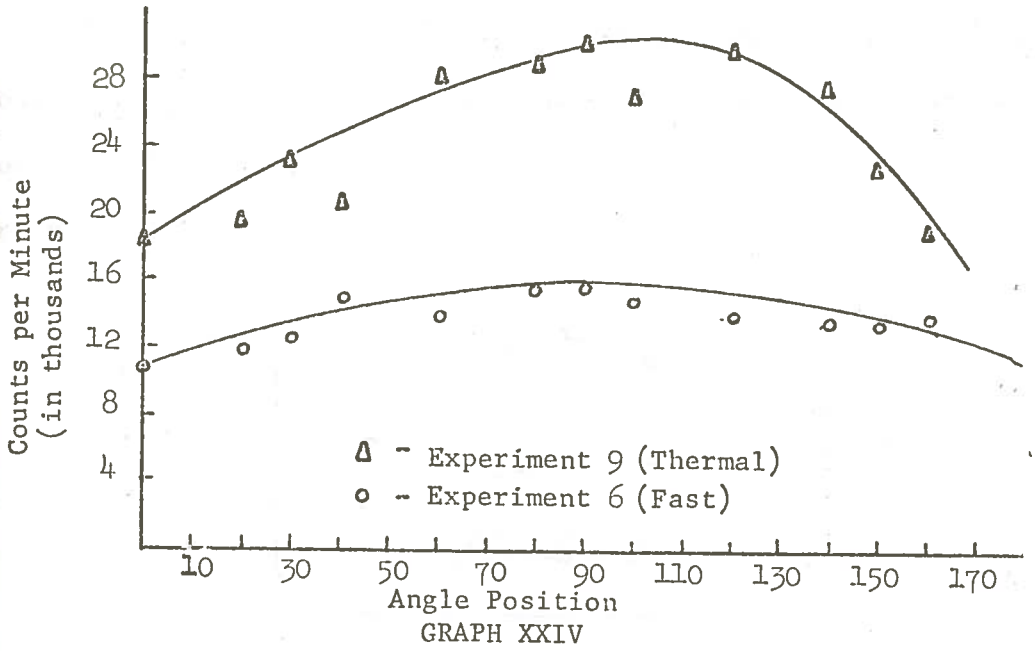

GRAPH XXIV

Comparison Between Thermal and Fast
Neutron Distribution from Experiments 9 and 6

First, the closer the foils were placed to the target the more pronounced an increase in thermal neutrons at the angle position 90°. This is seen clearly by comparing the thermal neutron curve in graph XXIII with that in graph XXIV. The slope of the thermal neutron curve in graph XXIII is greater than that of graph XXIV indicating a more rapid increase in thermal neutrons detected at angular position 90°. Another interesting fact is the large number of fast neutrons which have not yet been thermalized. This suggests that moderator designs with thicknesses greater than six centimeters will be needed to maximize the thermal flux at a point. This will be discussed further in subsection 1 of Series III.

D. Consideration of Series III Objective

1. Subseries 1. Different Dimension Hemispherical Polyethylene Moderators - Experiments 10-13 illustrate the increase in thermal counts as larger hemispherical polyethylene moderators were placed in front of the target. (See graph XXV).

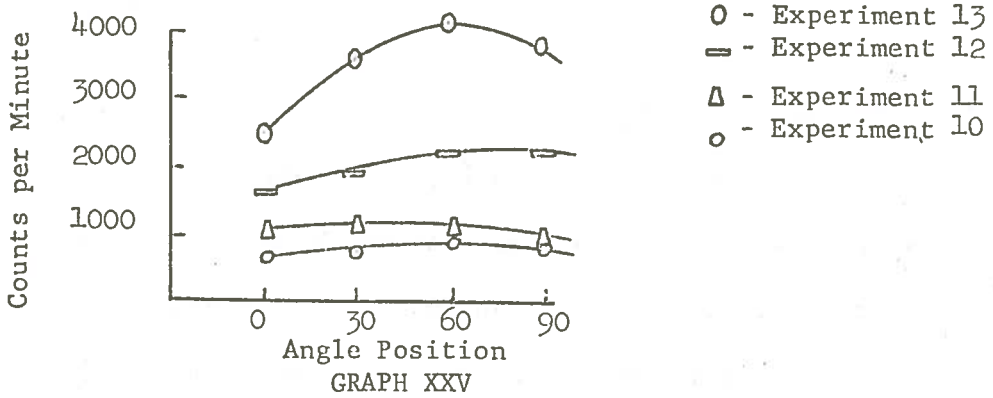

GRAPH XXV

Relationship Between Thermal Neutron Counts and Dimensions of Hemispherical Polyethylene Moderators

The flatness of the thermal neutron curve in Experiment 10 (no moderator) indicates that the deuterium beam was centered reasonably well on the accelerator target. However, the beam may have been moved off center on the subsequent experiments. The difficulty of getting the tightly fitting polyethylene spheres around the target may have resulted in moving the target. If so, this would account for the decrease in thermal counts observed at 90° in Experiments 11 and 13, and only a small increase in Experiment 12.

Two things may be noted from this subseries of experiments. First, the number of thermal neutrons increased as the size of the moderator increased. It also appears that the maximum increase in thermal neutrons has not been reached with the largest (6 cm) polyethylene hemisphere. Secondly, the observed number of fast neutrons increased with the increase in moderator size. This indicates that more of the fast neutrons are being moderated to lower energies (but still above 0.41 eV) where the absorption cross-section of the foil becomes greater. Thus the foil is activated more by the greater number of slower fast neutrons.

2. Subseries 2(a). Side and Back Block Wax Moderators - This subseries of experiments (14-20) was designed to obtain a rough approximation of how many of the fast neutrons originally scattered in directions other than to the foil might be moderated and scattered back to the foil placed two feet from the center of target.

The data (See graph XIV) indicates that 7.5 inches of paraffin along side the target results in the maximum number of thermal neutrons scattered back to the foil. When a fourth block of paraffin was placed along side the target (Experiment 18) the number of thermal neutrons observed decreased. It is believed, although not proven, that the fourth paraffin block moderated the neutrons to an energy low enough to result in a greater number of the neutrons being absorbed.

Next, fast neutrons originally scattered away from the back of the target were thermalized and scattered toward the foil. This was done in Experiment 19-20. (See figures 21 and 22). The results indicate that two blocks of paraffin around the accelerator tube results in the largest increase in thermal neutrons at the foil, C_n.

Because of only a small increase in C_n in Experiment 20 from Experiment 19 it was felt the addition of a third layer of paraffin would not do much good. Support for this assumption is found in the fast neutron data, C_m. There was only a small increase (54,375 versus 51,881) in the fast neutron count. This indicates that there was little increase in moderation of fast neutrons.

Because copper foils were used at the target to normalize the data, the assumption that all counts resulted from the $Cu^{63}(n,2n)Cu^{62}$ reaction must be examined.

Since T_2, time elapsed before copper target foil counted, was greater than 31 minutes for all experiments the above mentioned assumption is not as valid as would be desired. Furthermore, T_2 was

not the same for each experiment. Thus the degree of error varies among the experiments.

For the above reasons this subseries of experiments has been repeated using the Teflon target foils. For these results see Experiments 27-33 in Subseries 3 (a).

3. Subseries 2 (b). Paraffin Slabs as Moderator in Front of Target - In Experiment 25 one paraffin slab (2.5" x 2.5" x $\frac{5}{8}$") was placed before the target, while three slabs were used in Experiment 26 (See Figures 23 and 24). The data indicates a sharp decrease (471,664 to 70,713) in thermal neutrons observed when three slabs were placed in front of the target.

One possible explanation of the decrease is that the three slabs moderated the fast neutrons enough to allow them to be absorbed by the side paraffin blocks. Also fast neutrons first scattered into the side paraffin blocks may be absorbed when they are scattered back into the front paraffin slabs.

Again caution is urged in the exactness of the magnitude of difference. This caution results because of the use of copper foil at the target to normalize the data.

4. Subseries 2 (c). Paraffin Slabs in Conjunction with a Second Paraffin Block in Front of the Side Paraffin Blocks - A layer of paraffin blocks was placed in front of the side blocks mentioned earlier. Then experiments were run with different numbers of paraffin blocks placed in front of the target.

The purpose of this subseries was twofold: (1) to determine if the results from experiments 25 and 26 appear valid and (2) to determine the effect of the extra paraffin layer in front of the other side paraffin blocks.

Once again it must be noted that copper target foils were used.

As graph XVII clearly indicates, there was a marked reduction when more than two paraffin slabs were placed in front of the target. This supports the earlier findings that three slabs greatly reduces the thermal neutrons observed.

From this subseries of experiments little could be found about the effect of the extra paraffin layer placed in front of the side paraffin blocks. In Experiments 34-37 the effect is studied in more detail.

5. Subseries 3. Use of Teflon Target Foils to Correct Data Normalization Problem - Because of the uncertainties raised by the use of the copper target foils most of the conclusions reached were tested again, where a fluorine containing material (Teflon) was used as target foil.

In Part a (Experiments 27-33) the optimum number of side paraffin blocks was determined again. Once determined, the optimum number of rear paraffin blocks was next found for the configuration of interest.

Part b (Experiments 34-37) examined in more detail the effect of adding a paraffin layer in front of the side paraffin blocks.

The effect on thermal neutron production caused by the addition of paraffin blocks in front of the accelerator target was examined in Part c (Experiments 41-45).

Moderator effects after collimation of the thermal neutrons was studied in Part d (Experiments 38-40).

Finally, in Part e (Experiments 46-49) different paraboloid shaped paraffin moderators were placed around the accelerator target.

It should also be noted that several experiments (32, 36, and 42) were repeated in order that the reproducibility of the data might be examined. This will be dealt with in the concluding remarks.

(a) Part a. Optimizing Side and Rear Paraffin Moderators with a Teflon Target Foil

As before, when the copper target foils were used, little difference in the thermal neutrons observed could be detected when three or four block layers of paraffin were placed around the target (See figures 31 and 32). However, this time an increase rather than a decrease resulted. It was possible that the paraffin blocks might have been arranged in slightly different alignments to the target. A difference in alignment could have accounted for the increase in counts when four blocks were used. Since this increase (7,598,636 to 7,570,020) was so small (only 0.4%) a layer of three blocks thickness was considered optimum when other factors such as size, bulk, and support requirements were considered.

Contra to what the results indicated when copper target foils were used, a layer of three blocks of paraffin behind the target resulted in a substantial increase (6% if compare Experiment 32 with Experiment 31; 20% if compare Experiment 33 with Experiment 31) in thermal neutrons observed. These experiments demonstrate the advantage of using fluorine containing materials as foils, rather than copper foils.

(b) Part b. Consideration of a Second Layer of Paraffin Along Side the Target as A Moderator

When the data from Experiments 34-37 (with second layer) are compared with data from Experiments 32-33 (without second layer) there appears to be no increase to the number of thermal neutrons observed. In fact there is a decrease (See graph XXVI below):

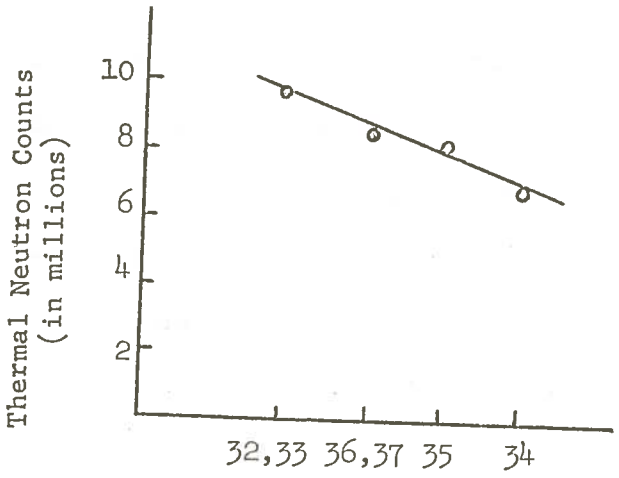

Experiment 32 has been averaged with 33

Experiment 36 has been averaged with 37

GRAPH XXVI

Effect of Second Side Paraffin Layer on the Number of Observed Thermal Neutrons

(c) Part c. Optimization of the Number of Front Paraffin Slabs

One to four slabs were tested in Experiments 41-45. The data indicates that three slabs resulted in the maximum observed thermal neutrons.

This data also is an indication of the effect using a second side layer of paraffin, and a back layer of paraffin in the moderator design. In Experiments 25 and 26 when no back or second side layer was used the data clearly indicated a decrease in observed thermal neutrons when three slabs were used. However, Experiment 44 which has a back layer shows an increase in observed thermal neutrons. This increase must be attributed to neutrons scattered from the back layer and thermalized by the three front paraffin slabs. On the other hand, Experiments 21-24 which had both a back and second side paraffin layer a decrease when more than two front slabs were used. This decrease must be attributable to the front layers if Experiments 41-45 are accurate.

The data from Experiments 41-45 is believed more accurate for several reasons. There is no copper target foil error as is found in Experiments 21-24. Secondly, the data in Experiment 42 was reproduced fairly closely by Experiment 43. When it is considered that these two experiments were run on different days, and after the moderator structure had been torn down and then reconstructed, the 11% difference in the normalized data appears acceptable. Therefore three front paraffin slabs appear to be the optimum number.

(d) Part d. Use of Different Moderator Designs And Collimation of Thermal Neutrons

As stated in the introduction neutron radiography requires a collimated beam of thermal neutrons. This series was designed to determine if the increase in observed thermal neutrons at a distance of two feet in front of target resulted in an increase in collimated thermal neutrons.

From previous neutron radiography work[37] a suitable collimator consisted of a water (or oil) tank with a tube running through it where thermal neutrons could pass (See figures 43-45). The tank was six feet square and the pipe had an inside diameter of four inches.

The moderator designs selected were those of Experiment 43 (figure 40), Experiment 45 (figure 42), and one similar except with six paraffin slabs in front of the target.

As expected there was a decrease in the observed collimated thermal neutrons as the number of paraffin slabs increased. The relationship between the decrease in observed thermal neutrons and observed collimated thermal neutrons is seen by the following table:

---

[37] Private Communications with Dr. Frank A. Iddings in August, 1969

NUMBER OF SLABS	OBSERVED THERMAL NEUTRONS	OBSERVED COLLIMATED THERMAL NEUTRONS
2	10,938,389	362,257
4	10,332,795	349,808
6	—	313,407

TABLE III

RELATIONSHIP BETWEEN OBSERVED AND OBSERVED COLLIMATED THERMAL NEUTRONS

There was a 5.5% decrease in the observed thermal neutron count when four slabs, instead of two, were used. For the observed collimated thermal neutrons there was a decrease of 3.4%. The closeness of these figures indicates that a direct relationship does exist between observed and observed collimated thermal counts. Therefore an increase in observed thermal neutrons due to a moderator design should indicate an increase in the collimated thermal neutrons, although it is expected that the increase will not be as large percentagewise.

(e) Part e. Paraboloid Shaped Moderator

A cylindrical mold was made in order to shape a moderator in the form of a doughnut (See figure 53 below):

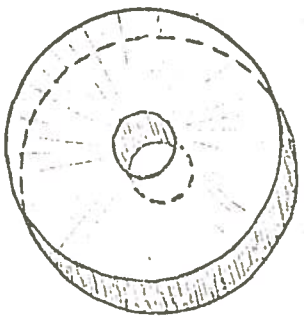

Figure 53

Doughnut Shaped Paraffin Moderator

Experiment 46 (only doughnut shaped moderator) indicates that the doughnut shaped moderator gives results of the magnitude obtained when a side paraffin layer of two block thickness was used.

Experiment 47 was designed to simulate Experiment 43. Data from 47 was 13,162,811 observed thermal neutron, while from 43 the observed thermal neutrons were 10,938,389. With this difference known comparisons can now be made between the paraboloid shaped moderators and other moderator designs studied.

The results from Experiments 48 and 49 indicate a substantial increase (50%) over the best results from previous moderator designs (See Experiment 44).

(f). Reproducibility of Data.

In order to test the accuracy of the data three experiments were run a second time. In each case a time period of 24 hours had passed, the moderator structure from the original run had been torn down and then restructured, and different Teflon target foils as well as different indium foils were used. The results are summarized in Table 3 below.

ORIGINAL EXPERIMENT NUMBER	REPRODUCED EXPERIMENT NUMBER	ORIGINAL C_n	REPRODUCED C_n	% CHANGE
32	33	9.08×10^6	10.33×10^6	13
36	37	9.11×10^6	8.62×10^6	5
42	43	9.87×10^6	10.94×10^6	11

TABLE IV

REPRODUCIBILITY OF EXPERIMENTS

when considering that the moderator structure had to be rebuilt a change of 13% is excellent.

CHAPTER VI

CONCLUSIONS

Most experimentation to this date has centered on health physics considerations. There was more interest in how much moderator was needed to absorb the neutrons. No experimental data has been found on moderator designs for accelerator which purpose has been to thermalize and not absorb the neutrons. Thus this experimental study is the first to approach the problem of selective moderation for accelerators.

The results from this study indicate a paraboloid shaped paraffin moderator leads to more thermal (< 0.041 eV) neutrons being located at a point two feet directly in front of the accelerator target, than with other shape moderators.

It is emphasized that the moderator designs tested in this study were only basic in structure. No attempt was made to achieve exact optimization in a particular design. For this reason much design needs be done to determine the utility of the moderator designs in neutron radiography applications.

VITA

David W. Kiesel was born in Orange, Texas on November 5, 1944.

Secondary education was obtained in Jennings, Louisiana at Jennings High School, from which he graduated in 1959. In September, 1959, he entered Louisiana State University, where he received his Bachelor of Mathematics degree in May, 1966 and his Juris Doctorate in Law in January, 1970.